ACS MATERIALS LETTERS

www.acsmaterialsletters.org

REVIEW

Multielectron Organic Redoxmers for Energy-Dense Redox Flow Batteries

Xiaoting Fang, Zhiguang Li, Yuyue Zhao, Diqing Yue, Lu Zhang,* and Xiaoliang Wei*

Cite This: *ACS Materials Lett.* 2022, 4, 277−306

Read Online

ACCESS | Metrics & More | Article Recommendations

ABSTRACT: Redox flow battery is a highly promising stationary energy storage method, but the limited energy density and high chemical cost are among the main barriers for commercialization. Multielectron organic redoxmers represent a family of structurally tailorable candidates that can achieve multiplied energy density with decreased materials consumption, potentially resulting in a viable solution to address these challenges. Here, the recent development of organic molecules with reversible multiredox activities in both aqueous and nonaqueous electrolytes is reviewed. The major focus is on the fundamental correlation between the chemical structures and the functional properties of reported multielectron organic molecules. Valuable insights are offered on rational structural design strategies for improving the relevant physicochemical and electrochemical properties. Finally, the current challenges are discussed to suggest future research needs along the avenue of using the multielectron approach to achieve energy-dense, stable, cost-effective redox flow batteries.

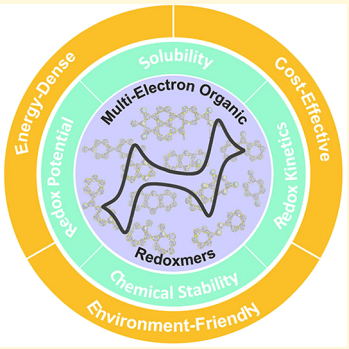

1. INTRODUCTION

The first 20 years of this century have witnessed a rapid evolution of our energy landscape with a transition from carbon-intensive fossil fuels to clean, abundant renewable energies. Solar and wind are expected to become the dominant energy sources in the future to reduce carbon footprint and improve societal sustainability.[1] However, critical challenges of power quality and grid stability are accompanied because of the intermittent nature of these renewables. Incorporation of large-scale, cost-effective electrical energy storage sectors represents a well-balanced approach to impart grid stability and reliability. Moreover, grid storage sectors can offer effective peak/off-peak managements, improve asset utilization efficiency, and defer the costly transmission and distribution (T&D) upgrading for our century-old power infrastructure. In addition, localized storage facilities can provide charging stations for electric vehicles, which can enhance the pace of transportation electrification. Among the variety of energy storage technologies, electrochemical methods including rechargeable batteries have gained momentum. Given the high energy density, lithium ion batteries have facilitated the widespread use of portable electronics, and recently have also been launched in grid storage market.[2,3] But the high cost, fire hazard and integrated electrode/carbon structure are the main roadblocks for lithium ion batteries in large-scale, safe, long-duration storage applications.[4] In this regard, redox flow batteries (RFBs) have unique advantages.[5−7] As shown in Figure 1a, RFBs capitalize on the pumped circulation of externally stored redox-active liquid electrolytes through the electrode compartments to trigger electrochemical reactions for conversion of energy forms. This cell structure spatially decouples the redox-active materials (or redoxmers) from the electrodes leading to readily and independently scalable energy and power, as well as other exceeding advantages such as fast solution reaction kinetics, minimal phase transformation, long cycle life, safety, and active thermal management. Therefore, RFBs have recently become an active field of research with significant industry involvement.

Traditional RFBs are based on inorganic redoxmers in aqueous electrolytes, such as $Cr^{II/III}$, $V^{II/III/IV/V}$, $Fe^{0/II/III}$, $Zn^{0/II}$, polyhalides, polysulfides, $Pb^{0/II/IV}$, etc.[8−10] By now, the all-vanadium RFBs are the benchmark system because of the use of a single element leading to minimal electrolyte contamination and long-term operational stability,[11] which however are plagued with low energy density (~25 Wh/L) and high chemical (V_2O_5) cost. A recent technoeconomic analysis of all-vanadium RFBs indicated a current capital cost as high as $320/kWh at the 1 MW/4 MWh scale, which is still several times higher than the DOE's cost target of $100/kWh, with V_2O_5 accounting for ~50% of the system cost.[12] RFBs based on

Received: October 21, 2021
Accepted: December 17, 2021
Published: January 6, 2022

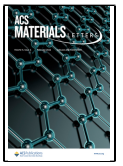

https://doi.org/10.1021/acsmaterialslett.1c00668
ACS Materials Lett. 2022, 4, 277−306

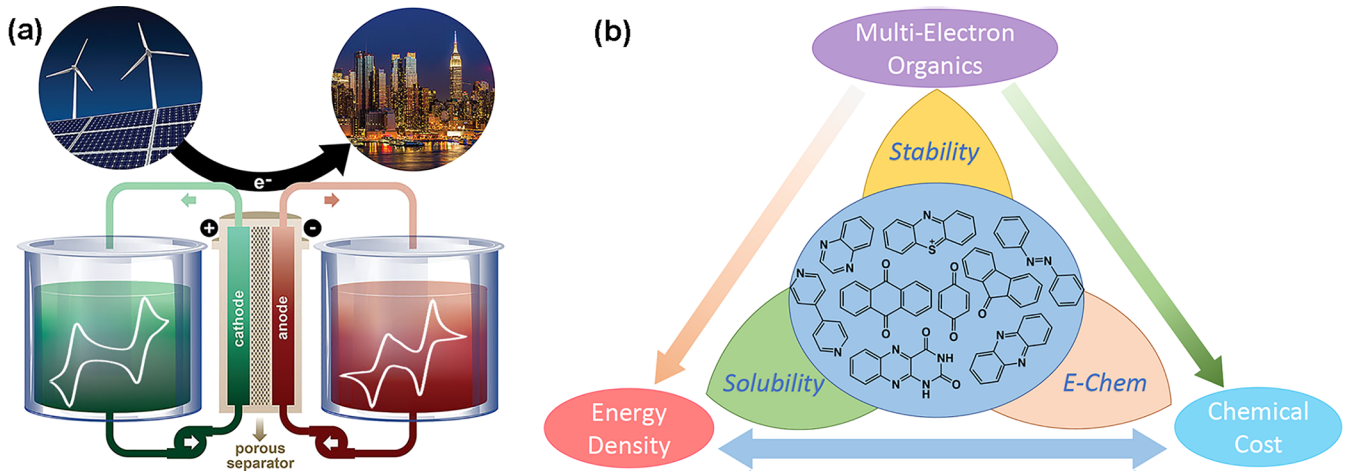

Figure 1. (a) Schematic diagram of 2e⁻ RFBs. Adapted with permission from ref 13. Copyright 2017 American Chemical Society. (b) Illustration of structure−property−performance correlations of multielectron organic molecules.

polysulfides, zinc, bromine, and iron are potentially cost-effective systems, but are facing their respective limitations such as species crossover, dendrite growth, low power, parts corrosion, stringent pH control, etc.[14,15] Nevertheless, for these inorganic species, there is limited space to tune their intrinsic characteristics to a wide range. On the contrary, organic redoxmers stand out as promising materials for RFBs because of their tremendous molecular diversity and tailorability thus have attracted substantial interest.[16−19] The versatile structures of these redoxmers can offer facile property adjustments to meet relevant requirements in solubility, chemical stability, redox potential, and kinetics. Moreover, these molecules have potentially broader uses because of their compatible properties with nonaqueous RFB electrolytes. Nonaqueous RFBs have been investigated to pursue high cell voltage and energy density, expand the pool of feasible materials and enable low-cost storage solutions, exploiting their wider electrochemical windows than aqueous counterparts.[20−22]

The versatile structures of these redoxmers can offer facile property adjustments to meet relevant requirements in solubility, chemical stability, redox potential, and kinetics.

Capital cost is one of the most important technoeconomic metrics that industry follows to commercialize a RFB technology. Achieving high energy density is a viable strategy to decrease the electrolyte volume and related component materials and thus overall cost. The energy density is calculated by $n \times C \times F \times V$, where n is the number of transferred electrons, C is the redoxmer concentration, F is Faraday's constant (96 485 C/mol), and V is the cell voltage. Following this equation, there are several approaches to achieve a high energy density in a RFB system. The first method is to increase redoxmer solubility. Thanks to modern synthetic organic chemistry, researchers have successfully attempted to introduce a variety of solubilizing functional groups or molecular asymmetry[23,24] onto redox cores to impart strong solvation interactions and thus increased solubility. The second method is to increase the cell voltage, which is the primary motivation for investigation of nonaqueous RFBs. The redox potential can be fine-tuned by incorporation of electron-withdraw groups (EWGs) or electron-donating groups (EDGs) to modulate the Fermi level of redoxmer.[25] The third method is to enable multielectron redox reactions. Multiredox activities are commonly observed in heteroaromatic organic molecules.[16−19] This approach has also been explored in inorganic redoxmers, such as $Zn^{0/2+}$, $Fe^{0/2+}$, $S_{2/4}{}^{2-}$, a mixture of multiple redox couples (e.g., mixed Fe^{2+} and V^{4+}[26]), and metal-coordination compounds especially those bearing redox noninnocent ligands. But these materials are out of the scope of this Review and excellent literature reviews are available to interested readers.[11,27−31]

In this Review, we first discuss the key material properties of organic redoxmers and the general strategies for achieving exceeding properties. Then, the recent advances in the development of multiredox organic molecules in the context of both aqueous and nonaqueous RFBs are summarized. The categorization of multielectron organic redoxmers is based on the location of the redox-active center in the molecular scaffold, as such including carbonyl-centered and N-centered candidates. Our purpose is to provide a perspective on the design and development of soluble, stable multiredox materials to achieve high energy density and long cyclability in RFBs (Figure 1b).

2. KEY PROPERTIES AND GENERAL STRATEGIES OF ORGANIC REDOXMERS

Aqueous RFBs have been extensively investigated with significant progress since the first invention of iron−chromium systems at NASA in the 1970s.[32] Aqueous electrolytes have significant technoeconomic advantages, including high ionic conductivity, low viscosity, wide pH range, available selective and conductive membranes, cost-effectiveness, and safety. These attributes have led to the development of high-power, long-cycling RFBs with great commercial promise, such as all-vanadium, all-iron, and zinc−bromine systems. However, aqueous electrolytes are generally limited by the narrow electrochemical window of water, typically <1.7 V. To avoid the parasitic H_2 or O_2 evolution reactions, the redox potentials of anolyte and catholyte materials must be constrained within this window. This feature has limited aqueous RFBs to low-voltage systems and also has excluded a number of redox candidates whose redox reactions occur outside this window.

To circumvent this limitation, nonaqueous electrolytes using water-free organic solvents have recently been explored,

https://doi.org/10.1021/acsmaterialslett.1c00668
ACS Materials Lett. 2022, 4, 277−306

exploiting their wider electrochemical windows of up to 8.2 V to achieve high-voltage and energy-dense storage systems.[21] Nonaqueous RFBs are currently in the infancy stage and are primarily focused on redoxmer design and development. A variety of technical challenges need to be addressed before commercialization standards are seriously discussed. The lack of suitable membranes with combined permselectivity and ionic conductivity has greatly hampered demonstration of redoxmers under practically relevant RFB conditions. In addition, the high viscosity, low ionic conductivity, and flammability of costly solvent and salts are other disadvantages of nonaqueous RFBs.

Nevertheless, despite these drawbacks, there has been great progress both in discovery of promising redoxmers and in understanding of fundamental structure−property relationships. We will strive to unravel the critical structural and mechanistic characteristics of multielectron organic redoxmers in aqueous and nonaqueous RFBs. The underlying property-controlling factors and the strategies to enable these factors will be discussed to suggest rational design principles. The key properties of redoxmers include solubility, redox behavior, and chemical stability. The prior art for property enhancement in one-electron organic redoxmers can be transferred to modify the multi-electron candidates. We will first illustrate the general materials engineering approaches for achieving favorable properties in reported organic redoxmers.

2.1. Solubility. Solubility is the maximum concentration testable in a RFB cell that determines its energy density. Reliable methods to accurately measure redoxmer solubility often rely on fitting a spectroscopic feature (e.g., peak intensity or area) of a millimolar-scale solution diluted from saturation to the predetermined linear peak-concentration relationship. These methods are started with the saturated solution thus eliminating the errors associated with preparing the redoxmer solution exactly at its solubility limit especially for deep-colored redoxmers. Ultraviolet−visible (UV−vis) spectroscopy is often used to serve this purpose.[33,34]

Theoretically, a high solubility originates from breaking of solid-phase molecular organization by the stronger solvent−solute (i.e., solvation) than solute−solute (i.e., ion/molecule pairing) interactions. Therefore, the solvate structures and ligand exchange dynamics mechanistically dictate the solubility of a solute molecule. Typically, organic redoxmer cores are inferiorly soluble in generally polar battery solvents including water because of the less polar structures. Common approaches work to increase solubility either through increasing solvent−solute interaction or via weakening solute−solute interactions. In the first case, polar substituents are usually introduced to polarize the core structures making them more soluble. For example, functional groups, such as phenolate ($-O^-$), sulfonate ($-SO_3^-$), carboxylate ($-CO_2^-$), phosphate ($-PO_3^{2-}$), quaternary ammonium ($-NR_4^+$), and oligo-ethylene glycol ($-EG_nOH$), have been extensively used to enable highly soluble organic molecules in aqueous electrolytes.[33−39] For nonaqueous RFB materials, carbonyl (−C=O), $-NR_4^+$ (with suitable anions) and oligo(ethylene glycol) ether ($-EG_nOMe$) have been widely installed.[23,40−42] In certain molecules, the nature of counterion plays a nontrivial role in enhancing solubility.[43] For example, compared to the Na^+/K^+ forms, NH_4^+ leads to several-fold increases in the solubilities of ferro/ferricyanide and anthraquinone disulfonate (AQDS).[44,45] For (ferrocenylmethyl)dimethylethylammonium, the $N(CN)_2^-$, $TFSI^-$, and PF_6^- anions result in significantly higher solubilities (>1.7 M) than BF_4^- (0.4 M) in nonaqueous carbonate solvents.[43] Spectroscopic and computational solvation studies have revealed that the solute−solvent interactions occurred preferentially at the polar substituent sites, confirming the importance of these functionalities in enhancing solvation interaction and solubility.[46,47]

In the second case, to weaken solute−solute interactions, the chemical structures are often designed such that molecular asymmetry occurs to disturb the propensity of ordered organization. It is noted that polar substituents alone do not always lead to high solubility; their geometric distribution in the molecular structure can also play a role. For example, in decorating phenazine and azobenzene cores, two symmetrically sited sulfonates yield near-zero polarity and low solubility in water, in sharp contrast with those structures having asymmetrical substituents.[33,48] This phenomenon is even more obvious in nonaqueous RFB materials. Structural asymmetry even eliminates the need of polar substituents in certain molecules. For example, ferrocene with two nonpolar methyl groups at its 1,1′-locations has a low melting point (37−40 °C) and high solubility (>3 M in carbonate).[24] Other asymmetrical examples include TEMPO (5.2 M in carbonate), 2,1,3-benzothiadiazole (4−5 M in common solvents), and 2,5-di-*tert*-butyl-1-methoxy-4-[2′-methoxyethoxy]benzene (liquid at room temperature).[13,23,49] Furthermore, in some circumstances, a hydrotropic additive, such as urea or nicotinamide that has strong hydrogen bonding with solute molecules, can effectively break the solute−solute interactions and enhance solubility.[48,50,51]

A nontraditional method for increasing the equivalent electron concentration is the redox-targeting approach that utilizes metal ion battery (MIB) materials as alternative charge storage hosts in the RFB framework.[52−54] This method capitalizes on redoxmer mediated intercalation chemistry to harvest combined RFB and MIB advantages, thus leading to high energy density and expanding the boundary of RFB-based storage.

2.2. Redox Potential and Kinetics. The redox potentials of anolyte and catholyte materials govern the cell voltage and energy density of a RFB system. They are expected to separate sufficiently apart to harvest a high voltage yet still within the electrochemical window of supporting electrolyte to avoid decomposition of solvent and salt. The redox potential of a compound is dependent on the energy levels of its frontier orbitals, that is, the highest occupied and the lowest unoccupied molecule orbitals (HOMO and LUMO).[55] Factors that can affect the electronic structure will have potential to tailor the frontier energy and thus the redox potential of a material. It has been established that, for a given redox-active core, an EDG increases its Fermi level and negatively shifts its redox potential, while an EWG operates in the opposite way. In addition, solvent and salt also have the capability of moving redox potential.[56] For example, Zhang et al. discovered that various cations (e.g., Li^+, Na^+, K^+, NEt_4^+) in MeCN-based electrolytes modulate the redox potential of 2,1,3-benzothiadiazole quite differently.[57] These features have offered generally useful molecular and electrolyte engineering methods to tune redox potential and cell voltage. Redox potential can be measured using voltammetric methods, usually cyclic voltammetry (CV).

Redox kinetics is an electrochemical parameter to characterize the rate of electron transfer at the electrode/electrolyte interface, which consequently influences the voltaic efficiency (VE) of RFBs. In general, organic redoxmers intrinsically have faster redox kinetics than metal ions and organometallic compounds,

https://doi.org/10.1021/acsmaterialslett.1c00668
ACS Materials Lett. 2022, 4, 277−306

presumably because they are mostly nonadiabatic processes accompanied by minimal covalent bond breaking/formation and reorganization. Moreover, RFBs typically use highly porous carbon electrodes to facilitate electrolyte flow and transport properties. The microstructure and surface chemistry of the electrodes largely impact redox kinetics. In general, the kinetic rate constant of a redox compound can be determined through two methods: (i) Koutecky−Levich analysis using linear sweep voltammetry (LSV) with a rotating disk electrode (RDE) to eliminate diffusion-related kinetic factors;[58] and (ii) Nicholson analysis using CV at a variety of scan rates.[59]

A special case is for certain organic molecules that undergo proton-coupled redox reactions in aqueous electrolytes, such as quinone,[34] alloxazine,[60] phenazine,[33] etc. The pH value of the electrolyte affects both the electrochemical window of water and the redox behaviors of these organic molecules; such effects are rather significant according to the Nernst Equation. For example, a phenazine analog, decorated with tri(ethylene glycol) groups (denoted as phenazine-$(EG)_3$) to make it soluble in all of the acidic, neutral, and alkaline electrolytes, exhibits pH-dependent redox responses (Figure 2). The change in pH from

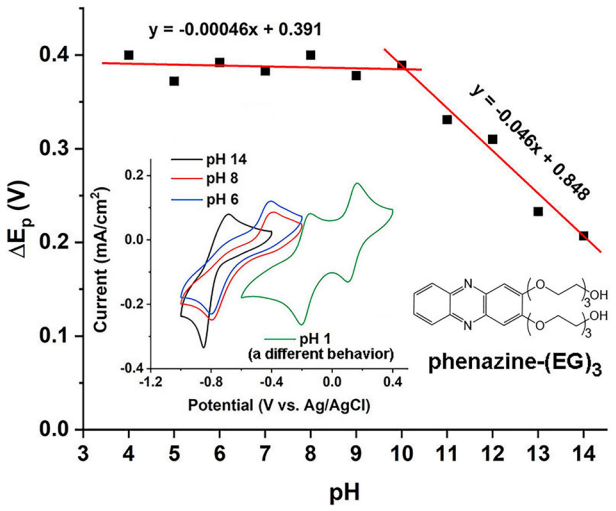

Figure 2. pH-dependent redox properties of phenazine-$(EG)_3$ (unpublished results by the authors).

alkaline to acidic not only shifts the redox potential positively, but also transforms the concerted $2e^-$ redox to stepwise activities. The exact mechanism for the evolution of peak separation (ΔE_P) is not well-understood but is hypothesized to be thermodynamically related with the varied protonation/deprotonation processes at different pH values.

2.3. Chemical Stability. Chemical stability of redoxmers in both electrochemically charged and discharged states can produce high cycling stability and long cycle life of corresponding RFBs. However, capacity fading has been observed in various RFBs using organic redoxmers. One of the major origins of such fading is decomposition of organic species, as the charged anolyte and catholyte species are reactive reducing and oxidizing agents, respectively. Moreover, organic compounds are multi-atom, multi-bond molecules usually bearing unsaturated groups, such as C═C, C═O, C═S, C═N, N═N, N−O•, N═O, etc. Thus, they are prone to parasitic side reactions which are often irreversible. Typical decomposition pathways include protonation, nucleophilic substitution/addition, bond breaking/formation/rearrangement, or a combination of multiple processes. The detailed mechanism is specific for given redox molecules because of their unique structures and redox reactions. The electrolyte rebalancing based capacity recovery, like the electrolyte remixing method used in all-vanadium RFBs,[61] is being pursued but with limited success.[45] Thus, replacement of aged electrolytes after degradation reaches a certain level seems to be a more reasonable approach to achieve continued service life, which is expected to change the way of calculating the levelized cost of RFB systems.[62]

Water is a special solvent with loose protons that can protonate anionic redox species in anolyte and simultaneously having electron lone pairs on O that can nucleophilically add to cationic redox species in catholyte. The protonation reaction is usually a fast, reversible process and often can be mitigated at high pH values. However, the water addition reaction is often irreversible followed by deprotonation and/or bond rearrangement, making the cationic redox species unstable. This is the primary reason the development of stable catholyte redoxmers is significantly more challenging. There is a very limited number of successful catholyte candidates particularly those having high redox potentials. In many cases, ferro/ferricyanide catholyte was used for investigating new anolyte materials,[34,63] although its long-term chemical stability in alkaline electrolytes remains questionable.[59,64]

Decomposition of redoxmers in nonaqueous RFBs are more complicated due to the multiple options of solvent and salt. Organic solvents may have electron-deficient functional groups that can undergo nucleophilic reactions with anionic redox species. For example, the radical anion form of 9-fluorenone and *N*-methylphthalimide may attack the C═O in carbonates or the proton in acetonitrile (MeCN), resulting in rapid capacity fading in the flow cells using these solvents.[42,58] For certain anionic redox molecules, such as PTIO and 2,1,3-benzothiadiazole, a NR_4^+ salt can afford reversible, stable redox activity with decent lifetime while a Li^+ salt fails to do so.[65,66] This observation is thought to be associated with the strong contact-ion pairing interactions between the anionic species and Li^+, but the bulk size of NR_4^+ obstructs formation of such ion pairs. Therefore, careful selection of supporting solvent and salt is critically essential to achieve high stability for nonaqueous RFB materials.

2.4. Theoretical Calculations. Theoretical calculation is playing an increasingly important role in fast screening of redox structure databases, identifying redox candidates with designed properties, and unraveling decomposition mechanisms. The computational efforts can corroborate with experimental tests to expedite the development pace of soluble, stable redoxmers with suitable redox potentials. The computational frameworks commonly used in the RFB field include density functional theory (DFT) and molecular dynamics (MD), which can provide molecular level insights of frontier energies, structural arrangements, reaction energetics, etc. Through calculating the

Theoretical calculation is playing an increasingly important role in fast screening of redox structure databases, identifying redox candidates with designed properties, and unraveling decomposition mechanisms.

https://doi.org/10.1021/acsmaterialslett.1c00668
ACS Materials Lett. 2022, 4, 277−306

frontier energy levels (i.e., HOMO and LUMO), the redox potentials of a series of derivatives of a redox-active core can be predicted with decently high accuracy and efficiency. The supporting solvent and salt may impact the redox potential, which can be understood via computational estimate of the ion pair effect.[67] Moreover, calculation of the solvation energy of a chemical structure in a liquid medium, typically via observing the bonding energy difference of the optimized structures in gas phase and with surrounding solvent molecules, can reflect the solubility.[33,48] In combination with spectroscopic characterizations (e.g., NMR), the solvate structures with spatial arrangements of counterion and solvent molecules in the close proximity of the redox moiety can be unraveled to determine the mechanisms for establishment of its solubility limit.[40,47] Furthermore, based on the positive or negative sign of the calculated Gibbs free energy change (ΔG) of a hypothetical parasitic reaction, its thermodynamic spontaneity under the electrolyte condition can be estimated to assess the possibility of the proposed decomposition pathway.[68−70] The trends offered by these calculations can help predesign redox molecules with promising properties, which can save a large amount of synthesis time and labor in candidate down-selection. Therefore, the molecular level computations can serve as useful tools to screen and develop soluble, stable redox structures with suitable redox potentials.

An important extension from the above calculations, which involve only a limited number of structures, is the high-throughput (HT) computational screening for accelerated discovery of propitious redox materials. For example, Aspuru-Guzik et al. developed a DFT-based HT screening protocol to identify possible anolyte and catholyte candidates from a pool of 1710 molecular variations to produce high-voltage all-quinone flow battery chemistries.[71] Mavrandonakis et al. investigated the HT-DFT calculations of the redox potentials of 200 phenazine structures to harvest a 2.8 V all-phenazine nonaqueous flow battery.[72] Persson et al. have developed an Electrolyte Genome database and established a virtual library of >100 000 molecules, using a big data strategy to offer successive evaluations of redox potential, solubility, and stability.[73] More recently, various machine learning (ML) approaches have been introduced to streamline the development process and accomplish inverse design of redox materials within shortened timeframes.[74,75] With the selected ML model, the property descriptors and training sets need to be carefully identified.

Other statistical models have also been developed to predict promising properties with high accuracy. Sanford et al. established a physical organic model to estimate the molecular structure of a persistent *N*-alkylpyridinium radical via inclusion of an electronic parameter and a steric parameter.[76] A training set of 12 synthetic *N*-alkylpyridinium radicals with a representative range of electronic and steric variations were tested to establish a quantitative structure−stability relationship, which was extrapolated to identify the stable radical structure. Similarly, Sigman et al. developed a solubility model to predict highly soluble (>1.6 M) cyclopropenium catholyte molecules in nonaqueous RFBs, through data set extrapolation of the molecular descriptor-solubility relationship obtained from the training set.[77]

3. MULTIELECTRON ORGANIC MOLECULES IN AQUEOUS RFBS

Currently, aqueous RFB systems are the major focus of RFB research and development because of the aforementioned technoeconomic advantages of aqueous electrolytes. However, most organic redox cores are hydrophobic and have scanty solvation interactions with water molecules and thus low solubility. This feature requires structural modification to increase solubility, which may meanwhile affect the redox properties and chemical stability. Therefore, for every type of multielectron organic compound, we will correlate their molecular structures with functional properties to offer insights of comprehensive property-dictating mechanisms.

3.1. Carbonyl-Centered Multi-Electron Organic Molecules.

3.1.1. Anthraquinone Derivatives. The carbonyl (C═O) group is redox-active with $1e^-$ or $2e^-$ reactions but the electrochemically reduced anionic structures typically require π-conjugation in the proximity to stabilize the charges. Among the various carbonyl-bearing compounds, quinone structures possess two naturally conjugated carbonyl groups in a six-membered unsaturated ring. The classical $2e^-$ electrochemistry converts between quinone and dihydroxybenzene. On the basis of the molecular structures, the "naked" quinone core can serve as a catholyte material because of its high redox potential, while the two electron-donating conjugative benzene rings in anthraquinone (AQ) result in a significant negative shift of its redox potential making it suitable as an anolyte material. Because of their different redox characteristics, benzoquinone (BQ) and AQ are discussed separately.

As the pioneer in the use of organic redoxmers for aqueous RFBs, Aziz's group have focused on the investigations of AQ compounds with an evolutionary structural design to address the solubility, stability and kinetics challenges existing for the chemical and electrochemical aspects of AQ. The first reported AQ compound was 9,10-anthraquinone-2,7-disulfonic acid (AQDS) as a $2e^-$ anolyte material (Figure 3a).[35] The two hydrophilic sulfonic acid ($-SO_3H$) groups boost the solubility of the pristine AQ from near-zero to >1 M at pH 0. The redox kinetics of AQDS ($k_0 = 7.2 \times 10^{-5}$ m/s) was measured using RDE-based LSV and is generally higher than those of inorganic metal ion based redoxmers.[8] The fast kinetics is beneficial to achieve high VE in corresponding flow cells. As a result, the traditional thermal or acid treatments to graphite electrodes, which are typical for all-vanadium systems to promote wettability and catalytic effects, are not strictly required. The AQDS anolyte is paired with HBr/Br_2 catholyte to form an aqueous organic−inorganic RFB chemistry and the cycling performance is shown in Figure 3b. The fast kinetics of both redoxmers and the high proton conductivity of acidic electrolytes lead to demonstration of an impressively high power density of 1 W/cm^2 in AQDS/Br_2 flow cells under optimized test conditions (Figure 3c).[78]

The long-term operational stability is a key performance metric for aqueous organic RFBs considering their expected >10 years of service life. One of the major causes for capacity fade in traditional inorganic-based RFBs is unbalanced species crossover such as in all-vanadium systems.[61] On the contrary, for organic redoxmers, this is often not the case because their bulky size and mostly ionic nature can prevent crossover through ion exchange membranes. However, due to the multi-atom and bond-unsaturation characteristics, their stability against external chemical attack and intramolecular structural rearrangement remains a significant concern, especially when seeking the root causes for capacity fade in organic RFBs. As shown in Figure 3d, the flow cells using 1 M AQDS in anolyte and 3 M HBr and 0.5 M Br_2 in catholyte exhibit high Coulombic efficiencies (CE, 98.35% on average) and relatively stable capacities (99.84%

https://doi.org/10.1021/acsmaterialslett.1c00668
ACS Materials Lett. 2022, 4, 277−306

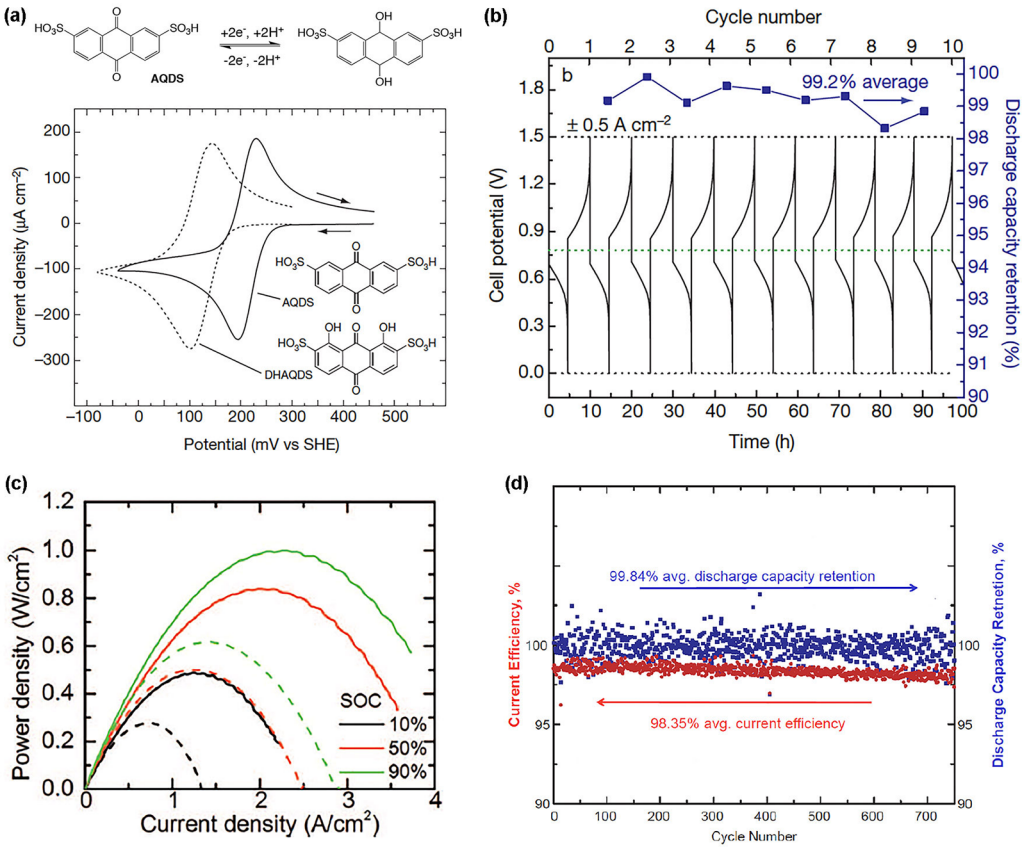

Figure 3. (a) Electrochemical reaction and CV scans of AQDS. (b) Voltage curve and discharge capacity of an AQDS/HBr flow cell at 40 °C. Reprinted with permission from ref 35. Copyright 2014 Springer Nature. (c) Power density vs current density of an AQDS/HBr flow cell. Reprinted with permission from ref 78. Copyright 2016 Electrochemical Society. (d) CE and capacity of an AQDS/HBr flow cell. Reprinted with permission from ref 81. Copyright 2014 Electrochemical Society.

capacity retention over 750 cycles at 0.75 A/cm^2).[79−81] But a significant amount of volume increase is observed as a result of high osmotic imbalance. Diffusion cell tests indicate bromine crossover through the Nafion membrane as the major cause for the CE loss. But the chemical degradation of AQDS especially in the reduced form is not excluded. A CO_2-assisted dimerization mechanism was proposed but the predicted result of 1.5 usable electrons per AQDS is in contradiction with the observed >90% of 2e$^-$ capacity in flow cells.[82] More recent studies also suggest desulfonation or disproportionation-based degradation pathways for AQDS, which however remain inconclusive due to a lack of detection of the decomposition products.[83,84]

The major drawback of anolyte AQDS is the too high redox potential (~0.21 V versus NHE), making it difficult to harvest high cell voltages with available catholyte materials. AQDS has been coupled with bromine in this report and with other redox couples such as hydroquinone and iron in other researchers' reports, all leading to ≤0.8 V voltages.[85,86] Simply removing one sulfonic acid (anthraquinone-2-sulfonic acid, AQS) or adding electron-donating hydroxyl groups in AQDS indeed negatively shift the redox potential but meanwhile yield chemical and cycling instability in AQ/Br_2 flow cells.[79,87]

Because of the proton-coupled nature of the redox reaction of AQ, electrolyte engineering via pH adjustment has been demonstrated as a feasible method to tune the redox potential. Aziz et al. developed 2,6-dihydroxylanthraquinone (DHAQ) with the electron-donating phenolate groups in an alkaline electrolyte resulting in a low redox potential of −0.69 V vs NHE and a cell voltage of 1.2 V when coupled with the ferrocyanide catholyte (Figure 4a).[34] Despite the relatively low solubility (0.6 M at pH 14 and 0.1 M at pH 12), the DHAQ-based flow cells demonstrate high power densities, for example, >0.45 W/cm^2 at 25 °C and 0.7 W/cm^2 at 45 °C. However, the DHAQ/ferrocyanide flow cells exhibit considerable capacity fade (0.1% per cycle), indicated in Figure 4b. While ferro/ferricyanide may undergo parasitic hydrolysis reactions at such a high pH of 14,[59] its contribution to the capacity fade is unclear since it was used in excess. Post-mortem spectroscopic analyses (NMR, HPLC, MS) of the cycled DHAQ after a symmetric flow cell test indicate that a disproportionation decomposition mechanism occurs forming redox-inactive anthrone and its dimer and resulting in the gradual loss of DHAQ (Figure 4d).[83,88] Similar anthrone dimer products were also detected from a cycled oligo(ethylene glycol)-bearing anthraquinone (1,8-PEGAQ) in neutral electrolyte,[39] suggesting a generally possible decomposition pathway of AQ and its derivatives. Interestingly, the anthrone can be oxidized back to DHAQ under aerobic conditions.[83] This is particularly beneficial for long-term flow cell cycling because air exposure can serve as a viable method to recover the lost capacity, which may eliminate the need of inert gas environment. Xiang et al. reported the use of a dihydroxylated anthraquinone, alizarin-3-methyliminodiacetic acid (AMA), as an anolyte material that displayed a slightly lower solubility (0.4 M) and a redox potential of −0.66 V versus NHE in pH 14 electrolytes.[89] The AMA/ferrocyanide flow cell produces a similarly high power density of 0.49 W/cm^2 and

https://doi.org/10.1021/acsmaterialslett.1c00668
ACS Materials Lett. 2022, 4, 277−306

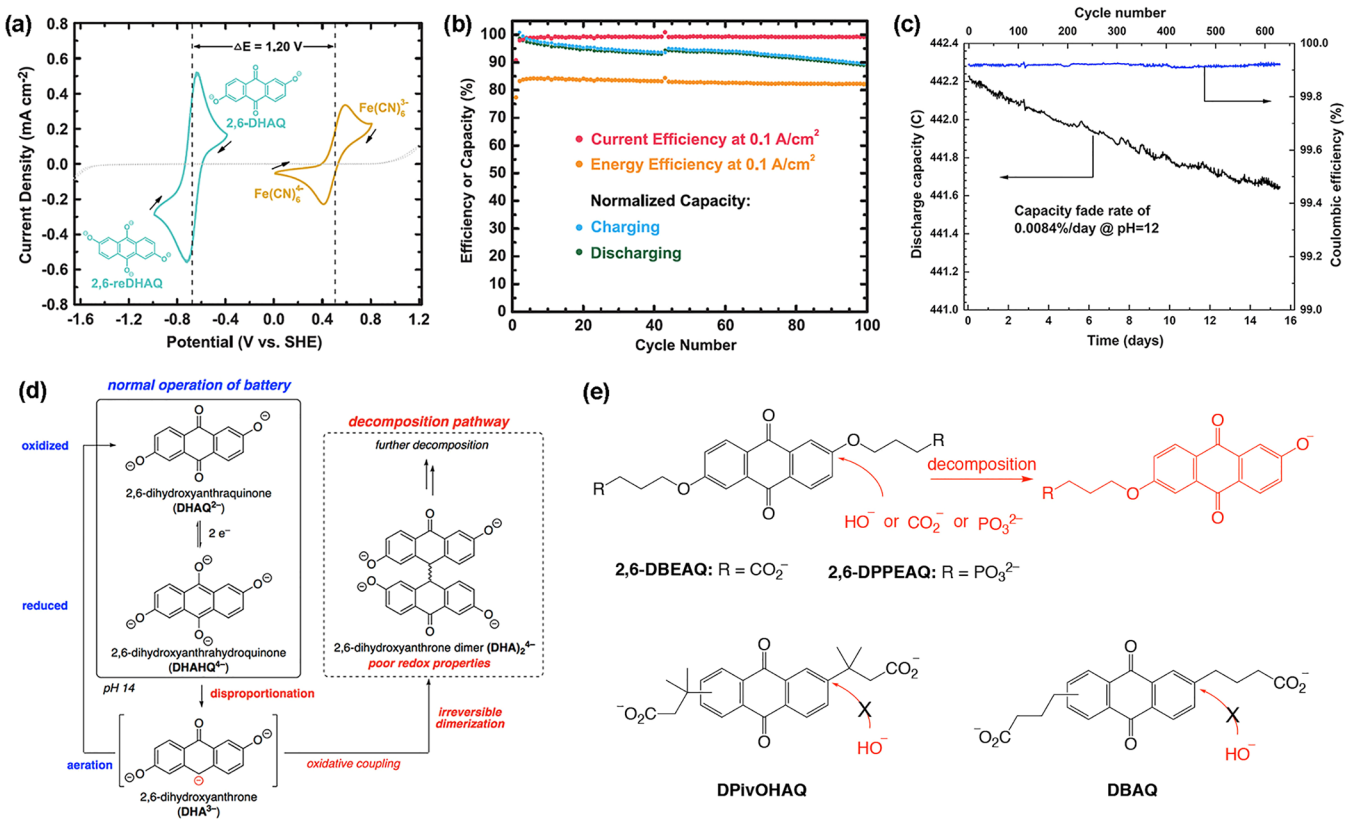

Figure 4. (a) CV scans of DHAQ in pH 14 alkaline electrolyte and (b) cycling efficiencies and capacities of 0.5 M DHAQ/ferrocyanide flow cell. Reprinted with permission from ref 34. Copyright 2015 AAAS. (c) CE and capacity of 0.5 M DBAQ/ferrocyanide flow cell. Reprinted with permission from ref 92. Copyright 2020 Cell Press. (d) Decomposition pathways of DHAQ. Reprinted with permission from ref 83. Copyright 2019 American Chemical Society. (e) Molecular structures of 2,6-DBEAQ, 2,6-DPPEAQ, DPivOHAQ, and DBAQ; dealkoxylation-based decomposition pathways are also illustrated.

relatively good capacity retention of 99.19% per day for 350 cycles.

Further introduction of carboxylate-terminated O-alkyl ether groups to 2,6-DHAQ yields the more soluble 4,4′-((9,10-anthraquinone-2,6-diyl)dioxy)dibutyrate (2,6-DBEAQ, 0.6 M at pH 12; 1.1 M at pH 14).[90] More importantly, the reduced form of 2,6-DBEAQ is impressively more chemically stable. The evidence includes the remarkably low capacity fade rate in flow cells and the detection of negligible NMR peak change in cycled 2,6-DBEAQ electrolytes. The improved stability against disproportionation may originate from the higher redox potential of 2,6-DBEAQ (∼−0.51 V vs NHE at pH 14). A prior computational study suggests an inverse correlation between the tendency to disproportionate and the redox potential of AQ,[91] but the molecular-level mechanism is not well understood. Moreover, accelerated aging tests (75 °C) indicate slow decomposition of the uncharged form of 2,6-DBEAQ via cleavage of a γ-hydroxybutyrate group through nucleophilic substitution by HO^- and $-CO_2^-$ (Figure 4e) The decomposition products including mono-debranched 2,6-DBEAQ and γ-hydroxybutyrate were detected in ^{1}H NMR. The decomposition is more serious at pH 14 than at pH 12. On the other hand, the reduced 2,6-DBEAQ is exempt from such decomposition routes presumably due to the higher electron density in aromatic rings excluding the approaching of HO^- and $-CO_2^-$. Nevertheless, the 2,6-DBEAQ based flow cells demonstrate exceptional capacity retention. Symmetric flow cells loaded with 0.1 and 0.65 M 2,6-DBEAQ (50%SOC), respectively, at pH 14 show low capacity fade rates of <0.01%/day. The 2,6-DBEAQ/ferrocyanide full cell using 0.5 M 2,6-DBEAQ in pH 12 electrolyte shows a low capacity fade rate of 0.05%/day. The results support the high resistivity of 2,6-DBEAQ to both disproportionation and dealkoxylation side reactions at room temperature.

Substituting the terminal carboxylates in 2,6-DBEAQ with phosphates further alleviates the dealkoxylation-based decomposition.[38] The phosphates are less nucleophilic and the chemical attack to the Ar−O bonds by the estereal O^- becomes weaker. In addition, the resulting analog 2,6-DPPEAQ has an enhanced solubility (0.75 M) at pH 9, compared to the <35 mM solubility for 2,6-DBEAQ at this pH. The milder, less alkaline electrolyte additionally reduces the HO^- induced parasitic dealkoxylation reaction. As a result, 2,6-DPPEAQ based flow cells show even better capacity retention. A 2,6-DPPEAQ/ferrocyanide flow cell operated with 0.5 M 2,6-DPPEAQ and at pH 9 demonstrates an even lower fade rate of 0.014%/day.

Recently, replacement of the ether linkers in 2,6-DBEAQ with pure alkyl linkers ($-CH_2CH_2CH_2-$ or $-C(CH_3)_2CH_2-$) completely eliminates the possibility of nucleophilic HO^- or ester-O^- attacks even at pH 14.[92] The AQ/ferrocyanide flow cells using the resulting structures, namely, 3,3′-(9,10-anthraquinone-diyl)bis(3-methylbutanoic acid) (DPivOHAQ) and 4,4′-(9,10-anthraquinone-diyl)dibutanoic acid (DBAQ), yield record low capacity fade rate (0.0018%/day for the former and 0.0084%/day for the latter, Figure 4c). The low redox potentials (−0.48 V vs NHE), decent solubilities (0.74 and 1 M at pH 12), exceptional chemical stability and recoverable materials decomposition (by air exposure) work together to

https://doi.org/10.1021/acsmaterialslett.1c00668
ACS Materials Lett. 2022, 4, 277−306

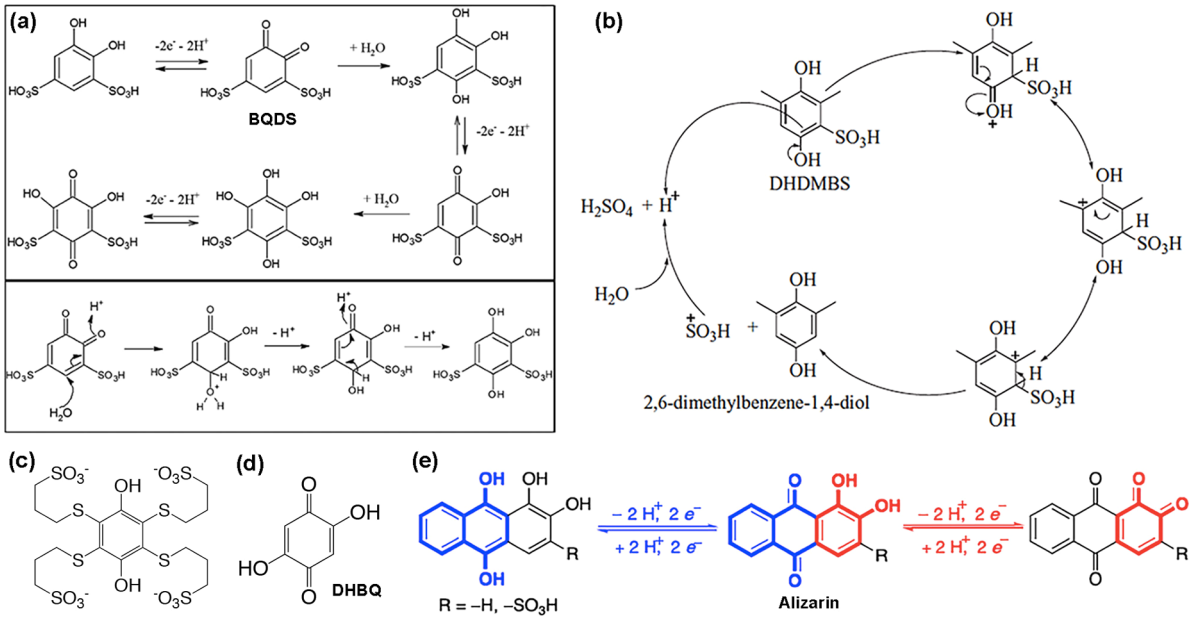

Figure 5. (a) Redox reaction and parasitic Michael addition pathway of BQDS: (Top) the pathways to side products and (bottom) the detailed Michael addition mechanism. Reprinted from ref 94 under the Creative Commons Attribution 4.0 License (CC BY 4.0, http://creativecommons.org/licenses/by/4.0/). (b) Decomposition of DHDMBS via proto-desulfonation. Reprinted from ref 96 under CC BY 4.0 (http://creativecommons.org/licenses/by/4.0/). (c) Molecular structure of benzoquinone bearing sulfonate-terminated thioether substituents.[98] (d) Structure of DHBQ.[99] (e) Ambipolar redox reaction of alizarin. Reprinted with permission from ref 101. Copyright 2019 American Chemical Society.

make DPivOHAQ and DBAQ exceeding anolyte candidates for mild-condition aqueous RFBs.

The investigations on AQ derivatives represent a progressive, steady advancement in the RFB field toward understanding degradation mechanisms and designing chemically stable redoxmers. The combined electrochemical, spectroscopic, and computational approaches should be transferred to investigating other redox structures. These extremely high cycling stability of flow cells demonstrates the great commercialization potential of AQ-based organic RFBs. Currently, the solubilities of these AQ derivatives revolve around 1 M or less, but the $2e^-$ redox reactions ensure decent energy densities in the generally used AQ/ferrocyanide RFB chemistries. Interestingly, the cation effect is found to positively impact the solubility of AQ. Liu et al. demonstrated that the use of NH_4^+ instead of alkali metal cations (e.g., Na^+) boosts the solubility of $AQDS^{2-}$ from 0.68 to 1.9 M in pH-neutral water, leading to greatly increased energy density.[44] This is presumably ascribed to the more hydrophilic NH_4^+ ions generating stronger solvation interactions with water, representing a promising electrolyte engineering strategy for technical enhancement.

3.1.2. Benzoquinone Derivatives. Compared to AQ, para- and ortho-benzoquinone (BQ) exhibit significantly higher redox potentials, making it promising for use as catholyte materials in RFBs. Narayanan et al. reported an aqueous all-quinone flow battery using AQS or AQDS anolyte and 1,2-dihydroxybenzene-3,5-disulfonic acid (BQDS) catholyte.[93,94] BQDS has a solubility of 1 M and a redox potential of 0.85 V versus NHE. However, the AQDS/BQDS flow cells demonstrate rapid capacity fade. While decomposition of AQDS may account for part of the fade, the degradation of BQDS via Michael addition of water molecules at the unsubstituted ring positions is the dominant cause (Figure 5a). NMR analysis of the cycled BQDS electrolyte detects the stepwise occurrence of the side products of trihydroxybenzene and tetrahydroxybenzene disulfonic acids.

To block the Michael addition route, Narayanan et al. designed and synthesized a new molecule, 3,6-dihydroxy-2,4 dimethylbenzenesulfonic acid (DHDMBS) with mostly occupied ring positions.[95] However, a significant capacity fade is still observed in AQDS/DHDMBS flow cells. Through NMR analysis of the cycled anolyte and catholyte solutions, the performance degradation is ascribed to two factors: through-Nafion crossover and parasitic proto-desulfonation of DHDMBS (Figure 5b).[96] Use of a mixed-reactant electrolyte (AQDS:DHDMBS 1:1) at the two sides of a symmetric flow cell, together with frequent electrolyte rebalancing, mitigates the DHDMBS crossover and derives a proto-desulfonation rate of 0.48%/day. Similarly, Stahl et al. designed and electrosynthesized a new BQ molecule that is fully substituted with sulfonate-terminated thioether groups (Figure 5c).[97,98] The thioether linker spaces the sulfonate away from the ring eliminating the possibility of proto-desulfonation. The four anionic sulfonates minimize crossover of this molecule and also afford a high solubility in acid form (1 M). These design characteristics effectively avoid the possible capacity fade mechanisms, leading to high cycling stability in flow cells coupled with AQDS. The major drawback is the too low redox potential (0.6 V vs NHE) due to the electron-donating thioether groups, which gives rise to a cell voltage of only ~0.4 V for the formed RFB chemistry. Future efforts to increase the redox potential while maintaining the current structural features should be dedicated to make it technically attractive.

Interestingly, because of the proton coupled redox reaction, BQ can be tailored for use as an anolyte material via molecular and electrolyte engineering. Aziz et al. grafted two hydroxyl groups to BQ to obtain 2,5-dihydroxy-1,4-benzoquinone (DHBQ, Figure 5d) and used it in alkaline electrolytes (pH 14), leading to a significant negative shift of the redox potential to −0.72 V versus NHE.[99] This feature, as well as the high solubility of >4 M in 1 M KOH, makes DHBQ a promising

https://doi.org/10.1021/acsmaterialslett.1c00668
ACS Materials Lett. 2022, 4, 277−306

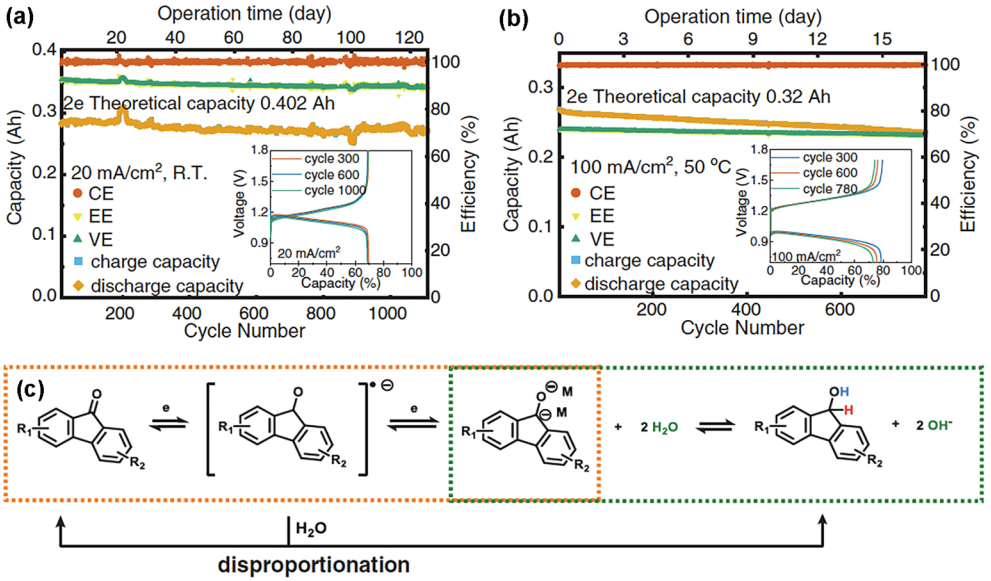

Figure 6. Performance of 4C7SFL: (a) reaction mechanism, (b) efficiencies, capacities, and voltage curves of a 4C7SFL/ferrocyanide flow cell using 1.36 M 4C7SFL and excess ferrocyanide at room temperature in a N_2-filled purge box, and (c) efficiencies, capacities, and voltage curves of a 4C7SFL/ferrocyanide flow cell using 1 M 4C7SFL at 50 °C outside a glovebox. Reprinted with permission from ref 63. Copyright 2021 American Association for the Advancement of Science.

anolyte candidate. However, the through-membrane crossover and Michael addition-based decomposition of DHBQ cause relatively fast capacity fade (0.24%/cycle). Functionalization of the unsubstituted ring position in DHBQ with bulky diphenylmethyl groups was carried out to block the Michael addition route but results in sluggish redox kinetics and poor solubility.

The drastic difference in the redox potentials of BQ and AQ is exploited to design ambipolar redox molecules. Carretero-González et al. reported that both alizarin bearing ortho-dihydroxyl and quinizarin bearing para-dihydroxyl groups show two sufficiently separated redox events and serve as both anolyte and catholyte materials in a RFB.[100] The AQ and the dihydroxybenzene parts contribute to the respective anolyte and catholyte redox activities with ~1 V cell voltages. Systematic electrolyte composition engineering results in high solubilities up to 1.6 M. However, no flow cell test results are reported in this work. Even the CV curves show complications in the redox reactions. Aziz et al. also utilized these two structures to assemble symmetric all-quinone full cells (Figure 5e).[101] A sharp capacity decay is observed after 100 cycles (55% loss) for the unfunctionalized alizarin-based cell. This decay is attributed to decomposition of oxidized alizarin via Michael addition. Similar to prior reports, structural modification with methyl groups to create dimethylquinizarin exhibits an ability to deter the Michael addition, thereby giving a boosted lifetime after 500 cycles. These efforts represent an interesting area of research to explore the full potential of quinone-based compounds in the RFB field. The previously described molecular engineering strategies can be transferred to develop more stable and soluble ambipolar quinone materials.

3.1.3. Single Carbonyl Compounds. All of the above AQ and BQ molecules are based on at least two π-conjugated carbonyl groups. Prior efforts pursuing ketone compounds with a single carbonyl, such as 9-fluorenone (FL), or multiple nonconjugated carbonyls, such as cyclohexanedione, have achieved limited success.[102,103] Normally, it is very challenging for single carbonyl compounds to undergo reversible $2e^-$ reactions in aqueous media because the benzylic deprotonation step in the electrochemical dehydrogenation (or reoxidation) of the protonated $2e^-$ product requires a much higher potential to proceed; typically a catalyst or chemical oxidant is needed to make it happen.[104]

Very recently, a significant breakthrough was made by Wang et al. by demonstrating that rationally functionalized FL molecules can fulfill a reversible hydrogenation/dehydrogenation reaction and harvest stable $2e^-$ charge storage.[63] DFT and NMR analyses were performed, suggesting that incorporation of EWGs can decrease the pK_a of the benzylic proton and potentially afford easier benzylic deprotonation. Such designed 4-carboxylic-7-sulfonate 9-fluorenone (4C7SFL) indeed demonstrates improved electrochemical reversibility, as well as solubility (up to 1.5 M) in alkaline electrolytes. With the rigid π conjugation providing high stability, an alkaline flow cell using 1.36 M 4C7SFL anolyte and excess ferrocyanide catholyte shows high efficiency and exceptional capacity retention with a low fade rate of 0.02%/day over 4 months (Figure 6a). Importantly, operation of such a flow cell at 50 °C outside a glovebox produces a high capacity retention of 87.8% over 780 cycles (16 days), as shown in Figure 6b; and the capacity decay is mainly due to 4C7SFL crossover, confirmed by NMR. Here, elimination of the need of inert atmosphere is a significant accomplishment for large-scale storage applications because of the potential simplification of operation conditions and reduction of atmosphere management cost.

Surprisingly, despite a redox control to FL/$FL^{\bullet-}$ only (one voltage plateau), the 4C7SFL-based flow cells still deliver $2e^-$ capacity. The $2e^-$ product, 4C7SFL−OH, is observed even at low SOCs. Combined NMR and electron paramagnetic resonance (EPR) studies confirm that, rather than following a direct electrochemical route, the second electron is accessed via a reversible chemical disproportionation reaction of the first redox product, $4C7SFL^{\bullet-}$ (Figure 6c). This work not only expands the redoxmer pool with an unexploited reaction mechanism but also opens an avenue to explore atypical organic molecules for the development of energy-dense aqueous RFBs.

https://doi.org/10.1021/acsmaterialslett.1c00668
ACS Materials Lett. 2022, 4, 277−306

3.1.4. Other Carbonyl Compounds. Besides quinone-based molecules, other π-conjugated carbonyl compounds have also been investigated. Carretero-González et al. demonstrated that indigo carmine (5,5′-indigodisulfonate), a natural dye based on two carbonyls conjugated through openly connected aromatic rings, can serve as an ambipolar redoxmer with sufficiently separated redox events (~0.8 V) in neutral electrolytes (Figure 7).[100] The anolyte redox activity is attributed to the carbonyls

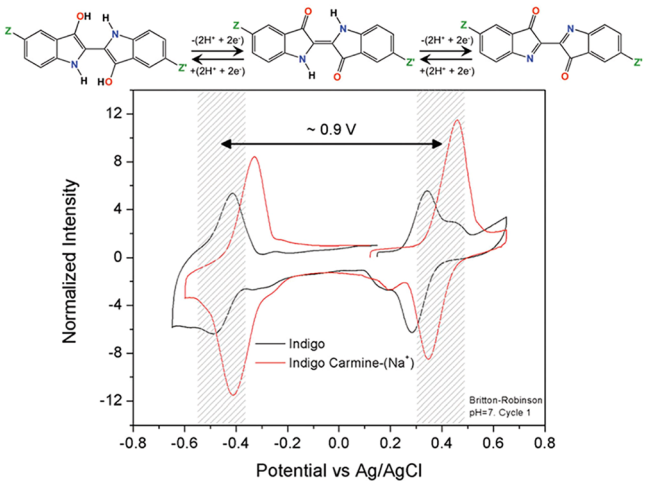

Figure 7. Ambipolar redox reactions and CV scans of indigo (black) and indigo carmine (red) in pH 7 BR buffer. Reprinted with permission from ref 100. Copyright 2016 Royal Society of Chemistry.

and the catholyte redox to the pyrrolyl N, both with $2e^-$ transfers. CV scans suggest that the use of pH 7 Britton–Robinson buffer greatly improves the electrochemical properties. However, no flow cell tests were carried out thus its RFB performance is not known. Zhu et al. used the anolyte side redox reaction of indigo carmine and paired it with bromine in acidic electrolyte to harvest a cell voltage of 0.85 V.[105] Substituting Na^+ in indigo carmine with H^+ boosts the solubility from 0.035 to 0.76 M. With excess bromine to compensate for its crossover, flow cell tests at high indigo carmine concentration (0.7 M) show relatively high capacity stability with a fade rate of 0.46%/day. But the fade mechanism is not discussed.

Naphthalene diimide (NDI) is an attractive molecular scaffold that may offer $2e^-$ reactions at its multiple carbonyl groups. The polyaromatic rings afford high chemical stability because of the extended π-conjugation, but its hydrophobic nature also presents a barrier to achieve high solubility. Ahlberg et al. introduced 3-trimethylammonium propyl groups to the amide N atoms in NDI resulting in a greatly enhanced solubility from near-zero to 0.68 M in water.[106] CV tests indicate a concerted $2e^-$ reaction at pH 0 and stepwise $2e^-$ reactions at pH 7. However, no flow cell data is provided. Byon et al. functionalized the two N atoms with glycinate groups and moderately increased the solubility of NDI to 0.17 M in water.[107] When coupled with 4-HO-TEMPO catholyte, the flow cell using pH neutral electrolytes demonstrates decent cycling stability at low redox concentrations.

3.2. N-Centered Multi-Electron Organic Molecules. *3.2.1. Phenazine Derivatives.* Phenazine is a type of redox-active $2e^-$ heterocyclic biomolecules with two imine-like nitrogen atoms (−N═) appending to the central of pyrazine core. The pristine phenazine is barely soluble in aqueous electrolyte and structural tailoring is needed to increase solubility. The earliest report of using phenazine based molecules in RFBs is from Schubert et al.[108] This team reported a $2e^-$ combi-molecule via incorporating two TEMPO catholyte moieties and a phenazine anolyte moiety linked via tri(ethylene glycol) ether spacers. A cell voltage of 1.2 V is obtained in pH 7 electrolytes. However, this molecule has a very low solubility in water and 10 vol % diglyme is added to enable the flow cell cycled at 10 mM. This flow cell maintains 80% of the original capacity after 1800 cycles. Because of the bipolar nature of its redox reactions, reversing the cell polarity yields the same capacity, indicating the chemical and electrochemical robustness of this molecule. Later, Zhu et al. utilized a phenazine-based natural dye, basic red 5 (BR5), as an anolyte and built two RFB systems including BQDS/BR5 and $Ce^{III/IV}$/BR5 in acidic electrolytes.[109] Albeit the low solubility (0.2 M in methanesulfonic acid), the $Ce^{III/IV}$/BR5 flow cell demonstrates a high cell voltage of 1.4 V and a remarkable stability with 99.9% capacity retention over 200 cycles. The BQDS/BR5 system displays a relatively fast capacity fade (26.7% over 360 cycles), mostly ascribed to the chemical instability of BQDS.

To predict feasible phenazine structures, Wang et al. carried out theoretical DFT calculations of the redox potential and solvation energy of a variety of phenazine derivatives (Figure 8a).[33] The down-selected 7,8-dihydroxyphenazine-2-sulfonic acid (DHPS) was synthesized and evaluated. An asymmetrical siting of sulfonate and phenolate groups in phenazine scaffold results in high molecular polarity boosting the solubility up to 1.8 M at pH 14. Because of the proton coupled redox reaction, the use of alkaline electrolytes, together with the electron-donating phenolates, greatly shifts the redox potential negatively to ~−0.9 V vs NHE. Consequently, a high cell voltage of 1.4 V is obtained when DHPS is coupled with ferrocyanide. A high volumetric capacity of 67 Ah/L is achieved in flow cell tests at near-saturation concentration with a capacity fade of 0.02% per cycle and 0.68% per day (Figure 8b). Temporal NMR monitoring over 21 days detects no spectral changes for DHPS in pH 14 electrolytes, indicating its high chemical stability, but the NMR peaks of the reduced DHPS become broadened. Recently, Jin et al. designed a benzene ring-fused hydroxyphenazine derivative (BHPC) using extended π-conjugation to stabilize the reduced phenazine.[110] This BHPC exhibits a solubility of 1.55 M and a redox potential of −0.78 V vs NHE at pH 14. When coupled with excess ferrocyanide, the flow cell using 0.5 M BHPC demonstrates high capacity retention with a fade rate of 0.08%/day, indicating the high stability of BHPC under flow cell conditions.

More recently, Ji et al. suggested a tautomerization-based degradation mechanism for a series of amino acid-functionalized phenazine molecules (Figure 8c).[111] Flow cell tests demonstrate that the 2,7- and 1,8-disubstituted phenazine analogs display obvious capacity fades. NMR analysis of both the cycled anolytes and the aged electrolytes of reduced phenazine determines formation of tautomerized byproducts, indicating a major degradation pathway via dearomatization of the phenyl ring by receiving protons transferred from the ring N atoms. On the contrary, for the 1,6-disubstituted phenazine, both flow cell tests and NMR analysis detect no obvious capacity and materials fade. Such a difference is in good agreement with theoretical DFT calculation of the energetics (ΔG) of side reactions and suggests the importance of functionality siting to the chemical stability of phenazine structures.

https://doi.org/10.1021/acsmaterialslett.1c00668
ACS Materials Lett. 2022, 4, 277−306

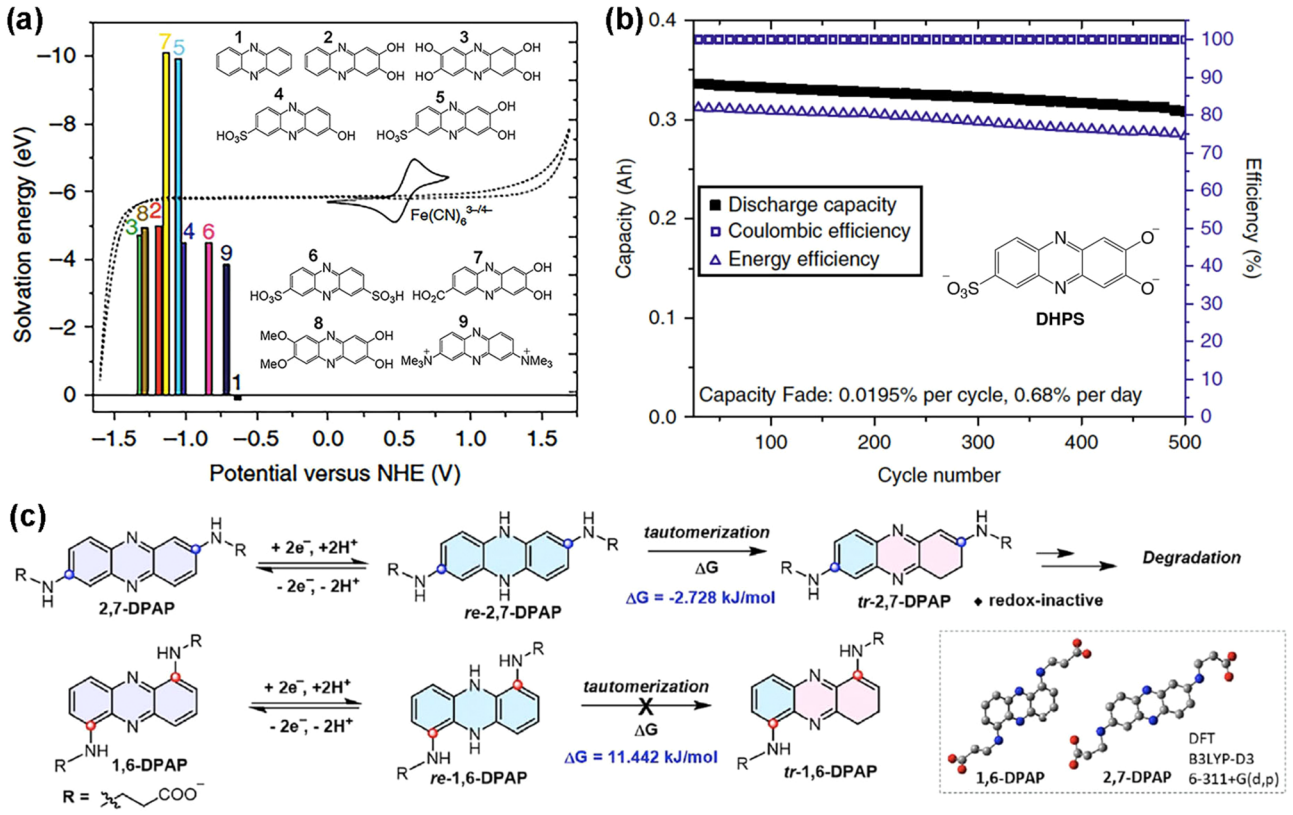

Figure 8. (a) DFT calculations of redox potentials and solvation energies of selected phenazine analogs and (b) efficiencies and discharge capacity of a DHPS/ferrocyanide flow cell using 1.4 M DHPS. Reprinted with permission from ref 33. Copyright 2018 Springer Nature. (c) Tautomerization-based decomposition of amino acid-functionalized phenazine molecules. Reprinted with permission from ref 111. Copyright 2021 Wiley.

A related molecular scaffold, quinoxaline bearing only one benzo group, has also been investigated as a highly soluble (4 M in water) anolyte material for aqueous RFBs. Brushett et al. investigated the voltammetric behaviors of quinoxaline in a variety of supporting electrolytes at different pH.[112] Quinoxaline exhibits a single-wave concerted $2e^-$ redox reaction, with improved electrochemical reversibility as the pH increases to alkalinity. At pH < 11, rapid decomposition is observed even at the CV time scale. Hjelm et al. confirmed a degradation mechanism via protonation of the N atoms followed by tautomerization resulting in loss of aromaticity and redox activity.[113] Substitution at the 2- and 3-positions (ortho to N) in quinoxaline can mitigate such a decomposition and improve chemical stability.

3.2.2. Alloxazine/Isoalloxazine. Isoalloxazine is the redox-active molecular scaffold of biologically important riboflavin (i.e., vitamin B2) or flavin mononucleotide (FMN), as shown in Figure 9a. Riboflavin and FMN are apt to undergo $2e^-$ reactions at low redox potentials (~−0.5 V vs NHE), promising to serve as anolyte materials in RFBs.[114] However, these materials are very insoluble in aqueous electrolytes. Moreover, they are not chemically stable in two aspects. First, riboflavin and FMN tend to stack with themselves and form dimeric structures. The dimers are still electrochemically reversible but can be reduced only at lower redox potentials because the dipole−dipole interactions between stacked monomers lower the energy states.[115] Such a transformation is beneficial for RFB use because of the higher cell voltages after dimer formation. Second, riboflavin and FMN can be decomposed into redox-inactive parasitic products, especially at elevated temperatures, via hydrolysis by water at the amidic carbonyl followed by ring opening (Figure 9b).[116] Although slow, this chemical reaction is irreversible and can cause gradual material loss. Therefore, suitable methods are needed to increase both chemical stability and solubility of isoalloxazine-based molecules for RFB use.

Meng et al. adopted an electrolyte engineering approach to improve the solubility and chemical stability of sodiated FMN (Na-FMN).[117] Hydrotropic nicotinamide (NA) is added to enhance the solubility of FMN-Na from 0.1 to 1.5 M at pH 14 through formation of extensive H-bonding interactions between nicotinamide and FMN. NA is electrochemically stable within the voltage range and shows no adverse effect on the redox properties of FMN. The dimerization of FMN is obvious in its alkaline solution, evidenced by the occurrences of more negative redox peaks in CV and a new higher voltage plateau (1.5 vs 1.1 V) in flow cell tests. The FMN/ferrocyanide flow cell demonstrates high capacity retention at a fade rate of 0.01%/cycle or 0.3%/day (Figure 9c). The slow fade is thought to be a consequence of the irreversible hydrolytic decomposition.

Approximately at the same time, Aziz et al. developed an alloxazine analog decorated with a carboxylic acid group (shortly, ACA, Figure 9d) that boosts the solubility to 2 M at pH 14.[118] On the basis temporal NMR observation, such a structural modification improves the chemical stability of alloxazine, albeit still with slow degradation (solution half-life time of 500 days). The ACA/ferrocyanide flow cell demonstrates a cell voltage of 1.2 V and relatively stable capacity with a decay rate of 0.013% per cycle or ~1% per day (Figure 9e). The dimerization of ACA is not detected as only one voltage plateau is observed in flow cell tests. The low pK_a of the amidic −NH−

https://doi.org/10.1021/acsmaterialslett.1c00668
ACS Materials Lett. 2022, 4, 277−306

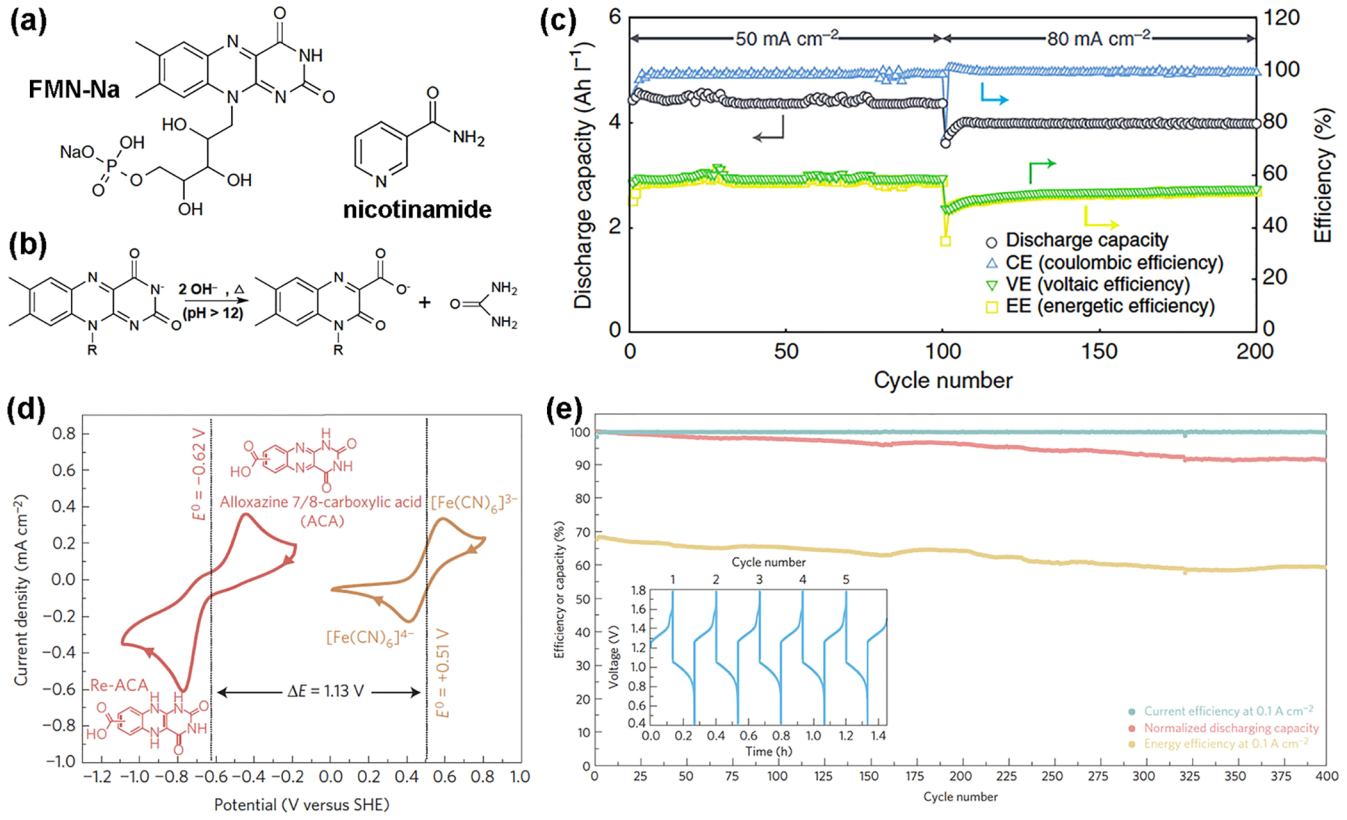

Figure 9. (a) Chemical structures of Na-FMN and hydrotropic nicotinamide (NA), (b) decomposition of alloxazine via hydrolytic ring opening reaction, and (c) efficiencies and discharge capacity of a Na-FMN/ferrocyanide flow cell using 0.24 M Na-FMN. Reprinted from ref 117 under CC BY 4.0 (http://creativecommons.org/licenses/by/4.0/). (d) CV curves of ACA in pH 14 electrolyte and (d) efficiencies and discharge capacity of an ACA/ferrocyanide flow cell using 0.5 M ACA. Reprinted with permission from ref 118. Copyright 2016 Springer Nature.

(~8.4 and ~11.4) results in complete deprotonation at pH 14 and consequent accumulation of negative charges, which repulses the approaching of HO^- and thus slows down the hydrolytic decomposition. But the non-negligible capacity loss still indicates a considerable loss of ACA. The chemical stability of reduced ACA is not investigated by NMR.

3.2.3. Dialkylated Viologen. Dialkylated viologens (4,4′-bipyridine) represent a family of quaternary pyridinium salts derived from 4,4′-bipyridine. Viologen-based materials such as methyl viologen (MV^{2+}) have attracted intensive interest for RFB anolyte uses, because of the unique properties such as high aqueous solubility, good chemical stability, excellent electrochemical reversibility, and accessible redox potential in neutral electrolytes.[119,120] In fact, MV^{2+} is capable of stepwise $2e^-$ reactions to form a radical cation ($MV^{+\cdot}$) in the first step and a neutral species (MV^0) in the second step, but the second redox is not usable because of the near-zero solubility of MV^0, which manifest as a deposition/stripping behavior in CV scan (Figure 10a, black line).[121] Liu et al. successfully achieved feasible designer $2e^-$ reactions for viologen through replacing the two methyls with two tetraalkylammonium end-functionalized propyls (namely, $(NPr)_2V$) to increase the solubility of the second redox product.[122] Such a structural modification largely alters the voltammetric behavior (Figure 10a, red line). This molecule was initially developed to sterically block the dimerization reaction of the $1e^-$ product,[123] but the ability to facilitate the $2e^-$ reaction is a significant bonus. The two redox events of $(NPr)_2V$ (Figure 10b) occur at −0.39 V and −0.78 V versus NHE, leading to 1.0 and 1.38 V cell voltages when FcNCl is used as the catholyte material. With the $2e^-$ operation, the $(NPr)_2V$/FcNCl flow cell at moderate concentrations (0.5 M electrons) demonstrates high capacity retention with a low fade rate of 0.01%/cycle (Figure 10c). Li et al. adopted a similar strategy by incorporating hydrophilic N-substituted hydroxyethyl groups to enable soluble $2e^-$ product.[124] The new viologen analog $(2HO\text{-}V)Br_2$ and its $2e^-$ reduced species have solubilities of 2.2 and 2.1 M, respectively, in water. Moreover, $(2HO\text{-}V)Br_2$ establishes itself as an ambipolar redoxmer with the viologen moiety responsible for the anolyte reaction and the Br^- for the catholyte reaction, which promises a minimal electrolyte cross-contamination and enables the use of cost-effective porous separators. The cell voltages of $1e^-$ and $2e^-$ redox reactions are 1.49 and 1.89 V, leading to a high theoretical energy density of 95 Wh/L. The symmetric flow cell at 0.1 M $(2HO\text{-}V)Br_2$ demonstrates an excellent capacity retention and almost no capacity fade was observed.

The low redox potential of the second redox of $(NPr)_2V$ raises a concern of hydrogen evolution. Liu et al. continued to introduce a thiazolo[5,4-*d*]thiazole (TTz) unit in between the two pyridinium rings to obtain a π-conjugation extended $(NPr)_2V$.[125] Such a TTz framework shifts the second redox activity of $(NPr)_2V$ from −0.78 to −0.44 V versus NHE, which can reduce the risk of water electrolysis. This is presumably because the electron-deficient TTz moiety increases the energy states. The π-conjugation also enhances the chemical stability of both $1e^-$ and $2e^-$ products without sacrificing the aqueous solubility (1.3 M). The flow cell using this viologen analog and a high-potential 4-trimethylammonium-TEMPO catholyte delivers an average cell voltage of 1.44 V and a theoretical energy density of 53.7 Wh/L.

https://doi.org/10.1021/acsmaterialslett.1c00668
ACS Materials Lett. 2022, 4, 277−306

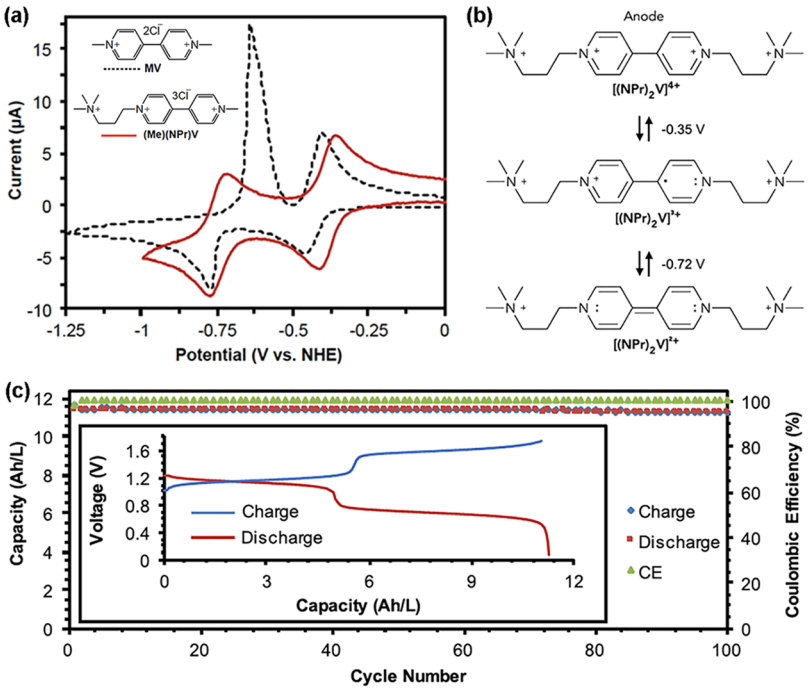

Figure 10. (a) Different CV characteristics of MV^{2+} and NPr-functionalized viologen; (b) stepwise electrochemical reactions of $(NPr)_2V$; and (c) CE, capacities, and voltage curves (inset) of a $(NPr)_2V$/FcNCl flow cell at 0.5 M electrons. Reprinted with permission from ref 122. Copyright 2017 Cell Press.

3.2.4. Phenothiazine. Phenothiazine (PT) is a redox-active tricyclic heteromolecule with a piperidyl−NH− and a thianyl−S− located at the para sites of the central ring. Compared to phenazine, the electron-withdrawing nature of S positively shifts the redox potential making PT a catholyte candidate. Because of the different electronic configurations of S and N, the central ring in PT is bent leading to an interrupted aromaticity throughout the molecule. Its $2e^-$ oxidized form, phenothiazinium (PT^{2+}), is an aromatic structure bearing a positive charge at the sulfonium moiety ($-S^+=$). However, such a structural feature brings a serious drawback of chemical instability in aqueous electrolytes. The sulfonium cation can undergo a hydrolysis side reaction via nucleophilic water addition followed by deprotonation, leading to oxidative formation of sulfoxide (S=O), as illustrated in Figure 11a.[126] This side reaction becomes more serious at high pH values. Even the $1e^-$ product (a radical cation, $PT^{\bullet+}$) is subject to a disproportionation reaction resulting in formation of the sulfoxide.[127] This is the case for the other analogue structure, thianthrene (the −NH− in phenothiazine replaced by −S−). Thianthrene has an even higher redox potential but has not been explored for RFB use because of the extreme water sensitivity of its charged species.[128,129] Therefore, deliberate structural or electrolyte engineering is necessary to stabilize the sulfonium and make them useful in aqueous RFBs.

Methylene blue (MB), a bioactive derivative of PT^{2+}, is commercially available and widely used in medical treatments, indicating its excellent chemical stability. The high stability originates likely from the charge resonance between the aromatic rings and the two dimethylamino substituents leading to delocalized charge density (Figure 11b). This suggests that MB can be a good candidate as RFB catholyte, but the low solubility in water (~0.13 M) is a barrier. Yu et al. demonstrated that the properties of MB are highly dependent on electrolyte composition and then carried out electrolyte engineering for property enhancement.[130] First is the redox property. Because of the proton-coupled redox reactions of MB, the addition of H_2SO_4 to MB solution positively shifts its redox potential (compared to 0 V vs NHE at neutral pH), converts the stepwise $2e^-$ redox to concerted, improves its electrochemical reversibility, and also increases its redox kinetics (Figure 11c). At 3 M H_2SO_4, MB has a redox potential of 0.57 V vs NHE, a redox peak current ratio of 1.02 and a kinetic rate constant of 0.32 cm/s. Second is the solubility. The presence of concentrated acetic acid (e.g., 3 M) results in an enhanced solubility of 1.8 M without compromising its chemical stability. This is ascribed to the strong acetic acid−MB H-bonding interactions breaking the lattice energy of solid MB. The electrolyte engineering renders MB with favorable catholyte properties. Excellent capacity retention is demonstrated in the symmetric MB flow cells and the vanadium ($V^{2+/3+}$)−MB flow cells both using concentrated MB (1 M or above), as shown in Figure 11d. The excellent performance reflects the high promise of MB as a catholyte candidate for aqueous RFBs.

3.2.5. Azobenzene. Azobenzene is composed of two phenyl rings bridged with a redox-active azo group (−N=N−) that undergoes reversible $2e^-$ redox activity converting between the azo and hydrazine forms. Yu et al. reported an azobenzene derivative, 4-amino-1,1′-azobenzene-3,4′-disulfonic acid monosodium salt (AADA), bearing asymmetrically sited hydrophilic groups to increase molecular polarity and aqueous solubility.[48] The solubility is enhanced from 0.12 to 2 M in 2 M NaOH when hydrotropic urea is added. The flow cells using AADS anolyte and ferrocyanide catholyte achieve a cell voltage of ~1 V and high efficiencies (98.8% CE and 87.6% EE at 10 mA/cm^2) but suffer from non-negligible capacity fading. The fading was ascribed to the possible air exposure during battery tests. The minimal NMR spectral change in the electrolytes after the first and fifth cycles suggest the molecular stability, although a stability study over longer periods of time is more affirmative.

https://doi.org/10.1021/acsmaterialslett.1c00668
ACS Materials Lett. 2022, 4, 277−306

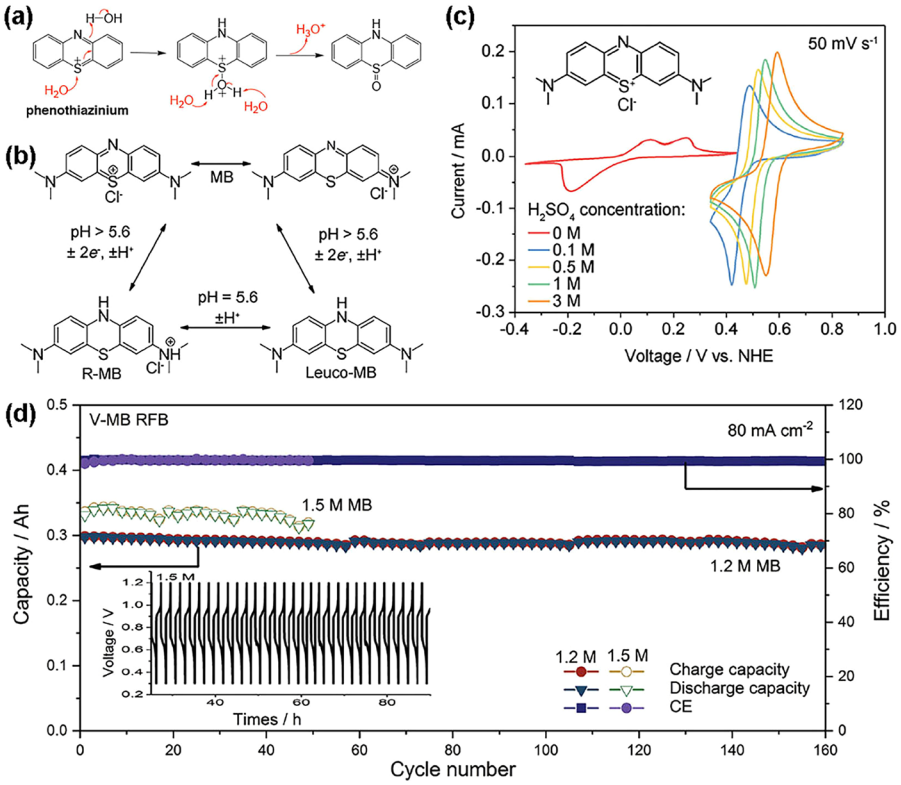

Figure 11. (a) Hydrolytic decomposition of phenothiazinium; (b) redox reactions of MB; (c) CV curves of MB at different H_2SO_4 concentrations; and (d) CE, capacities, and voltage curves of vanadium−MB flow cells at 1.2 and 1.5 M MB, respectively. Reprinted with permission from ref 130. Copyright 2019 Wiley.

Nevertheless, azobenzene-based molecules have the redox center in an open structure (in other words, not on an aromatic ring) but possess high electrochemical reversibility and chemical stability; such molecules have rarely been explored for RFB uses. In this sense, this study represents a unique approach in expanding the material pool and may inspire more research efforts.

4. MULTIELECTRON ORGANIC MOLECULES IN NONAQUEOUS RFBS

Nonaqueous RFBs have been extensively pursued exploiting the wider electrochemical windows to harvest higher cell voltages and utilize more redox candidates. Typical nonaqueous electrolytes contain lithium or tetraalkylammonium salts dissolved in organic solvents, such as carbonates, ethers, nitriles, etc. A number of organic molecules intrinsically have high solubilities in organic solvents, even without incorporation of solubilizing substituents, because of the similar molecular polarities. Interestingly, a number of $2e^-$ organic molecules that exhibit concerted redox behaviors in aqueous electrolytes demonstrate stepwise redox events in nonaqueous electrolytes; such examples include anthraquinone,[131] phenazine,[132] etc. The mechanisms are not well understood but may be related with the different modulations of their frontier energies by water and organic molecules. Compared to aqueous counterparts, the multiple choices of organic solvents and supporting salts may bring additional opportunities for property improvement. However, the chemical compatibility between organic solvents and organic redoxmers especially in the electrochemically charged states remains a concern because the multi-atom, multi-bond structures of both may result in a possibility of parasitic protonation and nucleophilic substitution/addition reactions.

Chemical compatibility between organic solvents and organic redoxmers especially in the electrochemically charged states remains a concern because the multiatom, multibond structures of both may result in a possibility of parasitic protonation and nucleophilic substitution/addition reactions.

One of the lethal limitations for nonaqueous RFBs is the lack of selective membranes. The crossover-induced redoxmer contamination has made reliable evaluations of redoxmers in flow cells highly challenging. To decrease cross-interference, the following methods have been adopted to investigate redoxmers in nonaqueous flow cells: (i) hybrid half-cell RFBs based on Li metal anode and interested catholyte redoxmer;[40] (ii) use of the same mixed-reactant electrolytes at both sides containing an equimolar mixture of anolyte and catholyte materials;[13] and (iii) symmetric flow cells using a mixture of uncharged and charged redoxmer at 50% state of charge (SOC).[41] Celgard or Daramic porous separators are used in these flow cells, but the large pore size (about several tens of nanometers) yields low selectivity. Limited success has been achieved in high concentration flow cell tests, which greatly weakens the reliability of redoxmer assessments in near-practical flow cell environments. Therefore,

https://doi.org/10.1021/acsmaterialslett.1c00668
ACS Materials Lett. 2022, 4, 277−306

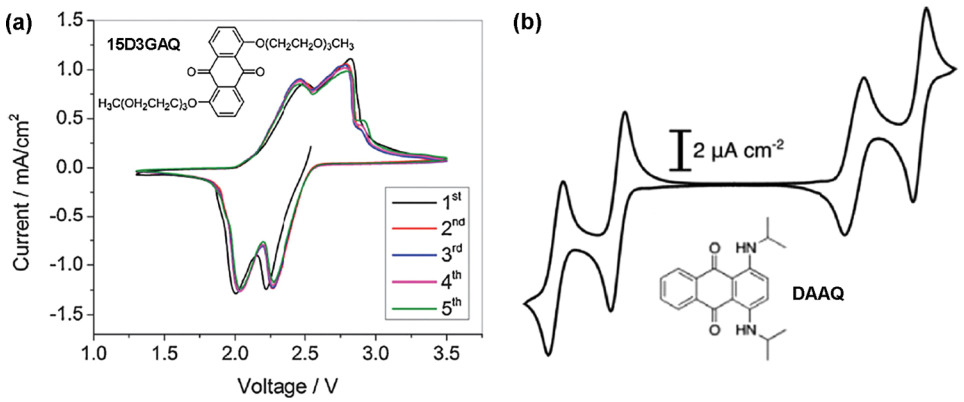

Figure 12. (a) CV scans of 15D3GAQ vs Li/Li^+ in $LiPF_6$/PC. Adapted with permission from ref 131. Copyright 2012 Royal Society of Chemistry. (b) Ambipolar redox activities of DAAQ. Adapted from ref 134 under the Creative Commons Attribution Non-Commercial No Derivatives 4.0 License (CC BY-NC-ND 4.0, http://creativecommons.org/licenses/by-nc-nd/4.0/).

we will summarize multiredox organic compounds reported in nonaqueous RFBs with more emphasis on property-controlling structural factors than on cell-level performance.

4.1. Carbonyl-Centered Multielectron Organic Molecules. *4.1.1. Anthraquinone Derivatives.* The anthraquinone (AQ) core contains symmetrically distributed C═O bonds and has almost no solubility in common RFB solvents. Wang et al. functionalized AQ with two $(EG)_3OMe$ groups at 1- and 5-positions to empower a new derivative (15D3GAQ) with improved solubility (>0.25 M) in carbonate electrolyte (Figure 12a).[131] This molecule exhibits stepwise $2e^-$ redox reactions to form a radical anion ($AQ^{\bullet -}$) at 2.53 V and then a dianion (AQ^{2-}) at 2.25 V vs Li/Li^+. A static Li/15D3GAQ hybrid RFB is used to electrochemically test 15D3GAQ at 0.25 M, yielding two plateaus in its voltage curve, as well as an energy density of 25 Wh/L yet with continuously decaying energy efficiency (EE).

Later, Zhang et al. synthesized several 2-methoxyethoxy ether functionalized AQ derivatives and evaluated their $2e^-$ properties in a supporting electrolyte of tetraethylammonium tetrafluoroborate ($TEABF_4$) in acetonitrile (MeCN) when paired with a $2e^-$ PT catholyte.[133] Interestingly, the analog having ether groups at 1,4-positions (AQ4) has a much higher solubility than the other derivatives (0.47 M vs <0.1 M), indicating the importance of substituent siting for solubility tailoring. AQ4 demonstrates two redox pairs at −1.33 ($AQ^{\bullet -}$) and −1.89 V (AQ^{2-}) vs Ag/Ag^+ and two voltage plateaus in bulk electrolysis (BE) tests, establishing robust evidence of $2e^-$ redox activity. However, the AQ4/PT flow cell quickly loses the $2e^-$ activity accompanied by rapid capacity fading. Interference from catholyte redoxmer crossover due to the porous separator used in the flow cell test is thought to be the main cause for the fading. In temporal UV−vis monitoring, the charged AQ4 electrolytes also exhibit quick peak intensity changes within 2 h. The results indicate the inferior chemical stability of $AQ4^{2-}$ in the $TEABF_4$/MeCN electrolyte.

In reality, AQ is quite picky toward the solvent and salt used. The charged AQ^{2-} dianion is highly nucleophilic bearing high electron density at the carbonyl O. Thus, it tends to chemically attack the electron-deficient C═O, C≡N, α-H, and BF_4^- groups in the solvent and salt. These side reactions may account for the performance fading in the above cell tests. Inspired by the study of solvent effects in related $1e^-$ carbonyl molecules, that is, 9-fluorenone[42] and *N*-methylphthalimide,[58] ether solvents, such as 1,2-dimethoxyethane (DME or glyme), may be a more suitable solvent for AQ redoxmers as they contains no electron-deficient groups.

Interestingly, Abruña et al. and Binnemans et al. developed symmetric nonaqueous RFBs using functionalized diaminoanthaquinone (DAAQ) molecules as ambipolar redoxmers (Figure 12b).[134,135] DAAQ exhibits 4 oxidation states; the two at −1.53 and −1.96 V vs Ag/Ag^+ are from the AQ moiety and are used as the anolyte redox. Introduction of aligo-ethylene glycol ether groups to the amine units affords high solubilities up to 1 M. However, despite the high theoretical energy density (122 Wh/L), the symmetric flow cell tests at 0.1 M yields rapid capacity fading in both MeCN and DME solvents, indicating the limited chemical stability. An understanding of the degradation mechanisms and corresponding structural modification is needed to overcome this drawback. In addition, the more serious fading in MeCN than in DME confirms our argument regarding the solvent-induced material decomposition.

4.1.2. Benzoquinone Derivatives. Benzoquinone (BQ)-based organic molecules have also been investigated for nonaqueous RFB applications. Yu et al. used a combined experimental and computational approach to systematically study a series of quinone-based $2e^-$ molecules including 1,4-BQ, 1,4-naphthoquinone (NQ), 9,10-phenanthrenequinone (PQ), AQ, and 5,12-naphthacenequinone (NAQ).[136] The frontier energies and Li^+ binding energies of these molecules are calculated using DFT to reveal the feasibility of redox reactions of these molecules. Among them, BQ has the highest redox potentials with two redox pairs at 2.75 and 2.80 V vs Li/Li^+ in a supporting electrolyte of LiTFSI in N,N-dimethylacetamide (DMA), but NQ results in the most stable capacity profiles in hybrid Li/NQ flow cells at both 0.1 and 1 M NQ. A major limitation for pristine BQ is the limited solubility in RFB solvents. Thus, incorporation of ether substituents to increase solubility is recommended in this report.

Electrolyte engineering can be another effective method to increase the solubility of BQ. Siroma et al. reported the use of soluble BQ in a nonflow lithium secondary battery.[137] Despite a different battery type, the reported high solubility (2.6 M) of unfunctionalized BQ in γ-butyrolactone solvent may inspire the use of solvent tailoring as an approach to increase solubility. However, the fast capacity fading in static Li/BQ cells suggests that such electrolyte engineering efforts should combine both solubility and stability requirements to harvest simultaneous property improvement.

https://doi.org/10.1021/acsmaterialslett.1c00668
ACS Materials Lett. 2022, 4, 277−306

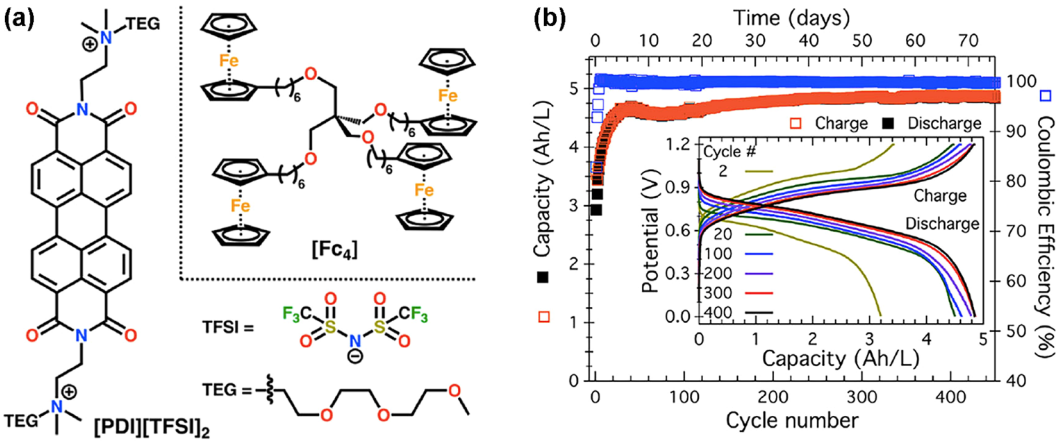

Figure 13. (a) Chemical structures of $[PDI][TFSI]_2$ and Fc_4. (b) CE, capacities, and voltage curves of a nonflow $[PDI][TFSI]_2/Fc_4$ cell at 0.4 M electron concentrations. Reprinted with permission from ref 138. Copyright 2017 American Chemical Society.

4.1.3. Perylene Diimide (PDI) Derivatives. The highly π-conjugated PDI core is promising to offer high chemical stability via electron delocalization but brings a drawback of low solubility in RFB solvents. Tailoring the molecular structure to increase solubility is often the central effort in applying PDI for nonaqueous RFBs. Sisto et al. introduced two cationic tetraalkylammonium groups each bearing an $(EG)_3OMe$ chain, coupled with $TFSI^-$ anions, as the solubilizing functionalities to increase the solubility to >0.5 M in MeCN (Figure 13a).[138] The new derivative ($[PDI][TFSI]_2$) has $2e^-$ redox activities forming $PDI^{\bullet-}$ and PDI^{2-} successively in supporting $LiPF_6$/MeCN electrolyte with almost overlapped redox peaks at −0.7 V vs Ag/Ag^+, leading to a cell voltage of 0.85 V when it is paired with a tetrameric ferrocene (Fc_4) catholyte. As expected, the static $[PDI][TFSI]_2/Fc_4$ cell using a dialysis separator at 0.4 M equivalent electron concentrations demonstrates an average CE of 99.955% and a decay-free capacity profile over 500 cycles (72 days) at 81% SOC (Figure 13b). Although no tests under flow cell conditions were reported, the static cell result still indicates the high chemical stability of both redoxmers.

Lin et al. functionalized the PDI scaffold with a redox-active phenoxyl radical moiety to enable redox activities up to $4e^-$ and also with 2,6-di-*tert*-butyl phenyl groups at the imide positions to enhance the solubility in 1:1 DME/DOL.[139] The two obtained derivatives are evaluated in static Li/PDI cells at 30 mM concentrations that demonstrate multiple voltage plateaus with slow capacity decays. The degradation mechanisms are not well understood, but, considering the high stability of PDI species, are thought to be associated with the phenoxyl radical.

4.2. N-Centered Multi-Electron Organic Molecules. *4.2.1. Quinoxaline.* The use of quinoxaline was among the earliest attempts to apply organic redoxmers in nonaqueous RFBs. Brushett et al. investigated the properties of quinoxaline as an anolyte material paired with 2,5-di-*tert*-butyl-1,4-bis(2-methoxyethoxy)benzene (DBBB) catholyte in an all-organic nonaqueous RFB.[140] Quinoxaline is extremely soluble in propylene carbonate (~7 M), plus the $2e^-$ redox reaction, making itself an attractive candidate; but the second redox event suffers from inferior reversibility. Among a series of molecular analogs, 2,3,6-trimethylquinoxaline (TMQ) exhibits improved electrochemical reversibility and low redox potentials (2.48 and 2.80 V vs Li/Li^+), as shown in Figure 14a. The 0.05 M TMQ/DBBB nonflow cell using Nafion 117 membrane under nonoptimized conditions demonstrates low CE (~70%) and VE (~50%), as well as low material utilization.

Brushett et al. also observed that addition of a Lewis acid BF_3 to the quinoxaline electrolyte not only greatly boosts its redox currents but also generates new redox peaks.[141] Quantum chemical calculation indicates that the electron deficient BF_3 strongly binds to the N atoms on quinoxaline, which increases its electron affinity and accounts for the varied redox behavior. On the basis of this understanding, a quinoxaline-(bis)-trifluoroborane adduct ($(BF_3)_2$•Q) is synthesized and electrochemically evaluated. Compared to bare quinoxaline, the CV curves of $(BF_3)_2$•Q show redox pairs with an order of magnitude increase in redox currents (Figure 14b) and the bulk electrolysis tests demonstrate 26-fold enhancement of charge capacity.

4.2.2. Phenazine. Motivated by the stable performance of phenazine in aqueous RFBs, researchers have explored its use in nonaqueous RFBs. Kang et al. reported that 5,10-dihydro-5,10-dimethyl phenazine (DMPZ) demonstrates two reversible redox events in a stepwise mode forming $DMPZ^{\bullet+}$ then $DMPZ^{2+}$ in MeCN solvent (Figure 14c).[132] DMPZ is actually the reduced form of phenazine. Interestingly, the two redox pairs are largely spaced at −0.15 and 0.61 V versus Ag/Ag^+, which may inspire the use of N,N′-disubstituted phenazine as ambipolar redox molecules in aqueous RFBs. DMPZ is paired with 9-fluorenone (FL) anolyte to harvest cell voltages of 1.24 and 2 V, respectively, for its two redox activities. Using a Celgard separator and mixed-reactant electrolytes with a stoichiometry of DMPZ: FL 1: 2, the DMPZ/FL flow cell demonstrates two voltage plateaus, an average CE of 90%, and an average EE of 70%. Remarkably, the stable capacity for 30 cycles (~25 h) suggests the chemical stability of $DMPZ^{\bullet+}$ and $DMPZ^{2+}$, although a longer cycling test is necessary to fully prove the durability. Despite the encouraging performance, the major drawback of DMPZ is its extremely low solubility (0.06 M) that is unable to make a practically interesting storage system.

To address this limitation, Kang et al. continued to modify the DMPZ structure by replacing the two methyls with 2-methoxyethyl groups.[142] The obtained BMEPZ has a boosted solubility of 0.5 M in MeCN, showing the importance of solubilizing substituents. BMEPZ exhibits similar $2e^-$ redox properties to DMPZ. DFT calculation indicates that the charged species, that is, $BMEPZ^{\bullet+}$ and $BMEPZ^{2+}$, are in near-planar geometries, leading to charge delocalization and thus the observed chemical stability. The DMPZ/FL flow cells at 0.1, 0.2,

https://doi.org/10.1021/acsmaterialslett.1c00668
ACS Materials Lett. 2022, 4, 277−306

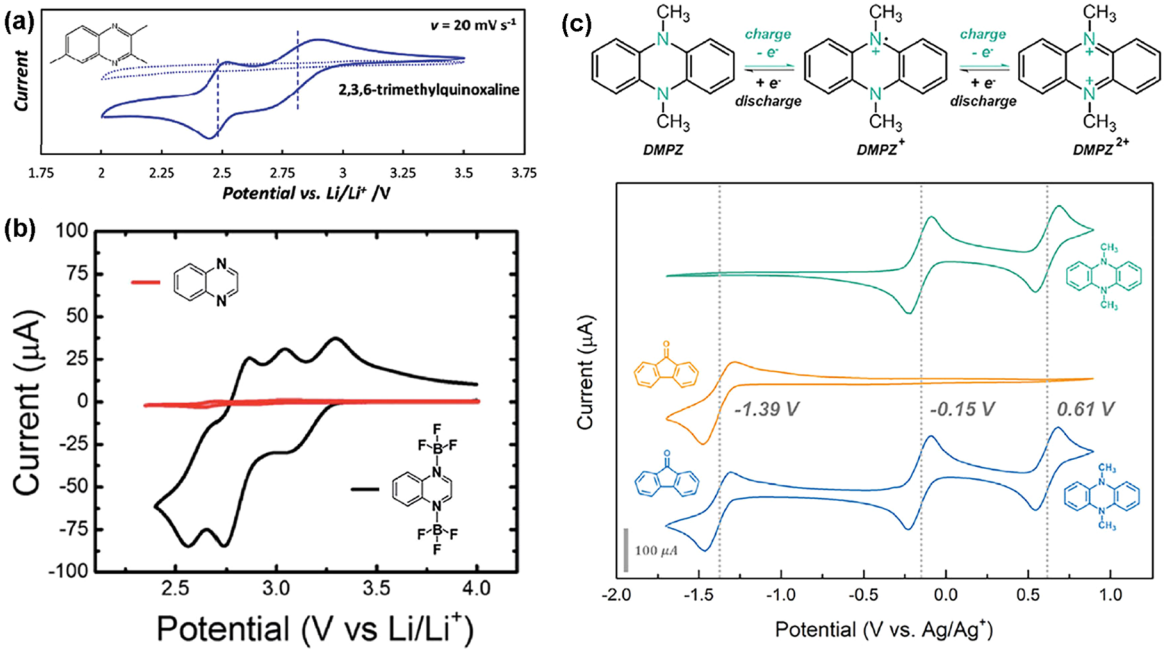

Figure 14. (a) CV scan of TMQ. Adapted with permission from ref 140. Copyright 2012 Wiley. (b) CV scans of quinoxaline (Q) and $(BF_3)_2$·Q adduct. Adapted from ref 141 under the Creative Commons Attribution 3.0 Unported License (CC BY 3.0, http://creativecommons.org/licenses/by/3.0/). (c) Two-step redox reactions and CV scans of DMPZ and FL. Adapted with permission from ref 132. Copyright 2018 Cell Press.

and 0.4 M equivalent electron concentrations all demonstrate relatively stable capacity profiles, validating the high stability of phenazine molecules under nonaqueous RFB conditions.

Despite the high stability, the drawbacks of these phenazine molecules include the limited solubilities and low redox potentials as catholyte candidates. In a recent report, an anolyte phenazine molecule bearing two $(EG)_2OMe$ substituents on the benzo ring exhibits a high solubility of 2.5 M and a low redox potential of −1.72 V vs Ag/Ag^+ in MeCN.[143] Although only the first redox activity is used for the nonaqueous RFB, the modification of solubility and redox potential offers insights on structural functionalization to afford favorable $2e^-$ properties. Computational studies can provide theoretical aspects on accelerated identification of molecular design strategies. Marvrandonakis et al. applied a HT-DFT calculation to explore the redox potentials of 200 phenazine derivatives in nonaqueous media.[72] By systematically investigating the effects of the nature, number and positioning of EDGs and EWGs, the redox potential is demonstrated to be tailorable between −0.65~2.25 V compared to the parent phenazine. The chemical stability of selected analogs is also estimated based on the reorganization energy and geometric distortion upon reduction. This study can provide theoretical structure−property insights for designing favorable phenazine structures.

4.2.3. Phenothiazine (PT). Phenothiazine (PT) can perform stepwise $2e^-$ redox reactions via successive formation of $PT^{\bullet+}$ then PT^{2+} in nonaqueous electrolytes. Zhang et al. investigated a series of PT derivatives as catholyte materials paired with AQ anolyte in $TEABF_4$/MeCN electrolyte.[133] The PT analog with two electron-withdrawing −Cl substituents at the locations para to N (i.e., 3- and 7-positions) on the conjugated rings has the highest redox potentials (0.54 and 1.12 V vs Ag/Ag^+), but the one (PT3) bearing electron-donating methyl groups at the same positions has the highest solubility of 0.43 M in MeCN. Although the AQ/PT3 flow cell encounters a capacity fading, the temporal UV−vis analysis indicates near-zero spectral changes over 2 h for the $2e^-$ oxidized $PT3^{2+}$ electrolyte, suggesting good chemical stability of the $PT3^{2+}$ species.

Odom et al. demonstrated that the $PT^{\bullet+}$ radical cation is stable in a variety of nonaqueous electrolytes, but the PT^{2+} dication is subject to decomposition with parasitic reactions often occurring at 3- and 7-positions.[41] This agrees with the good stability of the above $PT3^{2+}$ that has two methyl groups at the 3- and 7-positions blocking the parasitic reaction pathway. Later, they found that PT with strong EDG substituents such as methoxy groups (−OMe) at 3- and 7-positions (denoted as DMeOEPT) can enhance the chemical stability of PT^{2+} (Figure 15).[144] This effect is presumably attributed to the conjugation of the electron lone pairs on the ethereal O atoms to the aromatic rings leading to decreased charge density and stabilized dication state. Despite the decreased redox potential compared to the parent PT, accessibility of reversible $2e^-$ activity leads to a higher average redox potential and charge storage capacity. The major drawback of DMeOEPT is the very low solubilities in all three oxidation states (≤0.15 M).

To overcome this limitation, Odom et al. continued to introduce longer $(EG)_2OMe$ groups at the 3- and 7-positions of PT (abbreviated as B(MEEO)EPT).[145] Such a structural modification enhances the solubilities of all three oxidation states to >0.5 M. Interestingly, the radical cation and dication states of B(MEEO)EPT are prepared in purified solid forms via chemical oxidation by nitrosonium tetrafluoroborate ($NOBF_4$). Such chemical synthesis greatly facilitates property characterizations in all of the three oxidation states. A symmetric flow cell loaded with the same 0.3 M $B(MEEO)EPT^{\bullet+}$ electrolytes at both sides demonstrates a 27% capacity fade over 140 galvanic cycles (~460 h). Post-mortem CV and UV−vis analysis indicate that the fade is due to unbalanced redoxmer crossover through the nonselective separator rather than redoxmer decomposition.

https://doi.org/10.1021/acsmaterialslett.1c00668
ACS Materials Lett. 2022, 4, 277−306

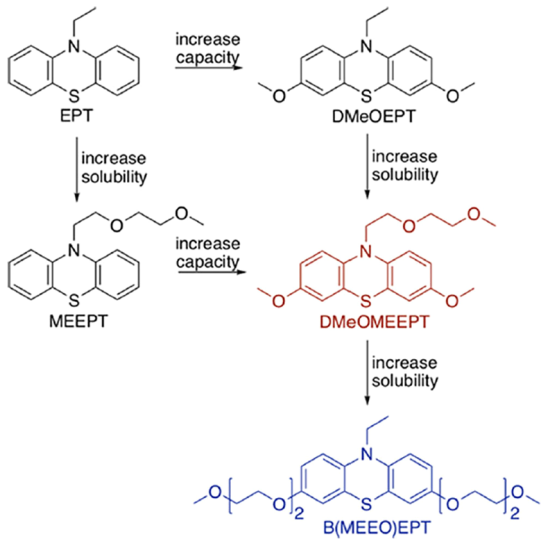

Figure 15. Evolutionary design of soluble, stable 2e⁻ PT molecules. Reprinted with permission from ref 145. Copyright 2019 American Chemical Society.

These studies represent an important example of multiproperty tuning of 2e⁻ redox molecules for increased charge storage.

4.2.4. Dialkylated Viologen. Dialkylated viologens are benchmark anolyte molecules frequently used in aqueous RFBs.[36,120] For MV^{2+}, access to the second electron is challenging because of the near-zero solubility of its 2e⁻ product (MV^0). But this is not the case in nonaqueous RFBs. Liu et al. demonstrated that methyl viologen bis(trifluoromethane)-sulfonamide (MVTFSI) achieves two reversible reduction reactions at −0.79 and −1.20 V vs Fc/Fc^+ in a nonaqueous LiTFSI/MeCN electrolyte.[146] Replacement of the Cl^- counterions in MV^{2+} with $TFSI^-$ boosts the solubility to 0.98 M in MeCN. MVTFSI is paired with (ferrocenylmethyl)-trimethylammonium bistrifluoromethanesulfonylimide (**FcNTFSI**) catholyte to achieve cell voltages of 1.06 and 1.47 V for the two redox steps. Using a Daramic porous separator, the **MVTFS/FcNTFSI** flow cell loaded with mixed-reactant electrolytes (MV: Fc 0.1: 0.2 M) displays an average CE of 95%, an average EE of 68%, and a capacity retention of 88% over 100 cycles at 40 mA/cm^2.

To mitigate the redoxmer crossover, Jiang et al. functionalized 4,4′-bipyridine with two $(EG)_{12}OMe$ groups at the two pyridyl N atoms to afford an oily viologen (PEG12-V) that is readily miscible with MeCN.[147] PEG12-V is electrochemically reversible in its two redox activities at −0.82 and −1.24 V vs Fc/Fc^+. The bulky size of PEG12-V can decrease its crossover through a house-prepared composite nanoporous aramid nanofiber (CANF) separator, evidenced by its an order of magnitude lower permeability than that of MV. As expected, the PEG12-V/Fc flow cell with excess Fc demonstrates a higher average CE (99.3%) and capacity retention (66% after 500 cycles or 185 h) than MV/Fc flow cell (98% CE, 22% after 205 cycles or 38.4 h). The capacity fade is ascribed mainly to the crossover of Fc due to its small size. Later, the same team demonstrated that replacing the Fc catholyte with $(EG)_{12}OMe$ substituted PT (PEG12-PT) to form an all-PEGylated non-aqueous RFB leads to decreased redoxmer crossover and consequently improved cycling stability in flow cell tests.[148]

An analogous 2,2′-bipyridine molecular scaffold has also been investigated as 2e⁻ anolyte materials for nonaqueous RFBs. *N*,*N*′-Ethylene or propylene-linked 2,2′-bipyridine derivatives (Diquats) exhibit two redox events in nonaqueous electrolytes, but suffer from major drawbacks of too high redox potentials for anolyte molecules, too large separations (>0.3 V) between the two redox potentials, and too low solubility.[149] To overcome these limitations, Sanford et al. developed a new Diquat molecule with a *N*−*N*′-propylene linker and two dimethylamino substituents para to N (denoted as M).[150] The dimethylamino groups afford a reversible concerted two-electron redox reaction between M and M^{2+}, shift the redox potential negatively to −1.67 V vs Fc/Fc^+, and enhance the solubilities to 0.7 M for M and to 0.6 M for $M^{2+}PF_6$ in MeCN. However, the 0.05 M symmetric flow cell shows a rapid capacity fade. Post-cycling analysis supports a material decomposition pathway via proton transfer from M^{2+} to M, followed by ring opening to form H_2M^{2+} that is detected with ^{1}HNMR and mass spectrum. Such chemical instability has limited its further use in nonaqueous RFBs.

Sigman et al. investigated the redox properties and stability of a series of functionalized 2,2′-bipyrimidine anolyte materials using combined experimental and computational approaches.[151] This scaffold is capable of reversible 2e⁻ redox reactions with redox potentials as low as ∼−2 V vs Fc/Fc^+ in MeCN, with modulations by both the substituents and the supporting cations. Interestingly, the use of tetrabutylammonium (TBA^+) or Li^+ salt yields stepwise 2e⁻ reactions, while Na^+ or K^+ causes the two redox steps to coalesce into a concerted event. This is speculated to be associated with the different interactions between the counterion and the reduced products. Moreover, combined BE tests and chemical analysis of aged 2e⁻ electrolytes indicate that the stability is adversely affected by the steric strain caused by the substituents ortho to N atoms. This finding agrees with the reported decomposition mechanism of dialkylated 2,2′-bipyridine (Diquat) molecules in an aqueous RFB.[68] A statistical stability−structure model is established offering insights on stability controlling factors. The predicted stable structure is subsequently synthesized and electrochemically evaluated, and the results validate the molecular design.

4.2.5. Azobenzene. Azobenzene (AB) contains a rarely seen open structure with the redox-active azo bond (−N═N−) bridging two benzene rings. Although the benzene rings offer charge delocalization, whether the open structure can enable sufficient conjugative stabilization remains questionable. Yu et al. explored the use of AB as an anolyte material in nonaqueous RFBs.[152] Indeed, the redox chemistry of AB is strongly dependent on the solvent and supporting salt used. The LiTFSI/DMF electrolyte is finally chosen because of the redox reversibility, fast kinetics, and high solubility (∼4 M). AB exhibits a concerted 2e⁻ redox activity at −1.78 V vs Ag/Ag^+. Moreover, the chemical stability of AB and its reduced state (AB^{2-}) is confirmed via no changes detected in temporal UV−vis, NMR and CV tests of cycled AB and aged AB^{2-} electrolytes. Impressively, using either LISICON or porous separator, the AB/Fc flow cells at both low (0.1 M) and high (1 M) concentrations demonstrate record-breaking cycling stability among reported nonaqueous RFBs, for example, 0.11% per day for 0.1 M cell and 0.16% per day for 1 M cell (both over 3 months). Interestingly, while the capacities remain rarely changed, the voltage curves of the flow cells show significant evolution during galvanic cycling. This uncommon phenomenon is mechanistically ascribed to the Li^+-coupled redox chemistry of AB because of possible coordination interactions between Li^+ and N atoms, which is confirmed through UV−vis, NMR (^{1}H, ^{13}C, and ^{7}Li) and DFT calculation. This factor

https://doi.org/10.1021/acsmaterialslett.1c00668
ACS Materials Lett. 2022, 4, 277−306

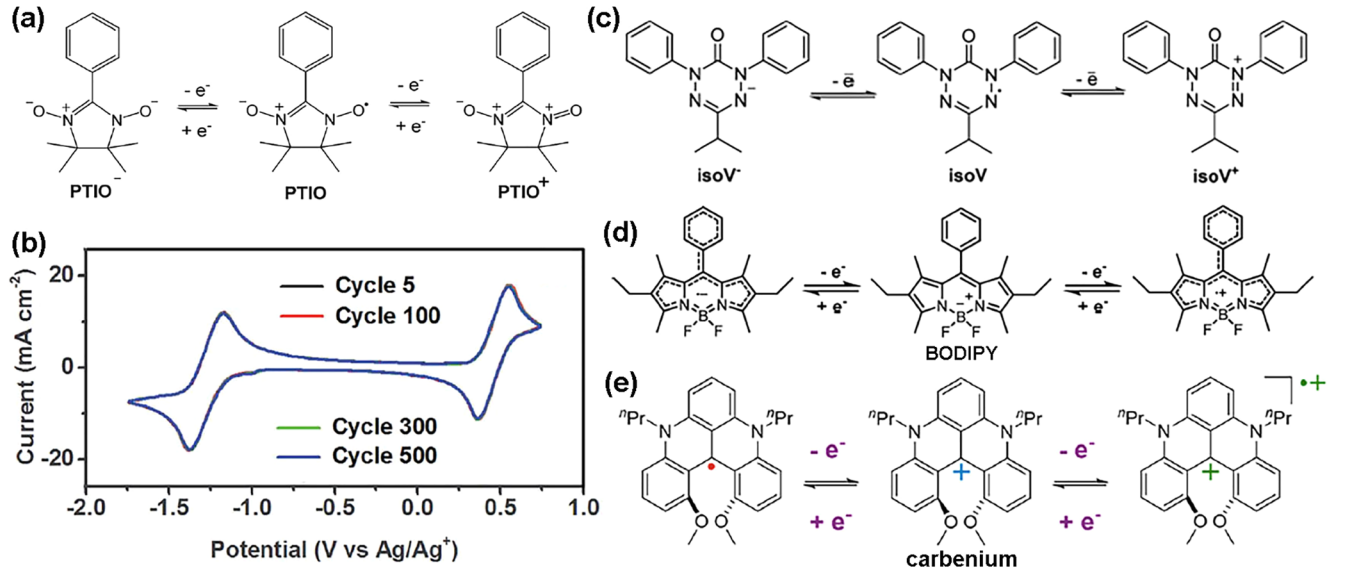

Figure 16. (a) Ambipolar redox reactions and (b) CV curves of PTIO. Reprinted from ref 65 under CC BY 3.0 (http://creativecommons.org/licenses/by/3.0/). (c) Redox reactions of the oxo-verdazyl isoV. Reprinted with permission from ref 158. Copyright 2020 Royal Society of Chemistry. (d) Redox reactions of BODIPY. Adapted with permission from ref 163. Copyright 2016 American Chemical Society. (e) Redox reactions of a helical carbenium (^{n}Pr-DMQA$^+$). Adapted with permission from ref 164. Copyright 2021 American Chemical Society.

contributes to the continuous voltage curve evolution throughout the repeated charging and discharging.

4.2.6. Pyridinium Derivatives. Typically, the pyridinium core itself undergoes one electron transfer.[76] When bearing a carbonyl group at the para position, the pyridinium molecule is capable of 2e$^-$ reactions because the carbonyl participates into the second redox forming an anionic enolate structure. Sanford et al. carried out an evolutionary study of the effects of pyridinium structure on its key properties to develop stable 2e$^-$ molecules in nonaqueous electrolytes.[153] The para carbonyl substituent plays an important role in stabilizing the 2e$^-$ enolate product. Ketone enolates are found to be strikingly more stable than ester enolates; no detectable decomposition is observed for days with temporal NMR and UV−vis monitoring. For the ester enolates, careful NMR and CV analyses reveal a decomposition pathway via protonation at the α-carbonyl position by the trace water impurity or MeCN solvent. The ketone enolate has an approximately 3 orders of magnitude lower basicity and, thus, is less susceptible to protonation.

Sanford et al. continued to investigate the effects of counterions on the stability of ketone enolates.[154] TBAPF$_6$ and KPF$_6$ produce better bulk electrolysis cycling stability than NaPF$_6$ and LiPF$_6$ for both 1e$^-$ and 2e$^-$ products of *N*-ethyl-4-benzoylpyridinium. This is ascribed mainly to the weaker Lewis acidity of TBA$^+$ and K$^+$ ions, which causes minimal reaction of PF$_6^-$ with trace water impurity in MeCN solvent and subsequent release of HF, preventing protonation-initiated decomposition of the ketone enolate. The use of KPF$_6$ yields significant technoeconomic benefits with low cost and stable cycling in a symmetric RFB loaded with the 1e$^-$ radical electrolyte at both sides.

4.3. Ambipolar Organic Molecules. Ambipolar redox molecules feature 2e$^-$ redox reactions but the two redox events are sufficiently separated to enable a decently high cell voltage on its own. Thus, these molecules can serve simultaneously as the anolyte and catholyte materials in symmetric RFBs. With the same redox scaffold used at both sides, such symmetric RFBs are architecturally similar to the all-vanadium or all-iron RFBs. A unique advantage is to make the crossover-induced capacity fade recoverable via electrolyte transfer or remixing, like in all-vanadium RFBs.[61] Thus, ambipolar organic redoxmers have been extensively investigated aiming to achieve minimal electrolyte cross-contamination and long-term cycling stability.[155] A few such examples have been discussed in the aqueous RFB section (see Figures 5e and 7), but there are more ambipolar systems in nonaqueous RFBs. A key challenge is to enable high solubility and stability in all involved oxidation states of the redoxmer. This requires well-planned molecular or electrolyte engineering methods to harvest combined properties.

4.3.1. N-Centered Ambipolar Organic Molecules. A number of N-centered organic molecules have demonstrated ambipolar redox activities in nonaqueous RFBs. Nitroxide radicals are typical two-center, three-electron (2c−3e) bonds with the spin density resonant between N and O. These radicals are capable of disproportionational redox reactions forming an aminoxyl anion via gain of an electron and an oxoammonium cation via loss of an electron. Of the two reactions, the oxidation reaction is commonly stable in both aqueous and nonaqueous electrolytes; for example, nitroxide radicals bearing the TEMPO moiety have been widely used as catholyte materials in RFBs.[49,156] However, the reduction reaction of nitroxide radicals is often irreversible, possibly degraded by protonation from H-donors, such as water or organic solvents. Wei et al. demonstrated that a stable nitronyl nitroxide radical, 2-phenyl-4,4,5,5-tetramethylimidazoline-1-oxyl 3-oxide (PTIO), exhibits a reversible reduction reaction and is used in a nonaqueous symmetric RFB (Figure 16a and b).[65] The reaction between the two redox products (PTIO$^+$ and PTIO$^-$) regenerates the neutral PTIO, demonstrating a good promise to recover crossover-induced capacity loss. The N−O$^-$ anion in PTIO$^-$ is stabilized via both π-conjugation and steric hindrance engendered by the alpha C-phenyl imine moiety. Nevertheless, the PTIO$^-$ product is still picky to the electrolyte composition; only the tetraalkylammonium counterion (e.g., TBA$^+$) affords the redox reversibility, while Li$^+$ fails to revert the reduction process presumably due to strong Li$^+$−PTIO$^-$ ion

https://doi.org/10.1021/acsmaterialslett.1c00668
ACS Materials Lett. 2022, 4, 277−306

pairing.[66] PTIO shows a solubility of 2.6 M in MeCN and two redox potentials at −1.27 and 0.46 V vs Ag/Ag^+, leading to a cell voltage of 1.73 V. Capacity fade is still observed in the symmetric PTIO flow cell tests at both 0.1 and 0.5 M. The degradation may originate from the MeCN solvent susceptible to deprotonation or nucleophilic addition by the N−O⁻. Interestingly, FTIR can estimate the SOC of the PTIO flow cell with high accuracy, providing a viable opportunity for convenient inline SOC monitoring.

Verdazyl radicals have grown as a family of potentially air- and water-stable radicals and are characteristic of ambipolar redox properties. The molecular core is a cyclic 1,2,4,5-tetrazine scaffold. The unpaired electron is highly resonant among the N1−N2−C3−N4−N5 atoms, which accounts for the high radical stability. There are two types of verdazyl structures: Kuhn verdazyl with two alkyl substituents at the C6 position and oxo-verdazyl with a carbonyl at the C6 position. The latter is typically more stable because C═O imparts additional resonance. Verdazyl radicals can undergo disproportionational redox properties with formation of leuco-verdazyl anion when gaining an electron and of verdazylium cation when losing an electron, making them promising ambipolar candidates for symmetric RFBs. Dyker et al. investigated the use of 3-phenyl-1,5-di-*p*-tolylverdazyl (PDTV), a Kuhn verdazyl, in a nonaqueous RFB for the first time.[157] This molecule exhibits two redox peaks at −0.17 and −1.15 V vs Ag/Ag^+ in supporting $TBAPF_6$/MeCN electrolyte, leading to a cell voltage of 0.98 V. Employing a Tokoyuma AHA anion exchange membrane, the 0.04 M symmetric nonflow cell test demonstrates high CEs (94−97%) but rapid capacity fade over 50 cycles. Post-analysis of the cycled electrolyte reveals decomposition of PDTV as the major cause for the performance degradation. To address the stability issue, Cekic-Laskovic et al. investigated the more stable oxo-verdazyl radicals for use in a nonaqueous symmetric RFB.[158] A series of oxo-verdazyl structures are characterized to down-select the final candidate, 1,5-diphenyl-3-isopropyl-6-oxoverdazyl (isoV, see Figure 16c), which has the optimal solubility (2.4 M in MeCN) and redox properties. IsoV exhibits two redox peaks at −0.72 and 0.70 V vs Ag/AgCl (sat.), resulting in a cell voltage of 1.42 V in a supporting electrolyte of tetrabutylammonium perchlorate (TBAP) in MeCN. However, the symmetric flow cell demonstrates serious capacity decay within 150 cycles. The performance degradation is attributed mainly to the mutual isoV-membrane interactions. The isoV species can be trapped in the used FAP-375-PP anion exchange membrane causing continuous increase in cell resistance and capacity loss.

Porphyrin is a heterocycle consisting of four pyrrole moieties connected via methine bridges. Chen et al. demonstrated that 5,10,15,20-tetraphenylporphyrin (H_2TPP) shows unique $2e^-$ redox events for both anolyte and catholyte reactions in a nonaqueous RFB.[159] The anolyte reaction occurs between H_2TPP and H_2TPP^{2-} at −1.88 and −1.55 V, while the catholyte reaction between H_2TPP and H_2TPP^{2+} at 0.69 and 0.95 V vs Ag/Ag^+, respectively, in a supporting electrolyte of TBAP in dichloromethane (CH_2Cl_2). Because of the low solubility (~10 mM) of H_2TPP, a suspension electrolyte based on H_2TPP/Ketjen black (KB) composites is used to go beyond the solubility limit. With a ClO_4^-−selective Y-zeolite-PVDF membrane, the nonflow symmetric H_2TPP cell demonstrates stable cycling in a temperature range of −40~20 °C, implying its versatile applications under cold weather conditions.

The hexazaanthracene scaffold contains three directly fused pyrazine rings and has demonstrated ambipolar redox activities in nonaqueous electrolytes. Schubert et al. synthesized a molecular analog, 2,3,7,8-tetracyano-5,10-diphenyl-5,10-dihydrodipyrazino[2,3-*b*:2′,3′-*e*]pyrazine and investigated its redox properties.[160] This molecule exhibits two redox peaks at −1.49 and 1.42 V vs Fc/Fc^+, yielding a high cell voltage of 2.91 V by itself in $TBAPF_6$/MeCN. However, the anolyte redox is not chemically stable as new redox peaks are observed under bulk electrolysis conditions.

Boron-dipyrromethene (BODIPY) is a versatile dye and consists of a boron difluoride group connected to the two N atoms in a dipyrromethene moiety to form a cyclic structure. Tailored BODIPY derivatives feature two sufficiently separated redox events forming $BODIPY^{\bullet-}$ at the anolyte side and $BODIPY^{\bullet+}$ at the catholyte side, respectively (Figure 16d).[161] Cook et al. investigated the chemical and electrochemical properties of a commercial BODIPY dye (PM567).[162] It shows reversible redox peaks at −1.59 and 0.73 V vs Ag/Ag^+ in $TBAPF_6$/MeCN, resulting in a cell voltage of 2.32 V. A nonflow symmetric cell loaded with an AMI-7001 anion exchange membrane and 1 mM PM567 exhibits rapid capacity fading. Mass spectra of the aged redox products indicate decomposition of PM567 species via loss of F and BF_2 fragments and dimerization of these defragmented species. Schubert et al. introduced BODIPY units onto copolymer backbones and investigated their redox properties in a supporting electrolyte of TBAP in carbonate solvent.[163] Similar capacity fading is observed, indicating necessary improvement in chemical stability as a prerequisite for using BODIPY molecules in RFBs.

4.3.2. Other Ambipolar Organic Molecules. Gianetti et al. reported the use of *N*,*N*′-di(*n*-propyl) dimethoxyquinacridiniums (^{n}Pr-$DMQA^+$), a helical carbenium ion, in a nonaqueous symmetric RFB.[164] This cationic ^{n}Pr-$DMQA^+$ is converted to a neutral radical ^{n}Pr-$DMQA^{\bullet}$ at −1.14 V and to a dicationic radical ^{n}Pr-$DMQA^{\bullet 2+}$ at 0.98 V vs Ag/Ag^+ in $TBAPF_6$/MeCN (Figure 16e). In a symmetric H-cell test loaded with 1.2 mM ^{n}Pr-$DMQA^+$, near-100% CE and stable capacity are obtained in the first 80 cycles, but sharp efficiency and capacity drops appear in the following cycles. CV tests of the cycled electrolytes indicate material degradation at the catholyte side. The detailed decomposition mechanism is not discussed, but possibly because the high charge density in ^{n}Pr-$DMQA^{\bullet 2+}$ makes it susceptible to nucleophilic attacks.

Jiang et al. investigated tetracyanoethylene (TCNE) as a two-electron organic candidate in nonaqueous RFBs.[165] TCNE is converted successively to $TCNE^{\bullet-}$ at −0.05 V then to $TCNE^{2-}$ at −1.08 V vs Ag/Ag^+ in $NaClO_4$/MeCN. Despite the largely separated redox events, this molecule is used as an $2e^-$ anolyte material, paired with a PT catholyte. TCNE is highly soluble in MeCN with a solubility of 2 M. The flow cell tests demonstrate decent cycling stability at both 0.2 and 0.5 M TCNE with slightly excess PT, for example, 73% retention over 200 cycles for the former and 100% retention over 50 cycles for the latter, but capacity fluctuations are observed. In addition, electrolyte crossover and increased cell impedance still remain a concern.

Toghill et al. studied the ambipolar redox properties of a dianionic croconate violet dye ($Croc^{2-}$) in nonaqueous $TBAPF_6$/MeCN.[166] Interestingly, this molecule has five oxidation states ($Croc^{4-}$, $Croc^{\bullet 3-}$, $Croc^{2-}$, $Croc^{\bullet -}$, Croc), but only the middle three of them are used in a symmetric cell due to their redox reversibility. Despite the high solubility (1 M in MeCN), the symmetric flow cell at 1 mM $Croc^{2-}$ produces rapid

https://doi.org/10.1021/acsmaterialslett.1c00668
ACS Materials Lett. 2022, 4, 277−306

capacity fading because of the decomposition of the anolyte product $Croc^{\bullet 3-}$ learned through post-mortem CV tests.

Yu et al. reported a novel biredox eutectic electrolyte (BEE) formed by direct mixing of low-melting-point *N*-butylphthalimide (BuPh) anolyte and 1,1′-dimethylferrocene (DMFc) catholyte at ambient temperature without addition of solvent (Figure 17a).[167] The mechanism of eutectic formation is based

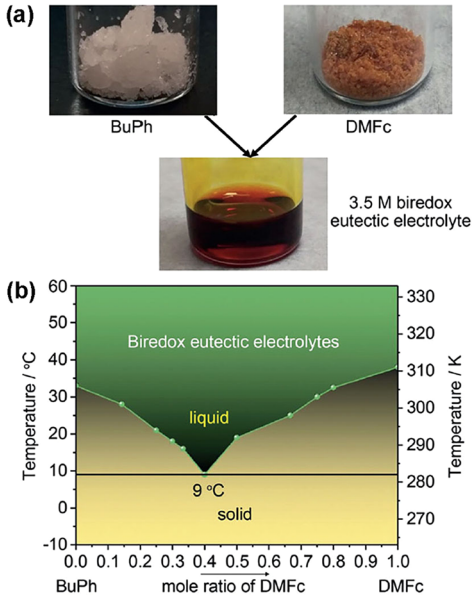

Figure 17. (a) Preparation of BEE based on 1:1 BuPh and DMFc and (b) phase diagram of the BuPh-DMFc BEE. Reprinted with permission from ref 167. Copyright 2019 Wiley.

on a combination of intermolecular dipole−dipole, $\pi-\pi$ stacking, and van der Waals interactions, indicated by FTIR and DFT analysis. The molarity of BuPh and DMFc reaches 3.5 M at 1:1 ratio with a low viscosity of 4.5 MPas at room temperature (Figure 17b). LiTFSI can be directly dissolved in the BEE with no solvent added, but because of the extremely low ionic conductivity, $TEABF_4$/MeCN is used as the supporting electrolyte in flow cell tests. The symmetric BEE flow cells at both 0.1 and 1 M deliver ∼50% EE and slow capacity fading when a Daramic porous separator is used. Such an "all-active" electrolyte design represents an attractive approach for the development of high-energy-density RFBs.

5. SUMMARY AND FUTURE OUTLOOK

An electrochemical feature of multiredox activities within a single molecular host is highly promising for achieving high energy density and low chemical cost in RFBs. We have reviewed the recent development of multielectron, mostly $2e^-$, organic redoxmers for use in aqueous and nonaqueous RFBs. The molecular structures, electrochemical reactions, and RFB-relevant properties including solubility, chemical stability, redox potential and kinetics of each type of these multielectron redoxmers are summarized in great details (Table 1). The key results obtained from this review are presented below:

(1) No matter aqueous or nonaqueous RFBs, conjugated carbonyl (C═O) and imine (C═N) compounds are the dominant redox centers that undergo multielectron reactions. (Anthra)quinone, phenazine, and (bi)-pyridinium are among the most investigated molecular scaffolds.

(2) Typically, the organic core dictates the multielectron activity, and the substituents modulate one or more of the key properties including solubility, stability, redox potential, and electrochemical kinetics. The substituents need to be carefully designed to achieve favorable properties and RFB performance. In some cases, factors affect properties in contradictory ways and compromise has to be accepted to achieve combined properties.

(3) It is quite often that the same $2e^-$ redox reactions are concerted in aqueous electrolytes but are stepwise in nonaqueous electrolytes. Most $2e^-$ reactions are proton-coupled in aqueous RFBs, thus these organic molecules exhibit strong pH-dependent electrochemical behaviors. In nonaqueous RFBs, the electrolyte composition needs to be attentively selected for property optimization.

(4) Understandings of property-limiting mechanisms, which have been progressively acquired for a number of redoxmers, are critically important for rationalizing design principles and realizing propitious multielectron candidates. A typical example is the development of anthraquinone derivatives in aqueous RFBs. The structure, number and siting of substituents have been systematically investigated leading to the discovery of a stable, soluble derivative (DBAQ).[92]

(5) Chemical stability is a common concern for organic redoxmers especially in electrochemically charged forms. Typical decomposition reactions include nucleophilic substitution/addition, protonation, disproportionation, or tautomerization. A combination of spectroscopic, electrochemical, and computational analyses is helpful to identify decomposition products and unravel decomposition pathways. Structural design of stable molecules should avoid these pathways.

(6) For stepwise two-electron reactions particularly in nonaqueous RFBs, reliable use of the second redox event is usually more challenging. For many such molecules, the solubility and stability of the $2e^-$ product are often inferior compared to the $1e^-$ redox.

Despite the significant progress, the development of multielectron organic compounds is not without challenges. Currently, candidates that meet commercialization requirements are still rather limited due to the lack of desired comprehensive property sets. The technoeconomic obstacles define the development needs and research directions for future pursuits.

(1) The multiredox activity involves multiple oxidation states for a single molecule, e.g., two for concerted reactions and ≥3 for stepwise reactions. Achieving high-value properties (solubility and chemical stability) in all of these oxidation states is a highly demanding task and has yet to be realized in most candidates. Groundbreaking design strategies need to be considered to push the boundary of molecular engineering.

(2) A variety of molecules are plagued with the low solubilities of post−$1e^-$ products, presumably because the altered charge density on the redox core counteracts the solubilizing substituents. Introduction of additional solvation interactions may be a viable approach for solubility improvement for post−$1e^-$ products. The development of $(NPr)_2V$ represents a good example of this effort. Decorating the viologen core with two tetraalkylammonium end-functionalized propyl pendants

https://doi.org/10.1021/acsmaterialslett.1c00668
ACS Materials Lett. 2022, 4, 277−306

Table 1. Solubilities, redox properties and RFB performance of representative multi-electron organic redoxmers in aqueous and nonaqueous RFBs

Redoxmer	Abbreviation	Solubility[a]	Redox Potential[b]	Kinetic Constant k_0 (cm/s)	Counter-Redoxmer	Tested Conc.[c]	Current Density (mA/cm²)	Cycle #	Capacity Fading
Aqueous RFBs									
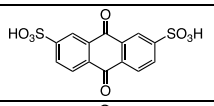	AQDS[35, 81]	>1 M	0.21 V (pH 0)	7.2×10^{-3}	Excess HBr/Br_2	1 M (1 M H_2SO_4)	750	~750	0.16%/cycle
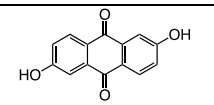	DHAQ[34]	0.6 M at pH 14	−0.69 V (pH 14)	7×10^{-3}	Excess $K_4Fe(CN)_6$	0.5 M (1 M NaOH)	100	100	0.1%/cycle
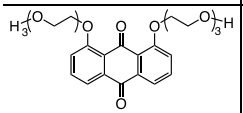	1,8-PEGAQ[39]	Miscible with water	−0.43 V (pH 7)	6.1×10^{-3}	Excess $K_3Fe(CN)_6$/ $K_4Fe(CN)_6$	1.5 M (1 M KCl)	50	220	0.043%/cycle, 0.5%/day
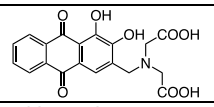	AMA[89]	0.4 M	−0.66 V (pH 14)	8.4×10^{-3}	Excess $K_3Fe(CN)_6$/ $K_4Fe(CN)_6$	0.4 M (0.2 M KOH)	100	350	0.02%/cycle, 0.81% /day
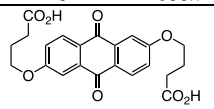	2,6-DBEAQ[90]	0.6 M at pH 12; 1.1 M at pH14	−0.51 V (pH 14)	7×10^{-3}	Excess $K_3Fe(CN)_6$/ $K_4Fe(CN)_6$	0.5 M (pH 12)	100	250	0.001%/cycle 0.05%/day
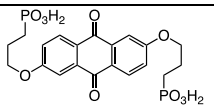	2,6-DPPEAQ[38]	0.75 M at pH 9	−0.47 V (1 M KCl, pH 9)	Not given	Excess $K_3Fe(CN)_6$/ $K_4Fe(CN)_6$	0.5 M (pH 9)	100	480	0.00036% /cycle 0.014%/day 5%/year
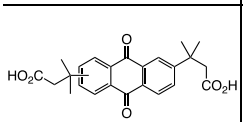	DPivOHAQ[92]	0.74 M at pH 12	−0.48 V (pH >11)	2.5×10^{-3}	Excess $K_3Fe(CN)_6$/ $K_4Fe(CN)_6$	0.5 M (pH 12)	100	650 at pH 12 then 750 at pH 14	pH 12: 0.014%/day, 5.1%/year pH 14: 0.0018%/day, 0.66%/year
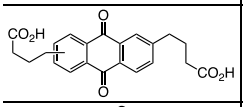	DBAQ[92]	1 M at pH 12	−0.47 V (pH 12)	2.9×10^{-3}	Excess $K_3Fe(CN)_6$/ $K_4Fe(CN)_6$	0.5M (pH 12)	100	650	0.0084%/day, 3.1%/year
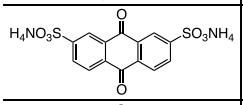	$AQDS(NH_4)_2$[44]	1.9 M	−0.2 V (pH 7)	0.077	Excess NH_4I	0.75 M (pH 7)	60	300	No fade
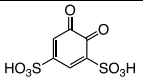	BQDS[93]	1 M	0.85 V (1 M H_2SO_4)	1.55×10^{-4}	AQDS or AQS	0.2 M (1 M H_2SO_4)	8	12	~1%/cycle
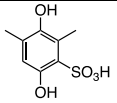	DHDMBS[96]	2 M in 1 M H_2SO_4	0.65 V (1 M H_2SO_4)	1.3×10^{-4}	AQDS	1 M (1 M H_2SO_4)	100	30	0.05%/cycle
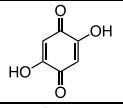	DHBQ[99]	>4 M in 1 M KOH	−0.72 V (1 M KOH)	2.12×10^{-3}	$K_4Fe(CN)_6$	0.5 M (2 M KOH)	100	150	0.24%/cycle
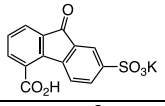	4C7SFL[63]	1.5 M in 2 M NaOH	0.7 V (1 M NaOH)	1.95×10^{-2}	Excess $K_3Fe(CN)_6$/ $K_4Fe(CN)_6$	1.36 M (1 M NaOH)	20	1111	0.02%/day 2.62%/4 months
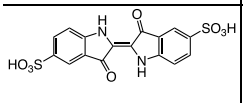	IC-H[105]	0.76 M in 0.1 M $HClO_4$	~0.2 V (0.1 M $HClO_4$)	1.86×10^{-4}	Excess HBr/Br_2	0.7 M (0.2 M $HClO_4$)	80	200	0.46%/day
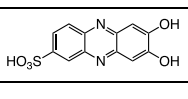	DHPS[33]	1.8 M at pH 14	−0.97 V (1 M NaOH)	Not given	Excess $K_3Fe(CN)_6$/ $K_4Fe(CN)_6$	1.4 M (1 M NaOH)	100	500	0.68%/day

https://doi.org/10.1021/acsmaterialslett.1c00668
ACS Materials Lett. 2022, 4, 277−306

Table 1. continued

Redoxmer	Abbreviation	Solubility[a]	Redox Potential[b]	Kinetic Constant k_0 (cm/s)	Counter-Redoxmer	Tested Conc.[c]	Current Density (mA/cm²)	Cycle #	Capacity Fading
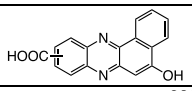	BHPC[110]	1.55 M in 1 M KOH	−0.78 V (1 M KOH)	1.55×10^{-3}	Excess $K_3Fe(CN)_6$/ $K_4Fe(CN)_6$	0.5 M (1 M KOH)	100	1305	0.08%/day
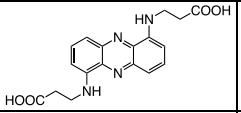	1,6-DPAP[111]	1.0 M	−0.5 V (1 M KCl, pH 12)	5.13×10^{-4}	Excess $K_3Fe(CN)_6$/ $K_4Fe(CN)_6$	0.5 M (pH 8)	20	90	0.0015% /day 0.5%/year
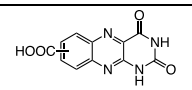	ACA[118]	2 M at pH 14	−0.62 V (1 M KOH)	1.2×10^{-5}	Excess $K_3Fe(CN)_6$/ $K_4Fe(CN)_6$	0.5 M (1 M KOH)	100	400	0.02%/cycle
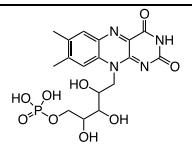	FMN-Na[117]	0.06 M in 1 M KOH, 1.5 M with 3 M NA	−0.52 V (pH 13)	5.3×10^{-3}	Excess $K_3Fe(CN)_6$/ $K_4Fe(CN)_6$	0.24 M (1 M KOH + 1 M NA)	50 then 80	100 then 100	0.01%/cycle at 50 mA/cm²
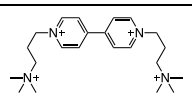	$(NPr)_2V$[122]	1.6 M	−0.35 V, −0.72 V (pH 7)	~0.31	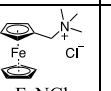 FcNCl	0.25 M (pH 7)	60	100	0.01%/cycle
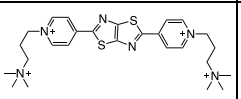	(NPr)2TTz[125]	1.3 M	−0.38 V, −0.50 V (pH 7)	~0.28	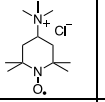	0.1 M (pH 7)	40	300	0.03%/cycle
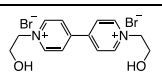	$(2HO\text{-}V)Br_2$[124]	2.2 M	−0.39 V, −0.79 V (pH 7)	0.36 (1st), 0.31 (2nd)	Self	0.1 M (pH 7)	40	200	no obvious decay
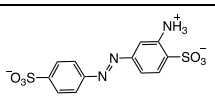	AADA[48]	2 M in 2 M NaOH with urea	~ −0.6 V (2 M NaOH)	4.85×10^{-4}	Excess $K_3Fe(CN)_6$/ $K_4Fe(CN)_6$	0.5 M (2 M NaOH + 2 M urea)	40	260	0.16%/cycle
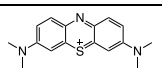	MB[130]	1.8 M in H_2O + CH_3CO_2H + H_2SO_4	0.57 V (3 M H_2SO_4)	0.32	V^{2+}	1.2 M (3.5 M H_2SO_4)	80	160	0.025%/cycle, 0.52%/day
Nonaqueous RFBs									
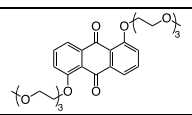	15D3GAQ[131]	0.25 M in PC	−1.0 V, −0.68 V	Not given	Li (non-flow)	0.25 M (1 M $LiPF_6$ in PC)	0.1	40	~8%/cycle
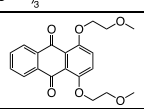	AQ4[133]	0.47 M in MeCN	−1.33 V, −1.89 V	Not given	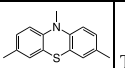 PT3	0.05 M (1 M $TEABF_4$ in MeCN)	10	10	~3%/cycle
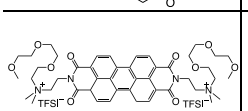	$[PDI][TFSI]_2$[138]	0.5 M in MeCN	−0.7 V	Not given	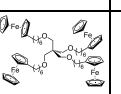 Fc_4 (non-flow)	0.2 M (0.5 M LiTFSI in MeCN)	Not given	450	No obvious decay
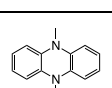	DMPZ[132]	0.06 M in MeCN	−0.15 V, 0.61 V	2.97×10^{-2} (1st), 5.53×10^{-3} (2nd)	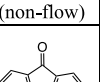	0.05 M (0.5 M LiTFSI in MeCN)	20	30	0.067%/cycle
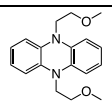	BMEPZ[142]	0.5 M in MeCN	−0.18 V, 0.61 V	1.18×10^{-2} (1st), 2.77×10^{-2} (2nd)	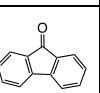	0.05 M (0.5 M LiTFSI in MeCN)	20	200	0.06%/cycle
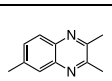	TMQ[140]	0.5 M in PC	−1.02 V, −0.7 V	Not given	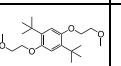 DBBB	0.05 M (0.2 M $LiBF_4$ in PC)	0.0625	30	Capacity fluctuation
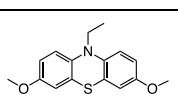	DMeOEPT[41]	0.15 M in PC	0.16 V, 0.72 V	Not given	Symmetric bulk electrolysis cell	0.001 M (1 M LiTFSI in PC)	0.804 mA (area not given)	50	0.08%/cycle

https://doi.org/10.1021/acsmaterialslett.1c00668
ACS Materials Lett. 2022, 4, 277−306

Table 1. continued

Redoxmer	Abbreviation	Solubility[a]	Redox Potential[b]	Kinetic Constant k_0 (cm/s)	Counter-Redoxmer	Tested Conc.[c]	Current Density (mA/cm²)	Cycle #	Capacity Fading
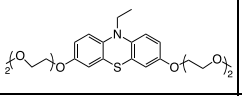	B(MEEO)EPT[145]	Miscible in MeCN	0.15 V, 0.74 V	Not given	Symmetric RFB	0.3 M (0.5 M TEATFSI in MeCN)	25	140	0.1%/cycle then 0.4%/cycle
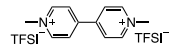	MVTFSI[146]	0.98 M in MeCN	−0.70 V, −1.11 V		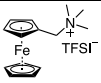 FcNTFSI	0.1 M (1 M LiTFSI in MeCN)	40	100	0.12%/cycle
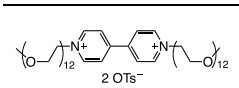	PEG12-V[147, 148]	Miscible in MeCN	−1.15 V, −0.74 V	0.22 (1st), 0.37 (2nd)	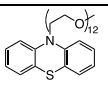 PEG12-PTZ	0.01 M (0.5 M $TBAPF_6$ in MeCN)	2	300	0.1%/cycle
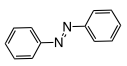	AB[152]	>5 M in DMF	−1.78 V	4.53×10^{-3}		0.1 M (0.5 M LiTFSI in DMF)	0.4	0.1 M: 3000;	0.007%/cycle, 0.35% /day
						1 M (1 M LiTFSI in DMF)	0.2	1 M: 100	0.15%/day, 0.16%/day
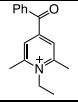	[154]	0.26 M in 0.5 M KPF_6/MeCN	−1.07 V, −1.57 V	Not given	Symmetric RFB	0.1 M (0.5 M KPF_6 in MeCN)	20 (50 cycles) then 40 (100 cycles)	100 at 40 mA/cm²	0.0028%/cycle
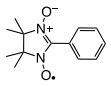	PTIO[65]	1.7 M in MeCN	−1.27 V, 0.46 V	Not given	Symmetric RFB	0.5 M (1 M $TBAPF_6$ in MeCN)	20	15	~4%/cycle
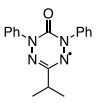	isoV[158]	2.4 M in MeCN	−0.72 V, 0.70 V	Not given	Symmetric RFB	0.01 M (0.3 M TBAP in MeCN)	2.2	150	~0.6%/cycle
	TCNE[165]	2 M in MeCN	−1.08 V, −0.05 V	8.38×10^{-3}, 1.81×10^{-3}	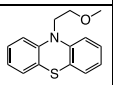 excess	0.5 M (1.2 M $NaClO_4$ in MeCN)	60	50	No obvious decay
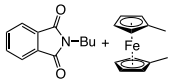	BEE[167]	3.5 M (1:1, neat)	−1.8 V, 0 V	Not given	Symmetric RFB	0.1 M (1 M $TEABF_4$ in MeCN)	60	500	0.056%/cycle

[a]Solubility in water, unless otherwise stated. [b]The reference electrodes are converted to SHE for aqueous redoxmers and to Ag/Ag^+ for nonaqueous redoxmers. [c]The supporting electrolytes are indicated in parentheses.

solubilizes the $2e^-$ product.[124] Moreover, understanding the mechanisms for establishment of solubility limit of the $2e^-$ product will offer useful clues to design solvation interactions that can defer the formation of contact ion pairs. Preparation of the $2e^-$ products in purified form via chemical methods will largely facilitate this effort.

(3) Similarly, a number of post−$1e^-$ products suffer from inferior chemical stability. Elucidation of decomposition pathways via identification of parasitic products will shed light on constructive structural designing to impede materials decomposition and improve molecular stability. Availability of purified $2e^-$ products will simplify temporal stability tests and expedite decomposition product analysis with minimal electrolyte complication.

(4) In many $2e^-$ RFB systems, it is challenging to develop organic anolyte and catholyte redoxmers that simultaneously have comparably high solubility and stability. For example, half-cell configurations using low-solubility yet stable inorganic redoxmers such as ferri/ferrocyanide in alkaline electrolytes are commonly employed to evaluate only one redoxmer at a time. Thus, there is an urgent need to develop multielectron anolyte and catholyte materials that have matched solubility and stability with high values and can be accommodated in the same RFBs to deliver practically attractive energy density and long operational stability.

(5) For aqueous RFBs, the development of multielectron catholyte molecules, particularly those having high redox potentials, lags significantly behind that of anolyte molecules. The major challenge is that the cationic multielectron products are more susceptible to nucleophilic water addition resulting in hydrolytic decomposition. Embracing electron-donating conjugation to the structural core to decrease charge density may be a feasible design strategy to mitigate this issue. The development of methylene blue (MB) catholyte is a typical example for this strategy.[130] The presence of the two dimethylamino groups offers electron conjugation to the cationic sulfonium leading to its high chemical stability in acid.

https://doi.org/10.1021/acsmaterialslett.1c00668
ACS Materials Lett. 2022, 4, 277−306

(6) For nonaqueous RFBs, the lack of selective membranes has formidably limited the capability of molecular evaluation under flow cell conditions. Currently, the closest tests are performed in symmetric flow cells, where redoxmer crossover is not a concern; but the conditions are still far from practical RFBs due to inability to demonstrate system-level energy density and operational stability. The development of selectively ion-conductive membranes is an urgent research task for nonaqueous RFBs and may need revolutionary design concepts to enable implementable membrane materials.

(7) At present, the cost and environmental impact of multielectron organic compounds are not widely considered. Ideally, these molecules should be commercially available with industrial-scale productions or can be scalably synthesized from commodity chemicals. Although some organic core structures are inexpensive, synthetic work to introduce substituents may increase the overall cost. Moreover, the often irreversible redoxmer loss may alter the method of levelized cost calculation. Comprehensive technoeconomic models need to be developed to identify cost-intensive factors in installation and operation of these RFBs. In addition, considering the large-scale use, they must have minimal adverse effects on human health, ecological system and environment. Thus, selection of multielectron molecules should reference related toxicity studies.

In conclusion, significant advancement in the development of multielectron organic molecules has been achieved with high-merit physicochemical and electrochemical properties in aqueous and nonaqueous RFBs. Fundamental structure–property understandings have been acquired for a variety of such molecules, offering valuable guidance for the design and development of more promising structures. These efforts have opened an important avenue toward realization of feasible multielectron redoxmers. In the meantime, the substantial technoeconomic challenges urge technical innovations at both materials and system levels to foster soluble, stable multielectron organic redoxmers that eventually lead to energy-dense, long-cycling, cost-effective RFBs.

AUTHOR INFORMATION

Corresponding Authors

Lu Zhang − *Argonne National Laboratory, Lemont, Illinois 60439, United States; Joint Center for Energy Storage Research, Argonne National Laboratory, Lemont, Illinois 60439, United States;* orcid.org/0000-0003-0367-0862; Phone: 630-252-5670; Email: luzhang@anl.gov

Xiaoliang Wei − *Indiana University–Purdue University Indianapolis, Indianapolis, Indiana 46202, United States;* orcid.org/0000-0002-7692-2357; Phone: 317-274-8983; Email: xwei18@iupui.edu

Authors

Xiaoting Fang − *Indiana University–Purdue University Indianapolis, Indianapolis, Indiana 46202, United States; Purdue University, West Lafayette, Indiana 47907, United States; Argonne National Laboratory, Lemont, Illinois 60439, United States*

Zhiguang Li − *Indiana University–Purdue University Indianapolis, Indianapolis, Indiana 46202, United States; Purdue University, West Lafayette, Indiana 47907, United States; Argonne National Laboratory, Lemont, Illinois 60439, United States; Joint Center for Energy Storage Research, Argonne National Laboratory, Lemont, Illinois 60439, United States*

Yuyue Zhao − *Indiana University–Purdue University Indianapolis, Indianapolis, Indiana 46202, United States*

Diqing Yue − *Indiana University–Purdue University Indianapolis, Indianapolis, Indiana 46202, United States; Purdue University, West Lafayette, Indiana 47907, United States*

Complete contact information is available at: https://pubs.acs.org/10.1021/acsmaterialslett.1c00668

Author Contributions

The manuscript was written through contributions of all authors. X.F. drafted the manuscript. X.F., Z.L., Y.Z., and D.Y. edited the manuscript. L.Z. and X.W. finalized the manuscript and supervised the project. All authors have given approval to the final version of the manuscript.

Notes

The authors declare no competing financial interest.

ACKNOWLEDGMENTS

The authors acknowledge financial support from National Science Foundation (Award No. CHE-2055222) and from the Joint Center for Energy Storage Research (JCESR), an Energy Innovation Hub funded by the U.S. Department of Energy, Office of Science, and Basic Energy Sciences. This research was also partially supported by Laboratory Directed Research and Development (LDRD) funding from Argonne National Laboratory, provided by the Director, Office of Science, of the U.S. Department of Energy under Contract No. DE-AC02-06CH11357.

REFERENCES

(1) Jacobson, M. Z.; Delucchi, M. A. Providing all global energy with wind, water, and solar power, Part I: Technologies, energy resources, quantities and areas of infrastructure, and materials. *Energy policy* **2011**, *39*, 1154–1169.

(2) Hesse, H. C.; Schimpe, M.; Kucevic, D.; Jossen, A. Lithium-ion battery storage for the grid—A review of stationary battery storage system design tailored for applications in modern power grids. *Energies* **2017**, *10*, 2107.

(3) *Energy Storage Grand Challenge: Energy Storage Market Report*, NREL/TP-5400-78461, DOE/GO-102020-5497; US Department of Energy, 2020.

(4) Trahey, L.; Brushett, F. R.; Balsara, N. P.; Ceder, G.; Cheng, L.; Chiang, Y.-M.; Hahn, N. T.; Ingram, B. J.; Minteer, S. D.; Moore, J. S.; et al. Energy storage emerging: A perspective from the Joint Center for Energy Storage Research. *Proc. Natl. Acad. Sci. U. S. A.* **2020**, *117*, 12550–12557.

(5) Dunn, B.; Kamath, H.; Tarascon, J. M. Electrical Energy Storage for the Grid: A Battery of Choices. *Science* **2011**, *334*, 928–935.

(6) Yang, Z. G.; Zhang, J.; Kintner-Meyer, M. C. W.; Lu, X.; Choi, D.; Lemmon, J. P.; Liu, J. Electrochemical Energy Storage for Green Grid. *Chem. Rev.* **2011**, *111*, 3577–3613.

(7) Wang, W.; Luo, Q.; Li, B.; Wei, X.; Li, L.; Yang, Z. G. Recent Progress in Redox Flow Battery Research and Development. *Adv. Funct. Mater.* **2013**, *23*, 970–986.

(8) Weber, A. Z.; Mench, M. M.; Meyers, J. P.; Ross, P. N.; Gostick, J. T.; Liu, Q. H. Redox flow batteries: a review. *J. Appl. Electrochem.* **2011**, *41*, 1137–1164.

(9) Noack, J.; Roznyatovskaya, N.; Herr, T.; Fischer, P. The Chemistry of Redox-Flow Batteries. *Angew. Chem., Int. Ed.* **2015**, *54*, 9776–9808.

(10) Perry, M. L.; Weber, A. Z. Advanced Redox-Flow Batteries: A Perspective. *J. Electrochem. Soc.* **2016**, *163*, A5064−A5067.
(11) Ding, C.; Zhang, H.; Li, X.; Liu, T.; Xing, F. Vanadium Flow Battery for Energy Storage: Prospects and Challenges. *J. Phys. Chem. Lett.* **2013**, *4*, 1281−1294.
(12) Crawford, A.; Viswanathan, V.; Stephenson, D.; Wang, W.; Thomsen, E.; Reed, D.; Li, B.; Balducci, P.; Kintner-Meyer, M.; Sprenkle, V. Comparative analysis for various redox flow batteries chemistries using a cost performance model. *J. Power Sources* **2015**, *293*, 388−399.
(13) Duan, W.; Huang, J.; Kowalski, J. A.; Shkrob, I. A.; Vijayakumar, M.; Walter, E.; Pan, B.; Yang, Z.; Milshtein, J. D.; Li, B.; Liao, C.; Zhang, Z. C.; Wang, W.; Liu, J.; Moore, J. S.; Brushett, F. R.; Zhang, L.; Wei, X. Wine-Dark Sea″ in an Organic Flow Battery: Storing Negative Charge in 2,1,3-Benzothiadiazole Radicals Leads to Improved Cyclability. *ACS Energy Lett.* **2017**, *2*, 1156−1161.
(14) Selverston, S.; Nagelli, E.; Wainright, J.; Savinell, R. All-iron hybrid flow batteries with in-tank rebalancing. *J. Electrochem. Soc.* **2019**, *166* (10), A1725.
(15) Li, B.; Liu, J. Progress and directions in low-cost redox-flow batteries for large-scale energy storage. *Natl. Sci. Rev.* **2017**, *4*, 91−105.
(16) Wei, X.; Pan, W.; Duan, W.; Hollas, A.; Yang, Z.; Li, B.; Nie, Z.; Liu, J.; Reed, D.; Wang, W.; Sprenkle, V. Materials and Systems for Organic Redox Flow Batteries: Status and Challenges. *ACS Energy Lett.* **2017**, *2*, 2187−2204.
(17) Winsberg, J.; Hagemann, T.; Janoschka, T.; Hager, M. D.; Schubert, U. S. Redox-Flow Batteries: From Metals to Organic Redox-Active Materials. *Angew. Chem., Int. Ed.* **2017**, *56*, 686−711.
(18) Ding, Y.; Zhang, C.; Zhang, L.; Zhou, Y.; Yu, G. Molecular engineering of organic electroactive materials for redox flow batteries. *Chem. Soc. Rev.* **2018**, *47*, 69−103.
(19) Luo, J.; Hu, B.; Hu, M.; Zhao, Y.; Liu, T. Status and prospects of organic redox flow batteries toward sustainable energy storage. *ACS Energy Lett.* **2019**, *4*, 2220−2240.
(20) Shin, S. H.; Yun, S. H.; Moon, S. H. A review of current developments in non-aqueous redox flow batteries: characterization of their membranes for design perspective. *Rsc. Adv.* **2013**, *3*, 9095−9116.
(21) Gong, K.; Fang, Q.; Gu, S.; Li, S.; Yan, Y. Nonaqueous redox-flow batteries: organic solvents, supporting electrolytes, and redox pairs. *Energy Environ. Sci.* **2015**, *8*, 3515−3530.
(22) Rhodes, Z.; Cabrera-Pardo, J. R.; Li, M.; Minteer, S. D. Electrochemical Advances in Non-Aqueous Redox Flow Batteries. *Isr. J. Chem.* **2021**, *61*, 101−112.
(23) Huang, J.; Cheng, L.; Assary, R. S.; Wang, P.; Xue, Z.; Burrell, A. K.; Curtiss, L. A.; Zhang, L. Liquid Catholyte Molecules for Nonaqueous Redox Flow Batteries. *Adv. Energy Mater.* **2015**, *5*, 1401782.
(24) Cong, G.; Zhou, Y.; Li, Z.; Lu, Y. A Highly Concentrated Catholyte Enabled by a Low-Melting-Point Ferrocene Derivative. *ACS Energy Lett.* **2017**, *2*, 869−875.
(25) Huang, J.; Duan, W.; Zhang, J.; Shkrob, I. A.; Assary, R. S.; Pan, B.; Liao, C.; Zhang, Z.; Wei, X.; Zhang, L. Substituted thiadiazoles as energy-rich anolytes for nonaqueous redox flow cells. *J. Mater. Chem. A* **2018**, *6*, 6251−6254.
(26) Wang, W.; Li, L.; Nie, Z.; Chen, B.; Luo, Q.; Shao, Y.; Wei, X.; Chen, F.; Xia, G.; Yang, Z. A new hybrid redox flow battery with multiple redox couples. *J. Power Sources* **2012**, *216*, 99−103.
(27) Zhang, S.; Guo, W.; Yang, F.; Zheng, P.; Qiao, R.; Li, Z. Recent progress in polysulfide redox-flow batteries. *Batter. Supercaps* **2019**, *2*, 627−637.
(28) Khor, A.; Leung, P.; Mohamed, M.; Flox, C.; Xu, Q.; An, L.; Wills, R.; Morante, J.; Shah, A. Review of zinc-based hybrid flow batteries: From fundamentals to applications. *Mater. Today Energy* **2018**, *8*, 80−108.
(29) Zhang, H.; Sun, C. Cost-effective iron-based aqueous redox flow batteries for large-scale energy storage application: A review. *J. Power Sources* **2021**, *493*, 229445.
(30) Jameson, A.; Gyenge, E. Halogens as Positive Electrode Active Species for Flow Batteries and Regenerative Fuel Cells. *Electrochem. Energy Rev.* **2020**, *3*, 431−465.
(31) Hogue, R. W.; Toghill, K. E. Metal coordination complexes in nonaqueous redox flow batteries. *Curr. Opin. Electrochem.* **2019**, *18*, 37−45.
(32) Thaller, L. H. *Recent Advances in Redox Flow Cell Storage Systems*, NASA TM-79186; 1974.
(33) Hollas, A.; Wei, X.; Murugesan, V.; Nie, Z.; Li, B.; Reed, D.; Liu, J.; Sprenkle, V.; Wang, W. A biomimetic high-capacity phenazine-based anolyte for aqueous organic redox flow batteries. *Nat. Energy* **2018**, *3*, 508−514.
(34) Lin, K.; Chen, Q.; Gerhardt, M. R.; Tong, L.; Kim, S. B.; Eisenach, L.; Valle, A. W.; Hardee, D.; Gordon, R. G.; Aziz, M. J.; Marshak, M. P. Alkaline quinone flow battery. *Science* **2015**, *349*, 1529−1532.
(35) Huskinson, B.; Marshak, M. P.; Suh, C.; Er, S.; Gerhardt, M. R.; Galvin, C. J.; Chen, X.; Aspuru-Guzik, A.; Gordon, R. G.; Aziz, M. J. A metal-free organic-inorganic aqueous flow battery. *Nature* **2014**, *505*, 195−198.
(36) Liu, T.; Wei, X.; Nie, Z.; Sprenkle, V.; Wang, W. A Total Organic Aqueous Redox Flow Battery Employing a Low Cost and Sustainable Methyl Viologen Anolyte and 4-HO-TEMPO Catholyte. *Adv. Energy Mater.* **2016**, *6*, 1501449.
(37) Hu, B.; DeBruler, C.; Rhodes, Z.; Liu, T. Long-Cycling Aqueous Organic Redox Flow Battery (AORFB) toward Sustainable and Safe Energy Storage. *J. Am. Chem. Soc.* **2017**, *139*, 1207−1214.
(38) Ji, Y.; Goulet, M. A.; Pollack, D. A.; Kwabi, D. G.; Jin, S.; De Porcellinis, D.; Kerr, E. F.; Gordon, R. G.; Aziz, M. J. A phosphonate-functionalized quinone redox flow battery at near-neutral pH with record capacity retention rate. *Adv. Energy Mater.* **2019**, *9*, 1900039.
(39) Jin, S.; Jing, Y.; Kwabi, D. G.; Ji, Y.; Tong, L.; De Porcellinis, D.; Goulet, M.-A.; Pollack, D. A.; Gordon, R. G.; Aziz, M. J. A water-miscible quinone flow battery with high volumetric capacity and energy density. *ACS Energy Lett.* **2019**, *4*, 1342−1348.
(40) Wei, X.; Cosimbescu, L.; Xu, W.; Hu, J.; Vijayakumar, M.; Feng, J.; Hu, M. Y.; Deng, X.; Xiao, J.; Liu, J.; Sprenkle, V.; Wang, W. Towards High-Performance Nonaqueous Redox Flow Electrolyte Via Ionic Modification of Active Species. *Adv. Energy Mater.* **2015**, *5*, 1400678.
(41) Milshtein, J. D.; Kaur, A. P.; Casselman, M. D.; Kowalski, J. A.; Modekrutti, S.; Zhang, P. L.; Harsha Attanayake, N.; Elliott, C. F.; Parkin, S. R.; Risko, C.; Brushett, F. R.; Odom, S. A. High current density, long duration cycling of soluble organic active species for non-aqueous redox flow batteries. *Energy Environ. Sci.* **2016**, *9*, 3531−3543.
(42) Wei, X.; Xu, W.; Huang, J.; Zhang, L.; Walter, E.; Lawrence, C.; Vijayakumar, M.; Henderson, W. A.; Liu, T.; Cosimbescu, L.; Li, B.; Sprenkle, V.; Wang, W. Radical Compatibility with Nonaqueous Electrolytes and Its Impact on an All-Organic Redox Flow Battery. *Angew. Chem., Int. Ed.* **2015**, *54*, 8684−8687.
(43) Cosimbescu, L.; Wei, X.; Vijayakumar, M.; Xu, W.; Helm, M. L.; Burton, S. D.; Sorensen, C. M.; Liu, J.; Sprenkle, V.; Wang, W. Anion-Tunable Properties and Electrochemical Performance of Functionalized Ferrocene Compounds. *Sci. Rep.* **2015**, *5*, 14117.
(44) Hu, B.; Luo, J.; Hu, M.; Yuan, B.; Liu, T. A pH-Neutral, Metal-Free Aqueous Organic Redox Flow Battery Employing an Ammonium Anthraquinone Anolyte. *Angew. Chem.* **2019**, *131*, 16782−16789.
(45) Luo, J.; Hu, B.; Debruler, C.; Bi, Y.; Zhao, Y.; Yuan, B.; Hu, M.; Wu, W.; Liu, T. Unprecedented Capacity and Stability of Ammonium Ferrocyanide Catholyte in pH Neutral Aqueous Redox Flow Batteries. *Joule* **2019**, *3*, 149−163.
(46) Deng, X.; Hu, M.; Wei, X.; Wang, W.; Mueller, K. T.; Chen, Z.; Hu, J. Nuclear magnetic resonance studies of the solvation structures of a high-performance nonaqueous redox flow electrolyte. *J. Power Sources* **2016**, *308*, 172−179.
(47) Han, K. S.; Rajput, N. N.; Vijayakumar, M.; Wei, X.; Wang, W.; Hu, J.; Persson, K. A.; Mueller, K. T. Preferential Solvation of an Asymmetric Redox Molecule. *J. Phys. Chem. C* **2016**, *120*, 27834−27839.

(48) Zu, X.; Zhang, L.; Qian, Y.; Zhang, C.; Yu, G. Molecular Engineering of Azobenzene-Based Anolytes Towards High-Capacity Aqueous Redox Flow Batteries. *Angew. Chem., Int. Ed.* **2020**, *59*, 22163−22170.
(49) Wei, X.; Xu, W.; Vijayakumar, M.; Cosimbescu, L.; Liu, T.; Sprenkle, V.; Wang, W. TEMPO-Based Catholyte for High-Energy Density Nonaqueous Redox Flow Batteries. *Adv. Mater.* **2014**, *26*, 7649−7653.
(50) Orita, A.; Verde, M. G.; Sakai, M.; Meng, Y. S. A biomimetic redox flow battery based on flavin mononucleotide. *Nat. Commun.* **2016**, *7*, 13230.
(51) Ding, Y.; Zhang, C.; Zhang, L.; Wei, H.; Li, Y.; Yu, G. Insights into hydrotropic solubilization for hybrid ion redox flow batteries. *ACS Energy Lett.* **2018**, *3*, 2641−2648.
(52) Chen, Y.; Zhou, M.; Xia, Y.; Wang, X.; Liu, Y.; Yao, Y.; Zhang, H.; Li, Y.; Lu, S.; Qin, W.; et al. A stable and high-capacity redox targeting-based electrolyte for aqueous flow batteries. *Joule* **2019**, *3*, 2255−2267.
(53) Huang, Q.; Yang, J.; Ng, C. B.; Jia, C.; Wang, Q. A redox flow lithium battery based on the redox targeting reactions between LiFePO 4 and iodide. *Energy Environ. Sci.* **2016**, *9*, 917−921.
(54) Zhou, M.; Huang, Q.; Pham Truong, T. N.; Ghilane, J.; Zhu, Y. G.; Jia, C.; Yan, R.; Fan, L.; Randriamahazaka, H.; Wang, Q. Nernstian-potential-driven redox-targeting reactions of battery materials. *Chem.* **2017**, *3*, 1036−1049.
(55) Tagade, P. M.; Adiga, S. P.; Park, M. S.; Pandian, S.; Hariharan, K. S.; Kolake, S. M. Empirical relationship between chemical structure and redox properties: Mathematical expressions connecting structural features to energies of frontier orbitals and redox potentials for organic molecules. *J. Phys. Chem. C* **2018**, *122*, 11322−11333.
(56) Wang, H.; Emanuelsson, R.; Banerjee, A.; Ahuja, R.; Strømme, M.; Sjödin, M. Effect of cycling ion and solvent on the redox chemistry of substituted quinones and solvent-induced breakdown of the correlation between redox potential and electron-withdrawing power of substituents. *J. Phys. Chem. C* **2020**, *124*, 13609−13617.
(57) Zhao, Y.; Yu, Z.; Robertson, L. A.; Zhang, J.; Shi, Z.; Bheemireddy, S. R.; Shkrob, I. A.; Li, T.; Zhang, Z.; Cheng, L.; et al. Unexpected electrochemical behavior of an anolyte redoxmer in flow battery electrolytes: solvating cations help to fight against the thermodynamic−kinetic dilemma. *J. Mater. Chem. A* **2020**, *8*, 13470−13479.
(58) Wei, X.; Duan, W.; Huang, J.; Zhang, L.; Li, B.; Reed, D.; Xu, W.; Sprenkle, V.; Wang, W. A High-Current, Stable Nonaqueous Organic Redox Flow Battery. *ACS Energy Lett.* **2016**, *1*, 705−711.
(59) Luo, J.; Sam, A.; Hu, B.; DeBruler, C.; Wei, X.; Wang, W.; Liu, T. Unraveling pH dependent cycling stability of ferricyanide/ferrocyanide in redox flow batteries. *Nano Energy* **2017**, *42*, 215−221.
(60) Lin, K.; Gomez-Bombarelli, R.; Beh, E. S.; Tong, L.; Chen, Q.; Valle, A.; Aspuru-Guzik, A.; Aziz, M. J.; Gordon, R. G. A redox-flow battery with an alloxazine-based organic electrolyte. *Nat. Energy* **2016**, *1*, 16102.
(61) Luo, Q.; Li, L.; Wang, W.; Nie, Z.; Wei, X.; Li, B.; Chen, B.; Yang, Z.; Sprenkle, V. Capacity Decay and Remediation of Nafion-based All-Vanadium Redox Flow Batteries. *ChemSusChem* **2013**, *6*, 268−274.
(62) Brushett, F. R.; Aziz, M. J.; Rodby, K. E. On lifetime and cost of redox-active organics for aqueous flow batteries. *ACS Energy Lett.* **2020**, *5*, 879−884.
(63) Feng, R.; Zhang, X.; Murugesan, V.; Hollas, A.; Chen, Y.; Shao, Y.; Walter, E.; Wellala, N. P.; Yan, L.; Rosso, K. M.; et al. Reversible ketone hydrogenation and dehydrogenation for aqueous organic redox flow batteries. *Science* **2021**, *372*, 836−840.
(64) Páez, T.; Martínez-Cuezva, A.; Palma, J.; Ventosa, E. Revisiting the cycling stability of ferrocyanide in alkaline media for redox flow batteries. *J. Power Sources* **2020**, *471*, 228453.
(65) Duan, W.; Vemuri, R. S.; Milshtein, J. D.; Laramie, S.; Dmello, R. D.; Huang, J.; Zhang, L.; Hu, D.; Vijayakumar, M.; Wang, W.; Liu, J.; Darling, R. M.; Thompson, L.; Smith, K.; Moore, J. S.; Brushett, F. R.; Wei, X. A symmetric organic-based nonaqueous redox flow battery and its state of charge diagnostics by FTIR. *J. Mater. Chem. A* **2016**, *4*, 5448−5456.
(66) Zhang, J.; Huang, J.; Robertson, L. A.; Assary, R. S.; Shkrob, I. A.; Zhang, L. Elucidating Factors Controlling Long-Term Stability of Radical Anions for Negative Charge Storage in Nonaqueous Redox Flow Batteries. *J. Phys. Chem. C* **2018**, *122*, 8116−8127.
(67) Qu, X.; Persson, K. A. Toward Accurate Modeling of the Effect of Ion-Pair Formation on Solute Redox Potential. *J. Chem. Theory Comput.* **2016**, *12*, 4501−4508.
(68) Huang, J.; Yang, Z.; Murugesan, V.; Walter, E.; Hollas, A.; Pan, B.; Assary, R. S.; Shkrob, I. A.; Wei, X.; Zhang, Z. Spatially Constrained Organic Diquat Anolyte for Stable Aqueous Flow Batteries. *ACS Energy Lett.* **2018**, *3*, 2533−2538.
(69) Zhang, J.; Shkrob, I. A.; Assary, R. S.; Tung, S. o.; Silcox, B.; Curtiss, L. A.; Thompson, L.; Zhang, L. Toward improved catholyte materials for redox flow batteries: what controls chemical stability of persistent radical cations? *J. Phys. Chem. C* **2017**, *121*, 23347−23358.
(70) Gerhardt, M. R.; Tong, L.; Gomez-Bombarelli, R.; Chen, Q.; Marshak, M. P.; Galvin, C. J.; Aspuru-Guzik, A.; Gordon, R. G.; Aziz, M. J. Anthraquinone Derivatives in Aqueous Flow Batteries. *Adv. Energy Mater.* **2017**, *7*, 1601488.
(71) Er, S.; Suh, C.; Marshak, M. P.; Aspuru-Guzik, A. Computational design of molecules for an all-quinone redox flow battery. *Chem. Sci.* **2015**, *6*, 885−893.
(72) de la Cruz, C.; Molina, A.; Patil, N.; Ventosa, E.; Marcilla, R.; Mavrandonakis, A. New insights into phenazine-based organic redox flow batteries by using high-throughput DFT modelling. *Sustain. Energy Fuels* **2020**, *4*, 5513−5521.
(73) Qu, X.; Jain, A.; Rajput, N. N.; Cheng, L.; Zhang, Y.; Ong, S. P.; Brafman, M.; Maginn, E.; Curtiss, L. A.; Persson, K. A. The Electrolyte Genome project: A big data approach in battery materials discovery. *Comput. Mater. Sci.* **2015**, *103*, 56−67.
(74) Sanchez-Lengeling, B.; Aspuru-Guzik, A. Inverse molecular design using machine learning: Generative models for matter engineering. *Science* **2018**, *361*, 360−365.
(75) Gao, T.; Lu, W. Machine learning toward advanced energy storage devices and systems. *iScience* **2021**, *24*, 101936.
(76) Sevov, C. S.; Hickey, D. P.; Cook, M. E.; Robinson, S. G.; Barnett, S.; Minteer, S. D.; Sigman, M. S.; Sanford, M. S. Physical Organic Approach to Persistent, Cyclable, Low-Potential Electrolytes for Flow Battery Applications. *J. Am. Chem. Soc.* **2017**, *139*, 2924−2927.
(77) Robinson, S. G.; Yan, Y.; Hendriks, K. H.; Sanford, M. S.; Sigman, M. S. Developing a predictive solubility model for monomeric and oligomeric cyclopropenium-based flow battery catholytes. *J. Am. Chem. Soc.* **2019**, *141*, 10171−10176.
(78) Chen, Q.; Gerhardt, M. R.; Hartle, L.; Aziz, M. J. A Quinone-Bromide Flow Battery with 1 W/cm(2) Power Density. *J. Electrochem. Soc.* **2016**, *163*, A5010−A5013.
(79) Gerhardt, M. R.; Beh, E. S.; Tong, L.; Gordon, R. G.; Aziz, M. J. Comparison of Capacity Retention Rates During Cycling of Quinone-Bromide Flow Batteries. *MRS Adv.* **2017**, *2*, 431−438.
(80) Chen, Q.; Eisenach, L.; Aziz, M. J. Cycling analysis of a quinone-bromide redox flow battery. *J. Electrochem. Soc.* **2016**, *163*, A5057.
(81) Huskinson, B.; Marshak, M.; Gerhardt, M.; Aziz, M. J. Cycling of a quinone-bromide flow battery for large-scale electrochemical energy storage. *ECS Trans* **2014**, *61*, 27−30.
(82) Carney, T. J.; Collins, S. J.; Moore, J. S.; Brushett, F. R. Concentration-Dependent Dimerization of Anthraquinone Disulfonic Acid and Its Impact on Charge Storage. *Chem. Mater.* **2017**, *29*, 4801−4810.
(83) Goulet, M.-A.; Tong, L.; Pollack, D. A.; Tabor, D. P.; Odom, S. A.; Aspuru-Guzik, A. N.; Kwan, E. E.; Gordon, R. G.; Aziz, M. J. Extending the lifetime of organic flow batteries via redox state management. *J. Am. Chem. Soc.* **2019**, *141*, 8014−8019.
(84) Mazúr, P.; Charvát, J.; Mrlík, J.; Pocedič, J.; Akrman, J.; Kubáč, L.; Řeháková, B.; Kosek, J. Evaluation of Electrochemical Stability of Sulfonated Anthraquinone-Based Acidic Electrolyte for Redox Flow Battery Application. *Molecules* **2021**, *26*, 2484.
(85) Yang, B.; Hoober-Burkhardt, L.; Wang, F.; Surya Prakash, G. K.; Narayanan, S. R. An Inexpensive Aqueous Flow Battery for Large-Scale

Electrical Energy Storage Based on Water-Soluble Organic Redox Couples. *J. Electrochem. Soc.* **2014**, *161*, A1371−A1380.
(86) Yang, B.; Murali, A.; Nirmalchandar, A.; Jayathilake, B.; Prakash, G. S.; Narayanan, S. A durable, inexpensive and scalable redox flow battery based on iron sulfate and anthraquinone disulfonic acid. *J. Electrochem. Soc.* **2020**, *167*, 060520.
(87) Gerhardt, M. R.; Tong, L.; Gómez-Bombarelli, R.; Chen, Q.; Marshak, M. P.; Galvin, C. J.; Aspuru-Guzik, A.; Gordon, R. G.; Aziz, M. J. Anthraquinone derivatives in aqueous flow batteries. *Adv. Energy Mater.* **2017**, *7*, 1601488.
(88) Goulet, M.-A.; Aziz, M. J. Flow battery molecular reactant stability determined by symmetric cell cycling methods. *J. Electrochem. Soc.* **2018**, *165*, A1466.
(89) Liu, Y.; Lu, S.; Chen, S.; Wang, H.; Zhang, J.; Xiang, Y. A Sustainable Redox Flow Battery with Alizarin-Based Aqueous Organic Electrolyte. *ACS Appl. Energy Mater.* **2019**, *2*, 2469−2474.
(90) Kwabi, D. G.; Lin, K.; Ji, Y.; Kerr, E. F.; Goulet, M.-A.; De Porcellinis, D.; Tabor, D. P.; Pollack, D. A.; Aspuru-Guzik, A.; Gordon, R. G.; et al. Alkaline quinone flow battery with long lifetime at pH 12. *Joule* **2018**, *2*, 1894−1906.
(91) Tabor, D. P.; Gómez-Bombarelli, R.; Tong, L.; Gordon, R. G.; Aziz, M. J.; Aspuru-Guzik, A. Theoretical and experimental investigation of the stability limits of quinones in aqueous media: implications for organic aqueous redox flow batteries. *ChemRxiv*, 2018. DOI: 10.26434/chemrxiv.6990053.v2.
(92) Wu, M.; Jing, Y.; Wong, A. A.; Fell, E. M.; Jin, S.; Tang, Z.; Gordon, R. G.; Aziz, M. J. Extremely stable anthraquinone negolytes synthesized from common precursors. *Chem.* **2020**, *6*, 1432−1442.
(93) Yang, B.; Hoober-Burkhardt, L.; Wang, F.; Surya Prakash, G. K.; Narayanan, S. R. An inexpensive aqueous flow battery for large-scale electrical energy storage based on water-soluble organic redox couples. *J. Electrochem. Soc.* **2014**, *161*, A1371−A1380.
(94) Yang, B.; Hoober-Burkhardt, L.; Krishnamoorthy, S.; Murali, A.; Prakash, G. K. S.; Narayanan, S. R. High-Performance Aqueous Organic Flow Battery with Quinone-Based Redox Couples at Both Electrodes. *J. Electrochem. Soc.* **2016**, *163*, A1442−A1449.
(95) Hoober-Burkhardt, L.; Krishnamoorthy, S.; Yang, B.; Murali, A.; Nirmalchandar, A.; Prakash, G. K. S.; Narayanan, S. R. A New Michael-Reaction-Resistant Benzoquinone for Aqueous Organic Redox Flow Batteries. *J. Electrochem. Soc.* **2017**, *164*, A600−A607.
(96) Murali, A.; Nirmalchandar, A.; Krishnamoorthy, S.; Hoober-Burkhardt, L.; Yang, B.; Soloveichik, G.; Prakash, G. S.; Narayanan, S. Understanding and mitigating capacity fade in aqueous organic redox flow batteries. *J. Electrochem. Soc.* **2018**, *165*, A1193−A1203.
(97) Gerken, J. B.; Stamoulis, A. G.; Suh, S.-E.; Fischer, N. D.; Kim, Y. J.; Guzei, I.; Stahl, S. S. Efficient electrochemical synthesis of robust, densely functionalized water soluble quinones. *Chem. Commun.* **2020**, *56*, 1199−1202.
(98) Gerken, J. B.; Anson, C. W.; Preger, Y.; Symons, P. G.; Genders, J. D.; Qiu, Y.; Li, W.; Root, T. W.; Stahl, S. S. Comparison of Quinone-Based Catholytes for Aqueous Redox Flow Batteries and Demonstration of Long-Term Stability with Tetrasubstituted Quinones. *Adv. Energy Mater.* **2020**, *10*, 2000340.
(99) Yang, Z.; Tong, L.; Tabor, D. P.; Beh, E. S.; Goulet, M. A.; De Porcellinis, D.; Aspuru-Guzik, A.; Gordon, R. G.; Aziz, M. J. Alkaline benzoquinone aqueous flow battery for large-scale storage of electrical energy. *Adv. Energy Mater.* **2018**, *8*, 1702056.
(100) Carretero-González, J.; Castillo-Martínez, E.; Armand, M. Highly water-soluble three-redox state organic dyes as bifunctional analytes. *Energy Environ. Sci.* **2016**, *9*, 3521−3530.
(101) Tong, L.; Jing, Y.; Gordon, R. G.; Aziz, M. J. Symmetric All-Quinone Aqueous Battery. *ACS Appl. Energy Mater.* **2019**, *2*, 4016−4021.
(102) Leung, P.; Martin, T.; Liras, M.; Berenguer, A.; Marcilla, R.; Shah, A.; An, L.; Anderson, M.; Palma, J. Cyclohexanedione as the negative electrode reaction for aqueous organic redox flow batteries. *Appl. Energy* **2017**, *197*, 318−326.
(103) Rodriguez, J.; Niemet, C.; Pozzo, L. D. Fluorenone Based Anolyte for an Aqueous Organic Redox-Flow Battery. *ECS Trans* **2019**, *89*, 49.
(104) Wang, F.; Stahl, S. S. Electrochemical oxidation of organic molecules at lower overpotential: Accessing broader functional group compatibility with electron− proton transfer mediators. *Acc. Chem. Res.* **2020**, *53*, 561−574.
(105) Mukhopadhyay, A.; Zhao, H.; Li, B.; Hamel, J.; Yang, Y.; Cao, D.; Natan, A.; Zhu, H. Abundant organic dye as an anolyte for aqueous flow battery with multielectron transfer. *ACS Appl. Energy Mater.* **2019**, *2*, 7425−7437.
(106) Wiberg, C.; Owusu, F.; Wang, E.; Ahlberg, E. Electrochemical evaluation of a napthalene diimide derivative for potential application in aqueous organic redox flow batteries. *Energy Technol.* **2019**, *7*, 1900843.
(107) Medabalmi, V.; Sundararajan, M.; Singh, V.; Baik, M.-H.; Byon, H. R. Naphthalene diimide as a two-electron anolyte for aqueous and neutral pH redox flow batteries. *J. Mater. Chem. A* **2020**, *8*, 11218−11223.
(108) Winsberg, J.; Stolze, C.; Muench, S.; Liedl, F.; Hager, M. D.; Schubert, U. S. TEMPO/phenazine combi-molecule: a redox-active material for symmetric aqueous redox-flow batteries. *ACS Energy Lett.* **2016**, *1*, 976−980.
(109) Lai, Y.; Li, X.; Liu, K.; Tung, W.-Y.; Cheng, C.-F.; Zhu, Y. Stable Low-Cost Organic Dye Anolyte for Aqueous Organic Redox Flow Battery. *ACS Appl. Energy Mater.* **2020**, *3*, 2290−2295.
(110) Wang, C.; Li, X.; Yu, B.; Wang, Y.; Yang, Z.; Wang, H.; Lin, H.; Ma, J.; Li, G.; Jin, Z. Molecular Design of Fused-Ring Phenazine Derivatives for Long-Cycling Alkaline Redox Flow Batteries. *ACS Energy Lett.* **2020**, *5*, 411−417.
(111) Pang, S.; Wang, X.; Wang, P.; Ji, Y. Biomimetic Amino Acid Functionalized Phenazine Flow Batteries with Long Lifetime at Near-Neutral pH. *Angew. Chem.* **2021**, *133*, 5349−5358.
(112) Milshtein, J. D.; Su, L.; Liou, C.; Badel, A. F.; Brushett, F. R. Voltammetry study of quinoxaline in aqueous electrolytes. *Electrochim. Acta* **2015**, *180*, 695−704.
(113) Pasadakis-Kavounis, A.; Baj, V.; Hjelm, J. Electrochemical Characterization of Aromatic Molecules with 1, 4-Diaza Groups for Flow Battery Applications. *Molecules* **2021**, *26*, 2227.
(114) Astuti, Y.; Topoglidis, E.; Briscoe, P. B.; Fantuzzi, A.; Gilardi, G.; Durrant, J. R. Proton-coupled electron transfer of flavodoxin immobilized on nanostructured tin dioxide electrodes: Thermodynamics versus kinetics control of protein redox function. *J. Am. Chem. Soc.* **2004**, *126*, 8001−8009.
(115) Grajek, H.; Drabent, R.; Bojarski, C.; et al. The structure of the flavomononucleotide dimer. *Biochim. Biophys. Acta Gen. Subj.* **1986**, *881*, 241−247.
(116) Smith, S. B.; Bruice, T. C. Mechanisms of isoalloxazine (flavine) hydrolysis. *J. Am. Chem. Soc.* **1975**, *97*, 2875−2881.
(117) Orita, A.; Verde, M. G.; Sakai, M.; Meng, Y. S. A biomimetic redox flow battery based on flavin mononucleotide. *Nat. commun.* **2016**, *7*, 13230.
(118) Lin, K.; Gómez-Bombarelli, R.; Beh, E. S.; Tong, L.; Chen, Q.; Valle, A.; Aspuru-Guzik, A.; Aziz, M. J.; Gordon, R. G. A redox-flow battery with an alloxazine-based organic electrolyte. *Nat. Energy* **2016**, *1*, 16102.
(119) Liu, T.; Wei, X.; Nie, Z.; Sprenkle, V.; Wang, W. A total organic aqueous redox flow battery employing a low cost and sustainable methyl viologen anolyte and 4-HO-TEMPO catholyte. *Adv. Energy Mater.* **2016**, *6*, 1501449.
(120) Beh, E. S.; De Porcellinis, D.; Gracia, R. L.; Xia, K.; Gordon, R. G.; Aziz, M. J. A Neutral pH Aqueous Organic-Organometallic Redox Flow Battery with Extremely High Capacity Retention. *ACS Energy Lett.* **2017**, *2*, 639−644.
(121) Bird, C.; Kuhn, A. Electrochemistry of the viologens. *Chem. Soc. Rev.* **1981**, *10*, 49−82.
(122) DeBruler, C.; Hu, B.; Moss, J.; Liu, X.; Luo, J.; Sun, Y.; Liu, T. Designer two-electron storage viologen anolyte materials for neutral aqueous organic redox flow batteries. *Chem.* **2017**, *3*, 961−978.

(123) Hu, B.; Tang, Y.; Luo, J.; Grove, G.; Guo, Y.; Liu, T. Improved radical stability of viologen anolytes in aqueous organic redox flow batteries. *Chem. Commun.* **2018**, *54*, 6871−6874.
(124) Liu, W.; Liu, Y.; Zhang, H.; Xie, C.; Shi, L.; Zhou, Y.-G.; Li, X. A highly stable neutral viologen/bromine aqueous flow battery with high energy and power density. *Chem. Commun.* **2019**, *55*, 4801−4804.
(125) Luo, J.; Hu, B.; Debruler, C.; Liu, T. A π-Conjugation Extended Viologen as a Two-Electron Storage Anolyte for Total Organic Aqueous Redox Flow Batteries. *Angew. Chem., Int. Ed.* **2018**, *57*, 231−235.
(126) Wiśniewska, J.; Rześnicki, P.; Topolski, A. A mechanistic study on the disproportionation and oxidative degradation of phenothiazine derivatives by manganese (III) complexes in phosphate acidic media. *Transit. Metal Chem.* **2011**, *36*, 767.
(127) Sackett, P. H.; Mayausky, J.; Smith, T.; Kalus, S.; McCreery, R. L. Side-chain effects on phenothiazine cation radical reactions. *J. Med. Chem.* **1981**, *24*, 1342−1347.
(128) Janietz, S.; Wedel, A. Electrochemical redox behavior and electroluminescence in the mixed energy-sufficient system thianthrene and 2-(4-Biphenyl)-5-(4-tert-butylphenyl)-1,3,4-oxadiazole. *Adv. Mater.* **1997**, *9*, 403−407.
(129) Rangappa, P.; Shine, H. J. An overview of some reactions of thianthrene cation radical. Products and mechanisms of their formation. *J. Sulfur Chem.* **2006**, *27*, 617−664.
(130) Zhang, C.; Niu, Z.; Peng, S.; Ding, Y.; Zhang, L.; Guo, X.; Zhao, Y.; Yu, G. Phenothiazine-Based Organic Catholyte for High-Capacity and Long-Life Aqueous Redox Flow Batteries. *Adv. Mater.* **2019**, *31*, 1901052.
(131) Wang, W.; Xu, W.; Cosimbescu, L.; Choi, D.; Li, L.; Yang, Z. Anthraquinone with tailored structure for a nonaqueous metal−organic redox flow battery. *Chem. Commun.* **2012**, *48*, 6669−6671.
(132) Kwon, G.; Lee, S.; Hwang, J.; Shim, H.-S.; Lee, B.; Lee, M. H.; Ko, Y.; Jung, S.-K.; Ku, K.; Hong, J.; et al. Multi-redox molecule for high-energy redox flow batteries. *Joule* **2018**, *2*, 1771−1782.
(133) Huang, J.; Yang, Z.; Vijayakumar, M.; Duan, W.; Hollas, A.; Pan, B.; Wang, W.; Wei, X.; Zhang, L. A Two-Electron Storage Nonaqueous Organic Redox Flow Battery. *Adv. Sustain. Syst.* **2018**, *2*, 1700131.
(134) Potash, R. A.; McKone, J. R.; Conte, S.; Abruña, H. D. On the benefits of a symmetric redox flow battery. *J. Electrochem. Soc.* **2016**, *163*, A338−A344.
(135) Geysens, P.; Li, Y.; Vankelecom, I.; Fransaer, J.; Binnemans, K. Highly soluble 1, 4-diaminoanthraquinone derivative for nonaqueous symmetric redox flow batteries. *ACS Sustain. Chem. Eng.* **2020**, *8*, 3832−3843.
(136) Ding, Y.; Li, Y.; Yu, G. Exploring bio-inspired quinone-based organic redox flow batteries: a combined experimental and computational study. *Chem.* **2016**, *1*, 790−801.
(137) Senoh, H.; Yao, M.; Sakaebe, H.; Yasuda, K.; Siroma, Z. A two-compartment cell for using soluble benzoquinone derivatives as active materials in lithium secondary batteries. *Electrochim. Acta* **2011**, *56*, 10145−10150.
(138) Milton, M.; Cheng, Q.; Yang, Y.; Nuckolls, C.; Hernández Sánchez, R.; Sisto, T. J. Molecular materials for nonaqueous flow batteries with a high coulombic efficiency and stable cycling. *Nano Lett.* **2017**, *17*, 7859−7863.
(139) Li, L.; Gong, H.; Chen, D.; Lin, M. Stable Bifunctional Perylene Imide Radicals for High-Performance Organic−Lithium Redox-Flow Batteries. *Chem.—Eur. J.* **2018**, *24*, 13188−13196.
(140) Brushett, F. R.; Vaughey, J. T.; Jansen, A. N. An All-Organic Non-aqueous Lithium-Ion Redox Flow Battery. *Adv. Energy Mater.* **2012**, *2*, 1390−1396.
(141) Carino, E. V.; Diesendruck, C. E.; Moore, J. S.; Curtiss, L. A.; Assary, R. S.; Brushett, F. R. BF3-promoted electrochemical properties of quinoxaline in propylene carbonate. *RSC Adv.* **2015**, *5*, 18822−18831.
(142) Kwon, G.; Lee, K.; Lee, M. H.; Lee, B.; Lee, S.; Jung, S.-K.; Ku, K.; Kim, J.; Park, S. Y.; Kwon, J. E.; et al. Bio-inspired molecular redesign of a multi-redox catholyte for high-energy non-aqueous organic redox flow batteries. *Chem* **2019**, *5*, 2642−2656.
(143) Romadina, E. I.; Komarov, D. S.; Stevenson, K. J.; Troshin, P. A. New phenazine based anolyte material for high voltage organic redox flow batteries. *Chem. Commun.* **2021**, *57*, 2986−2989.
(144) Kowalski, J. A.; Casselman, M. D.; Kaur, A. P.; Milshtein, J. D.; Elliott, C. F.; Modekrutti, S.; Attanayake, N. H.; Zhang, N.; Parkin, S. R.; Risko, C.; et al. A stable two-electron-donating phenothiazine for application in nonaqueous redox flow batteries. *J. Mater. Chem. A* **2017**, *5*, 24371−24379.
(145) Attanayake, N. H.; Kowalski, J. A.; Greco, K. V.; Casselman, M. D.; Milshtein, J. D.; Chapman, S. J.; Parkin, S. R.; Brushett, F. R.; Odom, S. A. Tailoring two-electron-donating phenothiazines to enable high-concentration redox electrolytes for use in nonaqueous redox flow batteries. *Chem. Mater.* **2019**, *31*, 4353−4363.
(146) Hu, B.; Liu, T. Two electron utilization of methyl viologen anolyte in nonaqueous organic redox flow battery. *J. Energy Chem.* **2018**, *27*, 1326−1332.
(147) Chai, J.; Lashgari, A.; Cao, Z.; Williams, C. K.; Wang, X.; Dong, J.; Jiang, J. PEGylation-enabled extended cyclability of a non-aqueous redox flow battery. *ACS Appl. Mater. Interfaces* **2020**, *12*, 15262−15270.
(148) Chai, J.; Lashgari, A.; Wang, X.; Williams, C. K.; et al. All-PEGylated redox-active metal-free organic molecules in non-aqueous redox flow battery. *J. Mater. Chem. A* **2020**, *8*, 15715−15724.
(149) Elliott, C. M.; Freitag, R. A.; Blaney, D. D. Electrochemistry, spectroelectrochemistry, and photochemistry of a series of new covalently linked tris (2, 2-bipyridine) ruthenium (II)/diquat complexes. *J. Am. Chem. Soc.* **1985**, *107*, 4647−4655.
(150) Vaid, T. P.; Sanford, M. S. An organic super-electron-donor as a high energy density negative electrolyte for nonaqueous flow batteries. *Chem. Commun.* **2019**, *55*, 11037−11040.
(151) Griffin, J. D.; Pancoast, A. R.; Sigman, M. S. Interrogation of 2, 2′-Bipyrimidines as Low-Potential Two-Electron Electrolytes. *J. Am. Chem. Soc.* **2021**, *143*, 992−1004.
(152) Zhang, L.; Qian, Y.; Feng, R.; Ding, Y.; Zu, X.; Zhang, C.; Guo, X.; Wang, W.; Yu, G. Reversible redox chemistry in azobenzene-based organic molecules for high-capacity and long-life nonaqueous redox flow batteries. *Nat. Commun.* **2020**, *11*, 3843.
(153) Sevov, C. S.; Brooner, R. E. M.; Chenard, E.; Assary, R. S.; Moore, J. S.; Rodriguez-Lopez, J.; Sanford, M. S. Evolutionary Design of Low Molecular Weight Organic Anolyte Materials for Applications in Nonaqueous Redox Flow Batteries. *J. Am. Chem. Soc.* **2015**, *137*, 14465−14472.
(154) Hendriks, K. H.; Sevov, C. S.; Cook, M. E.; Sanford, M. S. Multielectron Cycling of a low-potential anolyte in alkali metal electrolytes for nonaqueous redox flow batteries. *ACS Energy Lett.* **2017**, *2*, 2430−2435.
(155) Li, M.; Case, J.; Minteer, S. D. Bipolar Redox-Active Molecules in Non-Aqueous Organic Redox Flow Batteries: Status and Challenges. *ChemElectroChem.* **2021**, *8*, 1215−1232.
(156) Liu, Y.; Goulet, M. A.; Tong, L.; Liu, Y.; Ji, Y.; Wu, L.; Gordon, R. G.; Aziz, M. J.; Yang, Z.; Xu, T. A Long-Lifetime All-Organic Aqueous Flow Battery Utilizing TMAP-TEMPO Radical. *Chem.* **2019**, *5*, 1861−1870.
(157) Charlton, G. D.; Barbon, S. M.; Gilroy, J. B.; Dyker, C. A. A bipolar verdazyl radical for a symmetric all-organic redox flow-type battery. *J. Energy Chem.* **2019**, *34*, 52−56.
(158) Korshunov, A.; Milner, M. J.; Grünebaum, M.; Studer, A.; Winter, M.; Cekic-Laskovic, I. An oxo-verdazyl radical for a symmetrical non-aqueous redox flow battery. *J. Mater. Chem. A* **2020**, *8*, 22280−22291.
(159) Ma, T.; Pan, Z.; Miao, L.; Chen, C.; Han, M.; Shang, Z.; Chen, J. Porphyrin-Based Symmetric Redox-Flow Batteries towards Cold-Climate Energy Storage. *Angew. Chem.* **2018**, *130*, 3212−3216.
(160) Hagemann, T.; Winsberg, J.; Wild, A.; Schubert, U. S. Synthesis and Electrochemical Study of a TCAA Derivative − A potential bipolar redox-active material. *Electrochim. Acta* **2017**, *228*, 494−502.
(161) Nepomnyashchii, A. B.; Pistner, A. J.; Bard, A. J.; Rosenthal, J. Synthesis, photophysics, electrochemistry and electrogenerated chemiluminescence of PEG-modified BODIPY dyes in organic and aqueous solutions. *J. Phys. Chem. C* **2013**, *117*, 5599−5609.

(162) Kosswattaarachchi, A. M.; Friedman, A. E.; Cook, T. R. Characterization of a BODIPY dye as an active species for redox flow batteries. *ChemSusChem* **2016**, *9*, 3317−3323.
(163) Winsberg, J.; Hagemann, T.; Muench, S.; Friebe, C.; Haupler, B.; Janoschka, T.; Morgenstern, S.; Hager, M. D.; Schubert, U. S. Poly(boron-dipyrromethene)-A Redox-Active Polymer Class for Polymer Redox-Flow Batteries. *Chem. Mater.* **2016**, *28*, 3401−3405.
(164) Moutet, J.; Veleta, J. M.; Gianetti, T. L. Symmetric, Robust, and High-voltage Organic Redox Flow Battery Model Based on a Helical Carbenium Ion Electrolyte. *ACS Appl. Energy Mater.* **2021**, *4*, 9−14.
(165) Wang, X.; Chai, J.; Devi, N.; Lashgari, A.; Chaturvedi, A.; et al. Two-electron-active tetracyanoethylene for nonaqueous redox flow batteries. *J. Mater. Chem. A* **2021**, *9*, 13867−13873.
(166) Armstrong, C. G.; Hogue, R. W.; Toghill, K. E. Application of the dianion croconate violet for symmetric organic non-aqueous redox flow battery electrolytes. *J. Power Sources* **2019**, *440*, 227037.
(167) Zhang, C.; Qian, Y.; Ding, Y.; Zhang, L.; Guo, X.; Zhao, Y.; Yu, G. Biredox eutectic electrolytes derived from organic redox-active molecules: high-energy storage systems. *Angew. Chem., Int. Ed.* **2019**, *58*, 7045−7050.

https://doi.org/10.1021/acsmaterialslett.1c00668
ACS Materials Lett. 2022, 4, 277−306